LUND UNIVERSITY

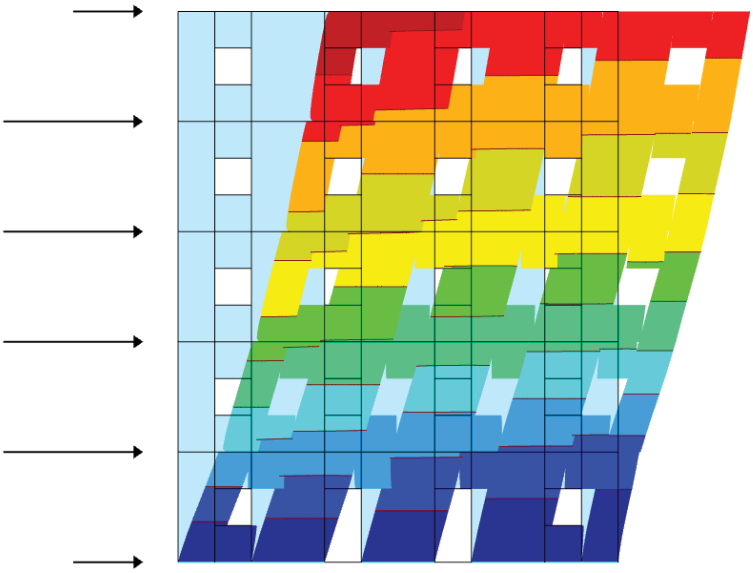

LATERAL STABILIZATION OF CLT BUILDINGS

Modelling approaches

SANNA KÄLLMAN GLEISNER
and LINA HOLMQVIST

Structural Mechanics

Master's Dissertation

DEPARTMENT OF CONSTRUCTION SCIENCES

DIVISION OF STRUCTURAL MECHANICS

ISRN LUTVDG/TVSM--22/5257--SE (1-88) | ISSN 0281-6679

MASTER'S DISSERTATION

LATERAL STABILIZATION OF CLT BUILDINGS

Modelling approaches

SANNA KÄLLMAN GLEISNER and LINA HOLMQVIST

Supervisor: Professor **ERIK SERRANO**, Division of Structural Mechanics, LTH.
Assistant Supervisor: Professor **JOSE M. CABRERO**, University of Navarra, Spain.
Examiner: Dr **HENRIK DANIELSSON**, Division of Structural Mechanics, LTH.

Printed by V-husets tryckeri LTH, Lund, Sweden, May 2022 *(Pl)*.

For information, address:
Division of Structural Mechanics,
Faculty of Engineering LTH, Lund University, Box 118, SE-221 00 Lund, Sweden.
Homepage: www.byggmek.lth.se

Abstract

Cross-laminated timber (CLT) is an environmentally positive building material with high stiffness and load-bearing capacity. In combination with a low self-weight, CLT is a beneficial material to use for the load-bearing structure of high-rise buildings. In this project, the lateral stabilization of a CLT building subjected to a wind load is analysed through several modelling approaches. The effect of modelling choice is investigated through predicted stiffness (displacement), internal force distribution and reaction force.

The modelling process considered in this work is divided into three parts. First, a single CLT panel is modelled as a truss and as a shell, respectively. The models are compared in terms of global horizontal displacement. The truss model consists of horizontal and vertical rigid bars and a diagonal spring. The spring stiffness is calculated to represent the stiffness of the CLT panel. Both shear deformations and bending deformations of the panel can be included. For wider panels bending and local effects are less decisive, and the shell model and the truss model have more similar results. Applying a vertical restriction at the top of the shell model makes the agreement between the two approaches, the shell model and the truss model, better.

In the second part, multi-storey models are built up by the single panels from part one. Shell models are compared to truss models, both including and not including a reduction for bending. The panels are connected to create different configurations with varying heights and lengths. The global horizontal displacement of the multi-storey models is of main interest. Applying a restriction for vertical displacement to the shell model makes the horizontal displacements between the models better coincide. The more slender the models are the greater is the difference in displacement between the truss and the shell model. This due to the greater influence of bending for more slender models.

The third part is a further investigation of the shell model. A full-scale gable of five storeys is modelled including door and window openings. Different subdivisions of the gable are investigated both including and not including a self-weight. The placement and stiffness of hold-downs as well as the stiffness of line hinges are investigated. The horizontal displacement, internal forces and reaction forces are all affected by the inclusion of the self-weight. A higher hold-down stiffness results in higher reaction forces and a smaller displacement. The line hinges have as well an effect on the displacement of the gable. The subdivisions of the gable are modelling approaches, especially affecting the distribution of internal forces in the gable.

The models are developed through simplifications of the reality and the modelling approaches are based on these properties. The modelling choice has a considerable effect on the result and the coinciding of the models. Limitations are made and the study leaves room for further developments of the subject and its models.

Sammanfattning

Korslimmat trä (KL-trä) är ett klimatpositivt byggnadsmaterial med goda styvhets- och hållfasthetsegenskaper. I kombination med KL-träs låga egentyngd är det ett fördelaktigt material att använda till den lastbärande stommen i höghus. I det här projektet har den horisontella stabiliseringen av KL-träpaneler som utsätts för vindlast analyserats med hjälp av olika modeller. Olika modelleringsmetoder har utvärderats genom att titta på horisontell förskjutning, invändig kraftfördelning och upplagskrafter.

Modelleringen i projektet är uppdelad i tre delar. I den första delen är en KL-träpanel modellerad både som ett fackverk och ett skalelement. Den horisontella förskjutningen jämförs mellan de båda modelleringsmetoderna. En ekvivalent styvhet för det diagonala fjäderelementet i fackverksmodellen beräknas och även en reduktion för att ta hänsyn till böjning är inkluderad. Resultatet för modellerna är mer överensstämmande när böjning är inkluderat i fackverksmodellen. Resultaten sammanfaller även bättre för längre paneler där lokala effekter och effekten av böjning är mindre avgörande. När ett villkor som begränsar vertikal rörelse i skalelementet är inkluderat, är den totala horisontella förskjutningen mer lik den för fackverksmodellen.

I den andra delen av modelleringen undersöks flervåningsmodeller uppbyggda av panelerna från den första delen, både som fackverk och skalelement. Även här undersöks inverkan av att inkludera en reduktion för böjning i fackverksmodellen. Panelerna kopplas samman i olika konfigurationer med varierande våningshöjd och längd. Här är det också den horisontella förskjutningen av modellerna som är av intresse. När en vertikal begränsning av skalmodellen införs sammanfaller resultatet av den horisontella förskjutningen, även inverkan av böjning är avgörande. Generellt är skillnaden i förskjutning mellan fackverksmodellerna och skalmodellerna större för slankare modeller eftersom böjning då har större inverkan.

Den tredje delen är en vidare undersökning av skalmodellen. En gavel med fem våningar modelleras med öppningar för dörrar och fönster, och även en indelning av gaveln i olika panelstorlekar görs. Placeringen av förankringsbeslag och deras reaktionskrafter undersöks samt styvheten/eftergivligheten mellan panelerna. De olika modellerna jämförs genom att både ta hänsyn till och försumma egentyngd. Inkluderad egentyngd påverkar förskjutningen, den invändiga kraftfördelningen och reaktionskrafterna. Ett högre värde på styvheten hos förankringsbeslagen resulterar i en mindre förskjutning samt en högre reaktionskraft. Styvheten mellan panelerna påverkar förskjutningen av gaveln och panelindelningen av modellen är ett modelleringsval som främst påverkar fördelningen av de invändiga krafterna.

Modellerna görs genom förenklingar av verkligheten och modelleringsvalen har stor betydelse för resultatet och hur väl modellerna sammanfaller med varandra. Avgränsningarna i projektet lämnar plats för vidare utveckling av modellerna och det aktuella ämnet.

Acknowledgements

We would like to take this opportunity to thank the people supporting us in this project. Foremost we would like to thank our supervisor Erik Serrano at the Faculty of Engineering, LTH at Lund University, for the dedication and interest in our project and the valuable guidance and input in the process. We would as well like to thank our examiner Henrik Danielsson for taking the role as our second supervisor and for the interest in our project and the valuable inputs.

We would like to send sincere gratitude to our supervisor at the University of Navarra José Manuel Cabrero for giving us the opportunity to write our master thesis at the Department of Building Construction, Services and Structures. He introduced us to the subject of this project and has given us valuable feedback. We would also like to thank Pablo González Serna for the interest he has been taking in our project and the guidance we have received throughout the project.

We would also like to show our appreciation to the people from the department for the entertaining conversations in Spanglish at the eleven-o-clock coffee breaks.

Pamplona, April 2022

Sanna Källman Gleisner & Lina Holmqvist

Contents

1 Introduction

The building industry and the built environment have a beneficial effect on the economy, labour market and quality of life. Aside from the positive qualities, the industry is responsible for about 50 % of the total materials produced in the world and buildings stand for about 40 % of the annual greenhouse gas emission in the EU. The operation of buildings, such as heating, cooling, and powering represent 28 % and the production and manufacturing of products, as well as the construction and renovation of buildings, result in about 8 % (World Green Building Council, 2021). By improving the production of building materials 80 % of the greenhouse gases emitted from the building industry could be prevented (European Commission, 2021).

Life cycle analysis of structures concludes that using timber as the main material in the load-bearing structure reduces the adverse environmental effects. The manufacturing of cross laminated timber (CLT) panels is energy efficient, and the by-products are returned to the process as energy, for example as fuel for the kilns that dry the timber in the first production step. Timber is a natural carbon sink, the carbon dioxide will be sequestrated within the material until the product is no longer used (or reused) and is either burnt or otherwise decomposed, releasing again the carbon dioxide to the atmosphere. Thereafter it is again available to take part in photosynthesis. The eco-cycle of timber through production is a closed loop with the steps of use, re-use, and energy production. Compared to other building materials such as concrete, a load-bearing structure of timber can relatively easy be re-used, as other timber products or as last resort to be used for energy production (Swedish Wood, 2019).

CLT is a product that is environmentally positive, renewable and has a long service life. Combined with these properties CLT has high stiffness and load-bearing capacity. The ability to pre-fabricate CLT panels is favourable both for the manufacturing, for transportation and the assembly on-site. CLT is a relatively new product, and although it is being used in practice there are still research questions of interest (Swedish Wood, 2019).

In this project different modelling approaches for CLT panels are investigated and compared. The lateral stiffness is of interest and the models are subjected to a lateral load. For analysis of CLT buildings, different modelling approaches can be used to include the properties of the material and the connections. The models are usually complex, and the finite element method is therefore used. In this project simplified models of CLT panels are modelled in RFEM, a structural analysis program. RFEM can be used to model complete structures of CLT buildings with walls and floors. The structural model can be exposed to loads and the software will, with a finite element analysis, calculate displacements, internal forces, stresses, etc.

1.1 Aims and objectives

The aim of the work is to continue with and contribute to the ongoing research about CLT as a load-bearing material in the building industry. In particular, the aim is to elucidate complex questions related to horizontal stabilization and the use of different engineering models.

The research questions are:

- What type of modelling approaches is used in previous research for design of CLT buildings experiencing lateral load?

- What is the effect of modelling choice (shell or truss models) for the predicted stiffness (displacement) of CLT panels experiencing lateral loads, in this case, wind loads?

- What is the effect of including self-weight in the models of CLT buildings in terms of displacement, internal force distribution and reaction forces?

- What is the effect of subdivision of panels and their connections for models of CLT buildings in terms of lateral stiffness (displacement), internal force distribution and reaction forces?

The objectives are to:

- Investigate different modelling approaches for CLT shear walls.
- Compare and discuss,
  - results from the use of different modelling approaches.
  - the pros and cons of different modelling approaches.
- Give recommendations for the choice of the modelling approach.
- Suggest improvements for further development.

1.2 Method

Initially, model approaches from literature are studied, using simple FE-models representing single panel walls. Knowledge about the software RFEM is gained as well as insight into the modelling approaches. The lateral stabilization of CLT panels is analysed through several modelling approaches. The main tool for comparing the different modelling approaches is through comparison of the results, in terms of stiffness (displacement), internal force distribution and reaction forces, especially anchorage forces. The modelling approaches applied are divided into three parts where the properties and the result of interest varies.

Part 1 – single panel: A single CLT panel is modelled as a truss and as a shell, respectively. Different supports are investigated, and a stiffness equivalent to a CLT panel is derived for the truss model.

Part 2 – multi-storey: The second part investigates multi-storey models built up by the single panels from Part 1. Truss models are compared to shell models. Models of a larger scale is of interest.

Part 3 – gable: The third part is a further investigation of the shell model. A full-scale gable is modelled including door and window openings as well as different subdivisions of the panels. The effect of varying the stiffness of line hinges and hold-downs, is investigated.

1.3 Limitations

The models of this project are made in 2D with the software RFEM, and the results reflect this choice. The limitation of only making 2D models gives a result easier to evaluate. Another software could have been used to compare different models and this is one of our main limitations. Also, no laboratory tests are made to compare the result of the modelling.

A further main modelling limitation is to not include any vertical forces except for self-weight. How seismic load affects multi-story buildings of CLT is of big interest, but it is not included in this project. A limitation is that only two types of models have been investigated, a truss model and a shell model. No regard for elasticity for the bar members of the truss model is considered. For the shell model, only one type of CLT panel is used with the same thickness and stiffness properties, this is a limitation.

2 Background

2.1 Cross laminated timber

Cross laminated timber (CLT) is an engineered wood product with a great range of use, and it can be adapted in different sizes and shapes. It is a structural material with stabilizing properties even though it has a relatively low self-weight. Because of its beneficial properties, it can favourably be used for multi-storey buildings. The ability to pre-fabricate CLT walls and floors is an advantage both for the manufacturing, transportation, and assembly on-site. An additional advantage of CLT is the economic use of wood material. Lower-grade timber can to some extent be used for CLT panels without compromising the final product. This results in that a bigger part of the stem is used, and less waste material is produced (Swedish Wood, 2019).

The material CLT has its origin in the alpine countries and was introduced in the early ’90s. CLT became common in the Swedish building industry a few years later, after the restrictions on the height of timber houses was dismissed in 1994 (Brandt, 2015). The annual production of CLT panels in the world was about 1.24 million m^3 in the year of 2020 and the industry continues to expand. Still, the alpine countries with Austria in front, are the region producing the greatest amount of CLT (IMARC Group, 2021).

2.1.1 Timber properties

The physical properties of timber are of importance when it is used for structural purposes. Timber behaves differently depending on the surrounding conditions, for example humidity, and different species are used for different purposes. Every tree is unique, and this reflects on the material properties, within the same species there can be a great variation. In general, it is the presence and distribution of knots that leads to the marked fibre deviation in the material (Swedish Wood, 2021).

The main parameter that affects the appearance of timber is the orthotropic property of wood i.e., the properties of the material differentiate along the three perpendicular axes: radial (*R*), longitudinal (*L*) and tangential (*T*). These directions are often assumed to be oriented in a cylindrical coordinate system, *see Figure 2.1*. The orthotropy is of importance since both the strength and the stiffness in the direction of the fibres, parallel to the longitudinal axis, are higher than perpendicular to the fibres. When timber is exposed to a force, the angle between the fibre direction and the force is decisive for the stiffness and the strength of the timber. Thus, for a piece of timber, the local fibre orientation close to a knot will have a great influence on its strength (Swedish Wood, 2019).

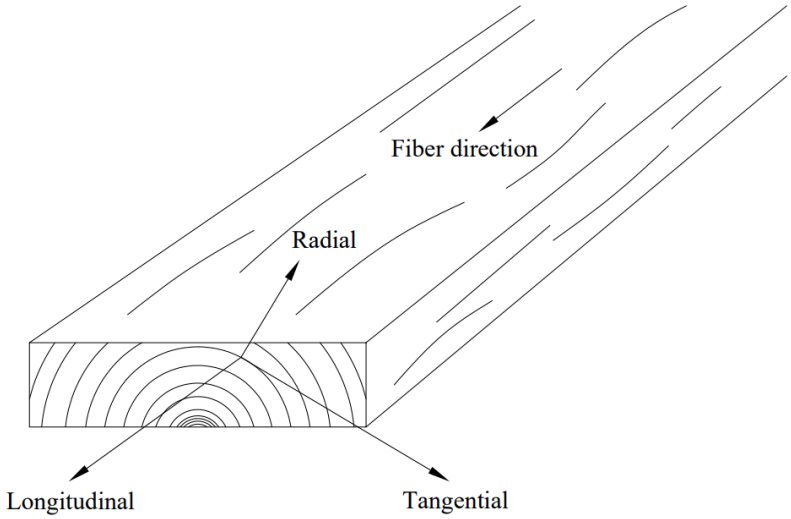

Figure 2.1: Orthogonal directions of timber. The orthogonal directions are often assumed to be oriented in a cylindrical coordinate system.

The mechanical properties of timber are best described relative to the orthogonal axes (*L*, *R*, *T*). The properties in the different directions are described with three different moduli of elasticity, three shear moduli and six values of Poisson's ratio. Only nine of these twelve material parameters are independent. The moduli of elasticity follow the mentioned axes, E_L, E_R and E_T. Since Poisson's ratio is the ratio between the strain in the loading direction and the transverse direction, the combinations of the directions are ν_{LR}, ν_{RL}, ν_{LT}, ν_{TL}, ν_{RT} and ν_{TR}. The resistance against shear stresses is described by three moduli of rigidity, G_{LR}, G_{LT} and G_{RT}.

The moisture content in timber and the temperature of the surrounding environment also affects the stiffness and the strength of the material. The duration of loading influences the strength, which is reduced with time. Timber has a low thermal conductivity and a high thermal capacity, compared to concrete and steel. This is a good quality for building materials since it makes the indoor climate stable, and it is also accurate for CLT. Like timber, CLT has good properties when it comes to fire resistance. The material is flammable, but the load-bearing capacity will decrease at a low and predictable pace since the burning rate of wood is rather slow (around 0.7 mm/min), thanks to the charcoal layer created on the outside acting as a thermally insulating layer (Swedish Wood, 2016).

2.1.2 Manufacturing and structure

The first step of the production of a CLT panel is to join lamellas by finger joints to get the desired length of the product. The finger jointed lamellas can either be bonded only on their wide faces to the adjacent layer of the CLT panels or be bonded first on their edges to form a single-layer panel, which is then bonded to the adjacent layer. The latter mode of production has the advantage of minimizing gaps in the CLT panel since the narrow sides of the lamellas are glued. (Brandner et al., 2016) Every other layer is glued with the lamellas being oriented with a 90-degree angle relative to adjacent layers. A CLT panel is typically constructed with 3–11 layers although more layers can be used in rare cases. There should always be an odd number

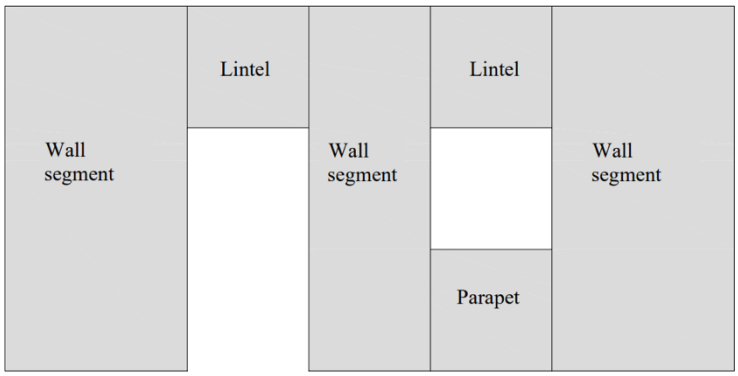

Figure 2.2: CLT wall, with openings, subdivided into wall segments, lintels, and parapets.

of layers (Brandt, 2015). Openings in CLT walls can either be performed through a cut out of the panel or through the use of smaller panel parts. The subdivided panels of a CLT wall are called wall segments, lintels, and parapets, *see Figure 2.2*. A wall segment is a subdivided panel on either side of the opening, a lintel is a part above the opening and a parapet is a part underneath a window opening (Casagrande et al., 2021a).

Spruce or pine are commonly used as raw materials. The thickness of the lamellas, strength class, the cross-section of the panels and the orientation of the layers differ between manufacturers. However, in Sweden, the thickness of a lamella is generally 20–45 mm. The dimensions of CLT panels can be up to 4.80 m in height and 30 m in length. For transportation reasons, panels with much shorter lengths are commonly used (Swedish Wood, 2019). The final step of the production of CLT is the shaping of the panel, such as channelling for installation, openings for windows and predrilling for joints (Swedish Wood, 2019).

The moisture content of timber is an important factor in the construction of CLT panels. When gluing the lamellas, the level of moisture content is important for the strength of the bond. Similar moisture content between the product and the surrounding environment will reduce the risk of splitting. Commonly, the lamellas arrive at the manufacturer already dried, planed and strength graded according to the used standard (Swedish Wood, 2019).

For calculations, CLT panels can be viewed in a coordinate system where the x-axis is parallel to the grain direction of the outermost lamella layer. The y-axis is parallel to the grain direction of the second outermost layer and the z-axis is perpendicular to both the y- and x-axis and parallel to the thickness of the CLT panel, *see Figure 2.3*. Due to the orthotropic structure of CLT, different construction setups utilize different properties of the panel. The structural design depends on different aspects, for example, the function of the building, economic reasons, and the architecture of the building (Swedish Wood, 2019).

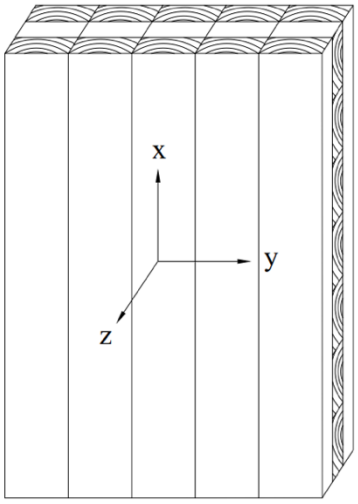

Figure 2.3: CLT panel with its local axes.

2.1.3 Design

Since CLT panels consist of several layers, and each layer consists of several lamellas the variation within each timber lamella evens out, and some effects of variability found in regular timber constructions are less apparent. The design of a CLT cross-section involves determining the strength and stiffness properties. In timber design, the stiffness is often decisive, and this is also the case for CLT. For CLT the tensile strength of the outer layers and the rolling shear strength of the transverse layers are commonly decisive for its strength (Swedish Wood, 2019).

In the design process of CLT panels, several parameters need to be considered. One aspect is the load direction, acting either in the direction perpendicular (out-of-plane loading) or parallel (in-plane loading) to the surface. Non-favourable actions are configurations that result in tension forces perpendicular to the surface and the phenomena of torsion and eccentricity (e.g., a vertically loaded wall where the load is not applied in the midplane of the wall). For panels with large openings, the remaining parts of the panel need to be checked for buckling. For CLT walls, this is typically done by assuming a buckling length equal to the storey height. The possibility to stiffen and strengthen floor panels with either glulam beams or other materials is common either for large spans, large loads, or when cut-outs of the panel are made (Swedish Wood, 2019).

The stiffness and strength of a CLT wall panel exposed to in-plane horizontal loading are related to four different types of deformations; bending, shear, translation (sliding), and rotation (rocking). The contribution from shear and bending deformations are often smaller than from translation and rocking. All deformations relate to in-plane behaviour, shear and bending deformations occur within the panel and translation and rocking are related to the connections of the panel (Lukacs et al., 2019). For CLT panels with out-of-plane loading, bending shear deformations or shear deformations are generally considered. For this, a method called the Gamma method is often used. Another alternative for this is to use a higher-order beam or plate theory, Timoshenko respectively Mindlin-Reissner theory (Swedish Wood, 2019).

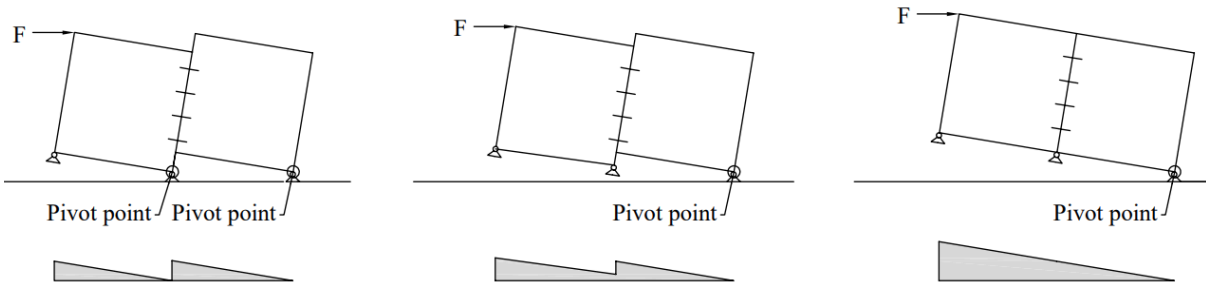

Figure 2.4: Coupled wall behaviour (left), single-coupled wall behaviour (middle) and single-wall behaviour (right). The distribution below the wall segments shows the uplift from the ground.

When modelling adjacent CLT walls three types of behaviours can be distinguished, depending on their interaction. The panels can act like a coupled wall, a single-coupled wall or a single wall, *Figure 2.4* shows the different behaviours. A single wall behaviour is when the panels act as one unit, and the panels are connected with rigid connections. The coupled wall behaviour is when each wall has one pivot point and vertical sliding occurs between the panels. This is the behaviour expected from walls with connections of small (or zero) stiffness as regards vertical sliding. A single-coupled wall is similar to a coupled wall except that a smaller vertical sliding occurs, and the panels have a common pivot point (Sandoli et al., 2016).

2.1.4 Connections

Connections are decisive for the load-bearing capacity and the stability of the entire structure. The fire resistance and acoustics of a building are additional properties affected by connections. A connection can be designed in many ways, and a more ductile failure is favourable. A ductile failure is commonly defined as a failure involving residual capacity after initiation and involving large deformation before the final collapse. The design of joinery depends on which type of panels and connections used. Some examples of fasteners are wood screws, metal plates and brackets, anchor nails, anchor screws and self-drilling screws. Connections are the weak point of a structure, and the joints should be able to transfer the forces between the structural elements. Depending on the structural system a connection can be modelled as rigid (moment resisting), pinned (allowing relative rotation) or something in-between rigid and pinned (including a resilience) (Swedish Wood, 2019).

In a master thesis by Olausson (2021) the shear stiffness of different types of connections between diaphragms is investigated. The connections are modelled with a spring stiffness with a value per meter from 1 kN/mm to 11 kN/mm per meter (meter along the edge of the panels). The analyzed connections are two types of butt joints with inclined screws, a lap joint, and a spline connection. In the present project when performing analyses, these values are used for reasonable estimates of the stiffness.

2.2 Finite element method

Problems based on differential equations can be too complex to solve with analytical methods, then the finite element method (FEM) is a good approach. The method is based on a subdivision of the region of interest into smaller elements and for each such element, a simplified approximation (e.g., a linear variation) is introduced. Problems analysed with the finite element method reach over a one-, two- or three-dimensional region. An assumption that a certain problem is linear over a smaller part of the complete region is reasonable if the variation within the element is small. By introducing more (smaller) elements in the region where the solution is expected to show high gradients, increased accuracy can be obtained (Zhu, 2018).

2.2.1 Element types

In modelling, different types of elements are commonly used to describe structures. A bar element only has axial forces and displacements; it has one degree of freedom in each end of the element. It is defined through its length and cross-section area. A spring element is similar to the bar element, but it is defined with a spring stiffness. The basic beam element is also a one-dimensional element, but with two degrees of freedom in each node: vertical displacement and rotation, due to shear force respectively bending moment. There is also a combination of a bar and beam element, that can take shear force, bending moment and axial forces (Ottosen Saabye & Petersson, 1992).

A membrane is a two-dimensional element that can be used for in-plane loading, either plane strain or plane stress. A plate is also a two-dimensional structure but with forces acting perpendicular to the plane of the plate. There are two common methods when analysing a plate structure, models based on the Kirchhoff thin plate theory respectively the Mindlin-Reissner plate theory. The first, also often called the Classical plate theory, is today not commonly used for CLT structures, since it neglects the shear strain of the axis parallel to the thickness of the plate. Mindlin-Reissner plate theory takes both shear deformation and rotary inertia into consideration and is therefore applicable for thick plates. A shell element is a combination of a membrane and a plate element (Liu & Quek, 2003).

2.2.2 RFEM design

RFEM is a structural analysis program that can be used to model complete structures with walls and floors. The structural elements can for instance be modelled as shells and membranes. The structural model can be exposed to loads and load cases and the software will, with a finite element analysis, calculate displacements, internal forces, stresses, etc. An additional property of RFEM is the ability to use different add-on modules, for example, to model laminate structures. This makes it possible to model the anisotropic material CLT as a shell, avoiding the use of a full three-dimensional description of the CLT (Dlubal, 2021a).

$$\mathbf{D} = \begin{bmatrix} D_{11} & D_{12} & D_{13} & 0 & 0 & D_{16} & D_{17} & D_{18} \\ & D_{22} & D_{23} & 0 & 0 & \text{sym} & D_{27} & D_{28} \\ & & D_{33} & 0 & 0 & \text{sym} & \text{sym} & D_{38} \\ & & & D_{44} & D_{45} & 0 & 0 & 0 \\ & & & & D_{55} & 0 & 0 & 0 \\ & & \text{sym} & & & D_{66} & D_{67} & D_{68} \\ & & & & & & D_{77} & D_{78} \\ & & & & & & & D_{88} \end{bmatrix} \quad (2.1)$$

2.2.2.1 CLT - Shell model

The stiffness of a CLT panel is described with a stiffness matrix **D** that incorporates the properties of the orthotropic material, *see Equation 2.1*. The values D_{11}–D_{33} relate to the torsional and bending properties, D_{16}–D_{38} relate to the eccentricity effects, D_{44}, D_{45} and D_{55} relate to the out-of-plane shear stiffness properties and the values D_{66}–D_{88} relate to the in-plane stiffness properties (axial stiffnesses and the in-plane shear stiffness). (Swedish wood, 2019) Stiffness reduction factors, k_{33} (≤ 1.0) and k_{88} (≤ 1.0), can be used to reduce the values in the matrix, affecting the torsional and shear stiffness of the panel, respectively. The factors are used to account for the effect of insufficient or non-existing edge gluing (e.g., for CLT with no bonding on the narrow sides of the lamellas). Theoretically, such edge bonding will increase the stiffness, but this might lead to an overestimated stiffness and the reduction factors k_{33} and k_{88} are commonly used (Dlubal, 2021b).

2.2.2.2 Connections

Nodal supports connect a structural element to its foundation and transfer the forces acting on the panel. For the node to function as a support, displacements in one or more degrees of freedom for the node needs to be prevented. Displacement and rotation in the direction of the current coordinate system can be set as completely free to displace (no force transfer) or more or less restricted (a stiffness is introduced at the support node for one or several degrees of freedom) depending on the type of support (Dlubal, 2021c). In RFEM, supports can also be modelled as line supports, and it considers all the FE nodes along the line of the structural element. As for nodal supports, the support conditions can either be free or more or less restricted (Dlubal, 2021d).

In RFEM, surfaces sharing a line are by default rigidly connected. *Line hinges* are releases that can be applied on such lines between surfaces, but also to any line defined within a surface. Both rotational and translational releases can be applied, in all three axes of the coordinate system (Dlubal, 2021e). *Member hinges* in beam and bar elements are an additional function to affect the transfer of internal forces. The hinges can only be placed at the end of members. Axial and shear forces as well as torsion and bending moment are factors that can be controlled by member hinges (Dlubal, 2021f).

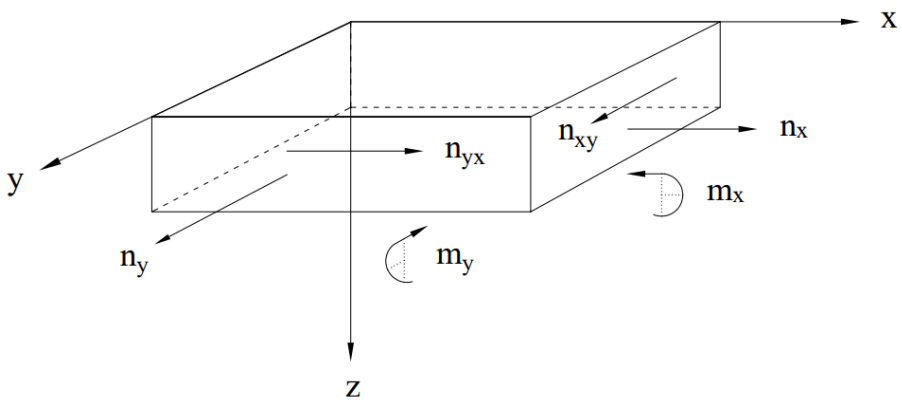

Figure 2.5: Plate with its local coordinate system, internal forces, and moments.

2.2.2.3 Internal forces

Basic internal forces (per length meter) are related to the local coordinate system (*x, y, z*) of the shell model. The surface is in the *xy*-plane and the *z*-axis is perpendicular to the plane. The bending moment that generates bending stresses in the *x*-direction is called m_x and in the *y*-direction called m_y, (thus a moment about the local *y*-axis respectively *x*-axis), *see Figure 2.5*. In the present work, the forces of concern are the axial forces. The axial forces in the direction of the local *x*-axis are n_x and the axial forces in the direction of the local *y*-axis are n_y. The shear flow is n_{xy} and n_{yx}. (Dlubal, 2022).

The principal internal forces are related to the principal axes (1, 2, 3) of the shell model. They have the value and direction of the extreme values of the internal forces. The maximum values of the internal forces are in the 1-axis direction and the minimum values are in the 2-axis direction. The angle alpha is the angle between the surface axis and the principal axis. Axial force in the direction of the principal 1-axis is n_1 and axial force in the direction of the principal 2-axis is n_2. Thus, presenting internal forces in terms of principal forces will depict the internal force transfer in pure tension and pure compression (Dlubal, 2022).

2.3 Scientific base

A summary of relevant research within the area of the project. Research investigating the stiffness and stabilization of CLT panels related to what type of connections are used and if openings are present or not.

2.3.1 Equivalent truss method

A method to analyse floor diaphragms with irregularities based on truss systems is proposed by Moroder et al. (2015). The approach contributes to research on high rise timber buildings subjected to seismic loading. Properties analysed with this approach are shear force in panels, deflection of diaphragms, torsional effects, reaction forces and forces in connections.

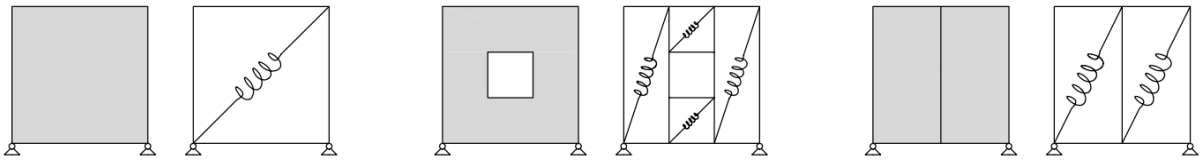

Figure 2.6: Shell models and their equivalent diagonal spring model. Shell model without irregularities (left) and shell models with irregularities (middle and right).

For timber diaphragms, a basic rectangular unit is constructed from bar or beam elements and a diagonal. The diagonal of the unit represents the behaviour of the floor diaphragm and its fasteners, and its stiffness is calculated based on the stiffness of both the diaphragm and the connections. The ideal angle of the diagonal is 45 degrees, to get a well-functioning truss structure. The method proposes that the diaphragms are connected through linear elastic connections.

In an analysis of a diaphragm with irregularities, such as openings, the structure is subdivided into separate panels with their own diagonal, *see Figure 2.6*. These diagonals are re-calculated from the one diagonal representing the whole diaphragm. The load is applied as a lateral load at the top corner of the diaphragm. Results from FEM analyses show that shear force distributions can be accurately represented. The diaphragm flexibility and the reaction forces are accurate as well when compared to models based on the use of shell elements. For as long as the equivalent stiffness is representable, the equivalent truss method presents reliable results (Moroder et al., 2015).

2.3.2 Stiffness of CLT panels with openings

The in-plane stiffness of CLT walls with openings is studied by Shahnewaz et al. (2016). They studied opening size, shape, and location, and how these parameters affect the stiffness of a CLT wall.

Modelling the CLT panel, the lamellas were set to behave as orthotropic elastic materials. The elastic stiffness of the lamellas is predicted with tests to be more accurate. The glue-line between the lamellas is assumed to be a non-linear contact element, with high stiffness. Linear spring elements are modelled for the connection between the floor and the walls. A parametric study is made to investigate the effect of openings and their placing. The input values for the study are the wall thickness, the aspect ratios of the wall and the size and shape of the openings and their ratio.

The stiffness of a wall, where half of the wall area is removed, is reduced by more than 70 %. FE-models additionally show that an opening placed with an offset to the centre of the wall results in a reduction of the stiffnesses. From the result, an analytical model is presented that describes the reduction of the in-plane stiffness, and a comparison between walls with and without openings is made. The presented equations are an improvement of former research (Shahnewaz et al., 2016).

2.3.3 Influence of openings on shear capacity

Dujic et al. (2007) investigate the shear capacity of timber walls with openings. In the design of buildings experiencing wind loads and earthquakes, only the shear capacities of the wall segments are considered i.e., the contribution from parapets and lintels is neglected (*see Figure 2.2* for a description of a lintel and a parapet). This might lead to an underestimation of the shear resistance in CLT buildings. The parapets and lintels contribute to the shear resistance, and they will transfer loads. If the contribution is considered, a more exact design can be made.

A general model is developed for different sizes of openings in walls. Laboratory tests are made to collect data about the wooden panels and the information is used as parameters for a computer-based model. In the tests, the response from the wall and the effect of the holes are studied in the matter of the non-linear behaviour of the supports and the elastic behaviour around the openings.

The mathematical model from the experiments is used to develop different patterns of openings. The result from parametric studies is summarized in a diagram presenting a ratio between area and racking load, and a comparison between the stiffness of walls with and without openings. The diagrams can be used by engineers in the design of CLT walls with openings. The conclusion is that an opening that is less than 30 % of the wall area has a low effect on the load-bearing capacity, but the stiffness is reduced by half (Dujic et al., 2007).

2.3.4 Model for coupled CLT walls

Sandoli et al. (2016) have created an equivalent frame model for coupled CLT walls, that is simplified but still detailed. A CLT panel subjected to horizontal loading will experience most of the displacements in the region of the connections, both anchor and vertical joints. The connections take a large part in the behaviour of coupled and uncoupled walls when experiencing horizontal loads. To prevent horizontal sliding of CLT panels angle brackets are used. The rocking effect of the panels is restricted by hold-downs. The vertical shear force between the panels is taken up by the vertical connection. For coupled walls, a vertical force between the walls is considered in addition to the anchoring force.

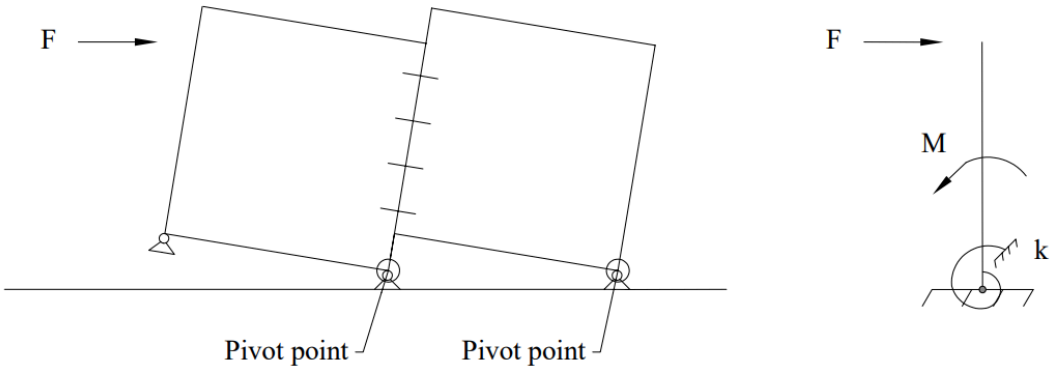

Figure 2.7: Simplified frame model: Coupled wall represented by a cantilevered beam.

Two different methods are used to analyse the effect of single and coupled CLT walls under horizontal loading, a simplified frame model and a detailed model. The simplified model consists of a cantilever beam representing two coupled walls, *see Figure 2.7*. This cantilever beam has both flexural and shear stiffness. An assumption is that the rocking of the wall is due to the rotation of each part around one point at the edge of the respective part. A rotational spring is placed at the support to consider the elastic stiffness of the connection and the coupling effect. The proposed detailed method, on the other hand, calculates the position of the pivot point (the neutral axis) of each panel.

When examining the horizontal displacement, it is noticed that the most contributing factors are the sliding and rocking components. The influences of shear and bending are almost insignificant. The conclusion is that the simplified method is relevant when looking at coupled CLT walls that are placed on a rigid foundation only. The detailed model is more accurate since it takes the base compression stiffness into account and can therefore be used for soft foundations and rigid foundations (Sandoli et al., 2016).

2.3.5 The effect of opening configuration and placing of hold-downs

Mestar et al. (2020) studied the kinematic behaviour of CLT walls with openings through numerical analyses and experimental testing. Different hold-down configurations are investigated as well as the degree of coupling of shear walls. Up to 63 different wall configurations are composed where the thickness of the panel, opening size and hold-down placement are the varying parameters.

The CLT panels analysed have either a centrically placed window or door opening. The hold-down configurations analysed are double hold-downs (hold-downs at the ends of the panel and at each end of the openings) and single hold-downs (hold-downs on the ends of the panel and not at the openings. The tensile stiffnesses of the hold-downs (including stiffnesses of angle brackets) used are 8, 14 and 20 kN/mm per hold-down and a value of 10^6 kN/mm is set for the compressive stiffness. Openings are made through cut-outs of the CLT panels i.e., there are no joints between the lintel beam and the rest of the panel. The inclusion of a self-weight is represented by a line load of 20 kN/m.

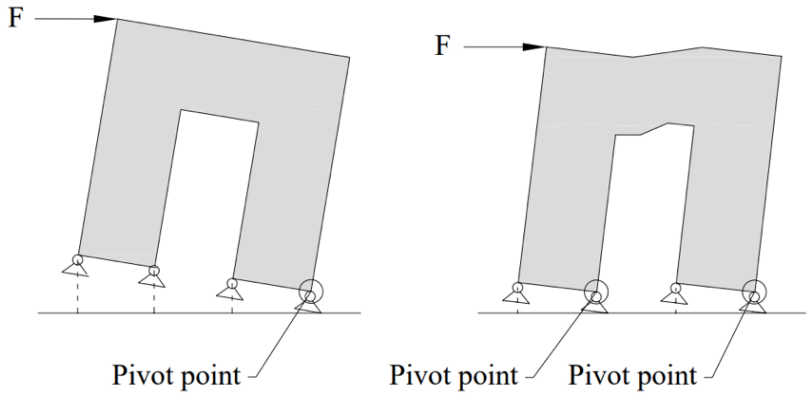

Figure 2.8: Two shell models (with door openings) subjected to a lateral load with different centres of rotation.

The horizontal load applied on the wall is 400 kN and no vertical load is applied. The displacement of the wall is described through four factors, bending, shear, translation, and rotation. Both rotational and vertical displacement of the wall are free, but the translation is restricted by adding steel rod blocking. The rocking behaviour of the CLT wall is described in terms of two kinematic behaviours: mode 1, where the wall has one centre of rotation and mode 2, where the segments of the wall (the parts on either side of the opening) have one centre of rotation each, *see Figure 2.8.* The kinematic behaviour depends mainly on the connections. For low values of hold-down stiffness, 8 kN/mm, the use of single- or double hold-downs does not affect the global kinematic behaviour. Greater values used, 14 kN/mm and 20 kN/mm, result in minor effects on the global kinematic behaviour.

The thickness of the CLT panel has a moderate effect on the kinematic behaviour, a wall with 150 mm thickness experiences more mode 1-alike behaviour than a wall of 100 mm. The horizontal load acting on the thicker wall, on either the model with single- or double hold-downs, results more frequently in a single centre of rotation, mode 1. The parapet (*see Figure 2.2* for a description of a parapet) has a great contribution to the stiffness of the entire wall and the only mode observed on walls with windows was the one with one centre of rotation. The slenderness of the wall segments appears to have a small effect on the kinematic behaviour (Mestar et al., 2020).

2.3.6 In-plane strength and stiffness of CLT shear walls

Shahnewaz et al. (2018) studied a platform-type building where the floor acts as a platform for the floor above, constructed with CLT panels. The coupled and single CLT panels are connected to the foundation with angle brackets and hold-downs. The CLT walls are connected either by lap joints or spline joints. The study aims to investigate the strength, stiffness, ductility, and energy dissipation of CLT walls, both single and coupled. The type of connections is the varying parameter.

With FE analysis and previous research, values for the elastic stiffness of connections are established. The shear connection between the wall is made with either a half-lap joint with a stiffness of the screw of 0.4 kN/mm or a spline joint with a screw stiffness of 0.2 kN/mm per screw. For half-lap joints and spline joints, the number of screws used is 20, respectively. Two types of hold-downs are used with the respective stiffness of 2.5 kN/mm and 4.9 kN/mm. The number of angle brackets and hold-downs used are varied. Coupled walls with four hold-downs showed larger resistance against seismic loading than the coupled walls with two hold-downs. The parameters analysed were peak load, ultimate load, displacement, and energy dissipation. Walls with the vertical half-lap joint connection showed a better result than the spline joint connection when looking at the peak and ultimate load (Shahnewaz et al., 2018).

2.3.7 Strength and stiffness of CLT panels - Analytical approaches

In the state-of-the-art publication by Lukacs et al. (2019) methods for strength and stiffness assessments of CLT panels are presented. The methods are all based on the same standardized

CLT panel subjected to one horizontal point load and a uniformly distributed load. The ground connection consists of three angle brackets and two hold-downs, one on either side of the panel. The methods used for strength and stiffness assessment are based on equilibrium equations, containing information about the geometry of the wall, loading, and connections.

For strength assessment i.e., load carrying capacity, the wall is considered a rigid element and the displacement will exclusively occur at the connections. The methods presented do all neglect overturning of the wall, by applying hold-downs, and the horizontal translation is restricted by angle brackets. The differences between the 10 methods are based on the different positions for the point of rotation (known or unknown), the usage of one or several lever arms for the hold-downs and angle brackets or the presence of a compression zone or not.

Five methods for stiffness assessment are presented. The differences between the methods are the inclusion of different deformation contributions (bending, shear, translation, or rotation) and the usage of effective values for the shear displacement. All methods can to some extent predict the elastic behaviour of a CLT wall, some with an over- respectively underestimation. The results should only be seen as a guideline, rather than be directly applied. The methods are all based on simple estimations and are only applicable to a panel with a single type of connection (Lukacs et al., 2019).

2.3.8 Distribution of internal forces

A numerical-analytical parametric study is performed by Casagrande et al. (2021b) and the distribution of internal forces in CLT panels is studied. The panels are subjected to a lateral load and anchored to the foundation with one hold-down on each side of the panel, and additional intermediate angle brackets. Finite element parametric analyses of the CLT panels are compared to analytical models. The axial forces and shear forces are examined, and the location and distribution of the maximum values are of interest. The study is done by considering several panels with different compositions, such as the size of door and window openings, thickness of the panel and the stiffness of the mechanical anchors, in a total of 162 different configurations. When analysing the results, the panel is divided into three parts, wall segments, lintels, and parapets (*see Figure 2.2* for a description of the parts).

Two anchorage systems are used, one flexible and one rigid. The values used for the flexible system, the tensile stiffness of the hold-downs, are 6609 kN/m and 13247 kN/m. The shear horizontal stiffness and tensile vertical stiffness of the angle brackets are 2090 kN/m and 2530 kN/m, respectively (Gavric et al., 2015a). To model the rigid contact between the shear wall and the foundation, a single value of 10^6 kN/m was used for the compressive stiffness of the hold-down, the angle brackets, and the gap elements. Pinned restraints are used to model the rigid anchor system for which horizontal and vertical displacement are completely prevented.

The results show that the location of the axial forces for panels with rigid anchors differs from the location in panels with flexible anchors. With rigid connections, the maximal internal forces

are located at the base section of the wall segment and with flexible connections, they are located at the end sections of the lintels. This is found for all the wall configurations, independent of the other parameters studied. This shows the importance of adopting a relevant CLT connection when modelling and calculating with finite element analysis.

The location of the maximal axial force in panels with openings is also dependent on the slenderness of the panel. For slender lintels with flexible or non-flexible connections, the maximal axial force occurs at the section of the parapet respectively at the base of the wall segment. For wider lintels, the location is at the bottom corner of the whole panel and there is no difference in the anchor used. The location of the maximal shear force is for all configurations at the corners of the openings (Casagrande et al., 2021b).

3 Method

The lateral stabilization of CLT panels is analysed by using several modelling approaches. The evaluation of the result is done through properties such as horizontal displacement, *see Figure 3.1*, vertical reaction forces and vertical internal forces. The modelling approaches that are used are described in three parts, where the properties and the result of interest vary and where each part refers to different stages of the work conducted, each part involving more detailed and complex models.

The first part consists of single CLT panels (i.e., one storey) modelled as a truss model and as a shell model, respectively. Different supports are investigated, and a stiffness equivalent to the CLT panel is derived for the truss model. The second part investigates multi-storey models built up by the single panels from part one, truss models are compared to shell models. Here the effect on the displacement of models of a larger scale is of interest. The third part is a further investigation of the shell model applied to a larger structure, a five-storey gable. Door and window openings are included as well as different subdivisions of the panels for a more realistic gable. The effect of modelling choice for connections between panels and to the ground is investigated.

3.1 RF-laminate

For the orthotropic shell model, the add-on module RF-laminate in RFEM is used to define material properties, layer thickness and orientation, thus establishing the stiffness properties of a CLT panel. The wall panels are built up by three layers. The strong direction of the panel i.e., the direction of the fibres of the outermost layers (the local *x*-axis), will be placed in the global vertical direction (global *z*-axis) of the coordinate system in RFEM.

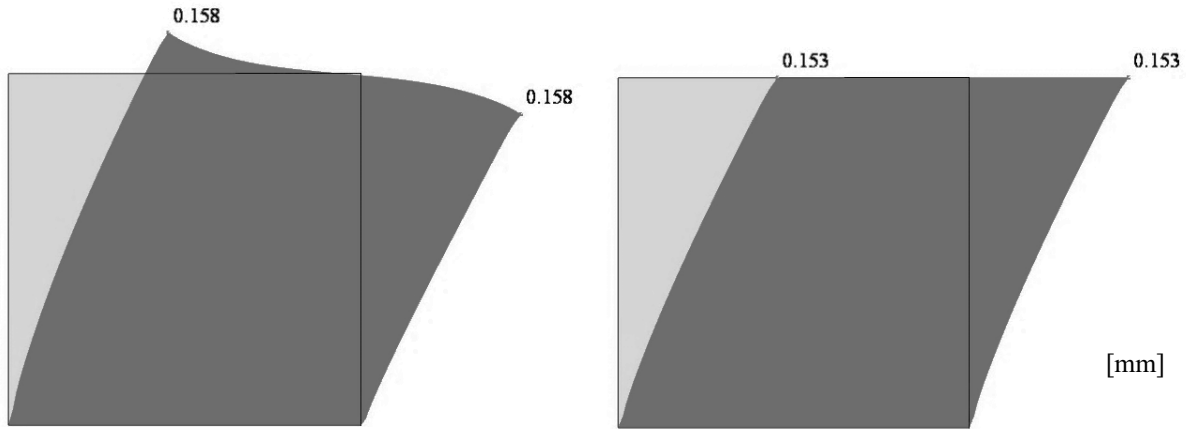

Figure 3.1: Global displacement (left) and horizontal global displacement (right) of the shell panel subjected to a line load.

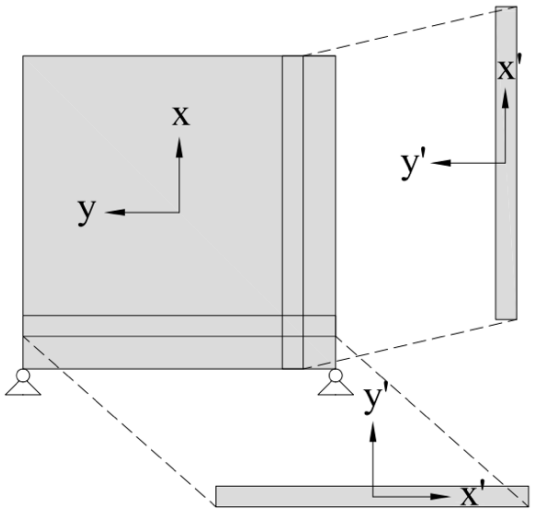

Figure 3.2: The laminate and the layers with its global and local axes.

The global coordinate system is orientated with the positive global *z*-axis downwards and the global *x*-axis placed horizontally, following the length of the models, see *Figure 3.2*. The modulus of elasticity E_x and shear modulus of the laminate G_{xz}, G_{xy} and G_{yz} are related to the coordinate system. The strength class used for the lamellas is C24, additional properties used in RF-laminate are presented in *Table 3.1*.

The extended stiffness matrix **D**, for the CLT shell model in RFEM, is presented in *Equation 3.1*. The stiffness is reduced according to the Austrian annexe of Eurocode 5 (ÖNORM B EN 1995-1-1, 2010). The torsional bending stiffness D_{33} is reduced by the factor k_{33}. The effect of the glue on the narrow side of the lamellas is neglected and the in-plane shear stiffness D_{88} is reduced by the factor k_{88}. This reduction affects the horizontal displacement of the wall. The reduction factors are found in *Table 3.1*.

$$\mathbf{D} = \begin{bmatrix} 634.5 & 0 & 0 & 0 & 0 & 0 & 0 & 0 \\ & 24.8 & 0 & 0 & 0 & 0 & 0 & 0 \\ & & 12.6 & 0 & 0 & 0 & 0 & 0 \\ & & & 8956.2 & 0 & 0 & 0 & 0 \\ & & & & 17250 & 0 & 0 & 0 \\ & & \text{sym} & & & 660000 & 0 & 0 \\ & & & & & & 330000 & 0 \\ & & & & & & & 31050 \end{bmatrix} \begin{matrix} \text{kNm} \\ \text{kNm} \\ \text{kNm} \\ \text{kN/m} \\ \text{kN/m} \\ \text{kN/m} \\ \text{kN/m} \\ \text{kN/m} \end{matrix} \quad (3.1)$$

Table 3.1: Properties of the RF-laminate.

Properties	Parameter	Value	Unit
Thickness lamella	t	30	mm
Thickness panel	d	90	mm
Effective thickness panel	d_{ef}	60	mm
Modulus of elasticity	E_x	11 000	MPa
Shear modulus (mean values)	G_{xz}	690	MPa
	G_{xy}	690	MPa
	G_{yz}	69	MPa
Stiffness reduction factor	k_{88}	0.5	-
Stiffness reduction factor	k_{33}	0.4	-

3.2 Models part 1 – single panel

Two different modelling approaches are used to model a single CLT panel experiencing lateral load. A comparison is made to examine the convergence of the two models. The first model is a shell structure, and the other is a truss structure. The shell model consists of quadrilateral 2D elements. The equivalent truss model is made of rigid bar members forming a frame, with a diagonal spring element representing the equivalent stiffness of the CLT panel. The horizontal displacement of the models is of interest, and the aim is to get the behaviour of the two models, as similar as possible. The properties of the truss elements and 2D elements in the finite element mesh are related, although the models cannot be expected to respond completely equal.

3.2.1 Dimensions

The length l and height h of the modelled CLT panels are inspired by earlier research. Sandoli et al. (2016) used the aspect ratio of h/l=1 and h/l=0.5 for the dimensions of the CLT panels in their modelling approach. Moroder et al. (2015) point out the importance of the angle of the equivalent diagonal of the frame, for it to be a well functional truss structure. The ideal angle is 45 degrees, i.e., thus ideally one should have a panel height and length of the same value.

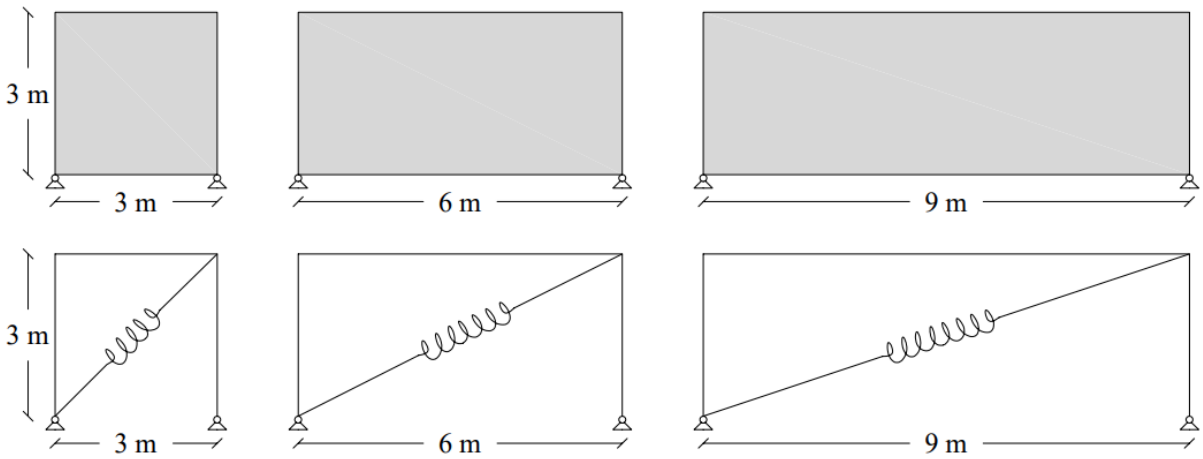

Figure 3.3: Shell models (upper) and truss models (lower) with lengths of 3, 6 and 9 m.

The height of the models is 3 m since it is a common height of a level in a building and a commonly used dimension of CLT panels. The lengths of the panels that are used are 3, 6, 9, 12, and 15 m and *Figure 3.3* presents the models of the three first mentioned lengths. The impact of the angle of the diagonal spring element, as well as the required stiffness, is examined by using different lengths of the panels.

3.2.2 Load

The wind load is represented by a horizontal load acting as a point load on the upper left node of the truss model and as a line load on the upper line of the shell model. The point load is set to 3 kN and the line load is chosen so that it corresponds to a point load of 3 kN, thus the magnitude of the line load expressed in kN/m is dependent on the length of the panel. Using a line load and not a point load for the shell model prevents local displacements that otherwise would occur at the point of loading. The line load acts as a uniform load over the whole top of the model and the displacement of the upper right and left corner of the shell model are therefore more equal. The self-weight of the CLT panel itself is neglected when modelling as well as any additional load, for example, live load.

3.2.3 Shell model

A CLT panel is created with properties given in the add-on module RF-laminate for the shell model. The ground support is modelled as a line support preventing displacement but allowing rotation in all directions. The top support of the shell model is modelled in two different ways. The first model has two point supports at the top part of the panel, to prevent out-of-plane movement, in the *y*-direction. The second model uses a line support along the top line of the panel to better mimic the behaviour of the truss model, *see Figure 3.4*. For the truss model, with rigid elements that do not elongate, the vertical bars only rotate around their respective support. This means that the horizontal top bar must remain horizontal during loading. To mimic the behaviour the vertical displacement of the nodes in the shell model, along with the top-line support, is therefore prevented.

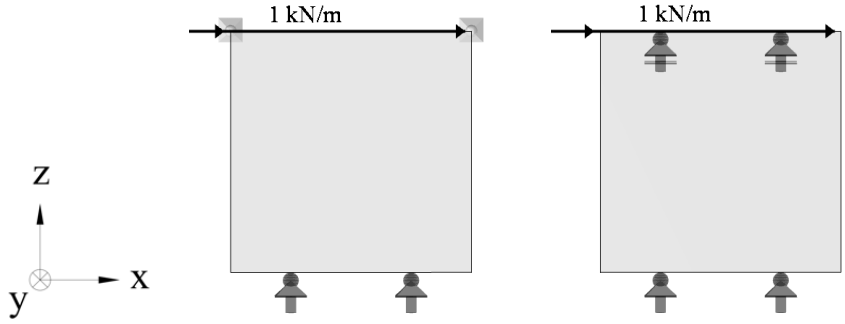

Figure 3.4: Shell model subjected to a line load with two types of upper supports: nodal supports (left) and line support preventing vertical displacement (right).

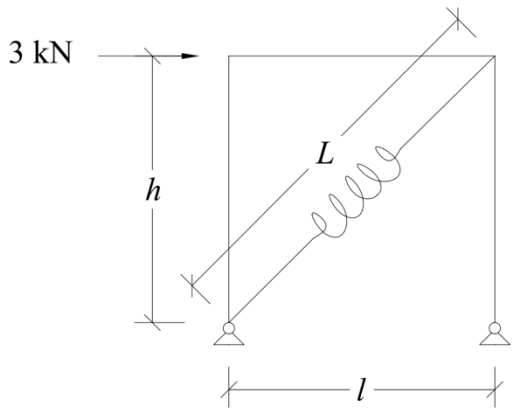

Figure 3.5: Truss model with an applied wind load of 3 kN.

3.2.4 Truss model

The truss model is intentionally simplified, to reduce the variable parameters and to make the calculations simpler. In the software RFEM, the diagonal spring element both takes tension and compression forces in the direction of its axis into account. Two truss models are used; Truss model A which does not include a reduction for bending of the CLT panel and Truss model B which includes a reduction to account for the bending stiffness. Top supports are applied to prevent the panel from out-of-plane movement, in the global *y*-direction. Ground supports are applied to prevent displacements along all axes and allow rotation around the *x*- and *y*-axes. The rigid bars share the same node in the corner connection and rotation in *y*- and *z*-direction is allowed by adding a member hinge. The wind load is applied at the upper left node of the model. *Figure 3.5* shows the geometry of the truss model with the acting load.

3.2.4.1 Spring stiffness- Truss model A

The equivalent stiffness of a CLT panel is represented by a diagonal spring element and the stiffness is calculated according to the method presented by Moroder et al. (2015), the equivalent shear-through-thickness rigidity of the panel is shown in *Equation 3.2*.

The value *G* is the shear modulus of the panel and *d* is the panel thickness, values found in *Table 3.1*. The slip modulus of the fastener parallel to the panel edge is represented by K_{ser}, the parameter is assumed to be infinitely large since no fasteners are included in the models of the single panels. The values c_1, c_2 and *s* are related to the fastener's spacing which is neglected. A reduction factor for shear stiffness k_{88} is applied, the factor is related to the edge gluing of the lamellas, s*ee Table 3.1* for a value. The other reduction factor related to edge gluing that effects torsion k_{33} is not relevant for this model since the models are restricted for out of plane movement.

$$(Gd)_{\text{ef}} = \frac{1}{\frac{1}{G \cdot d} + \frac{s}{K_{\text{ser}}}\left(\frac{c_1}{b} + \frac{c_2}{h}\right)} \longrightarrow (Gd)_{\text{ef}} = \mathrm{G} \cdot d \cdot k_{88} \tag{3.2}$$

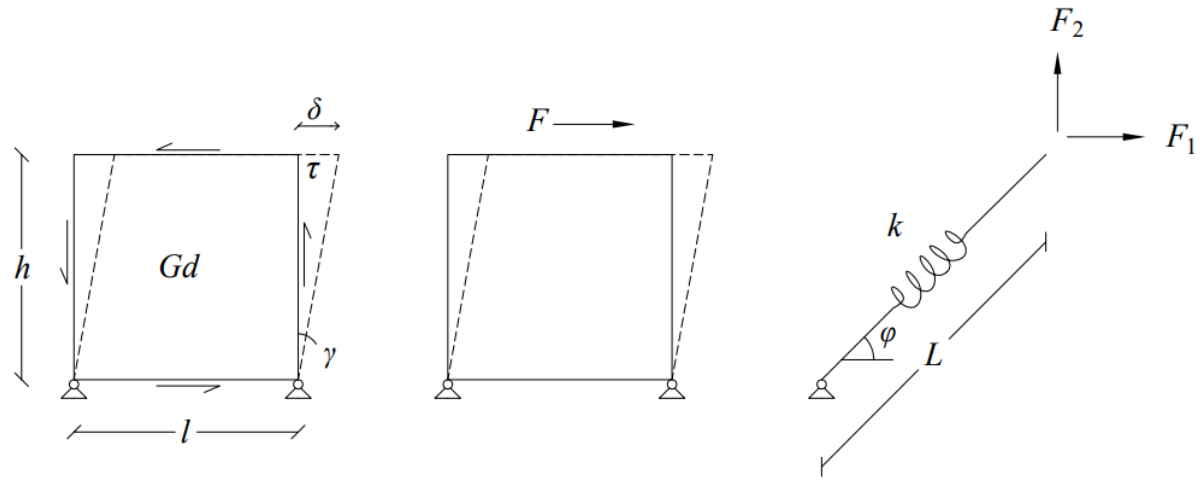

Figure 3.6: The derivation of the equivalent spring stiffness from an elastic plate element.

The cross-sectional area A of the diagonal in *Equation 3.3* is set to the same numerical value as the diagonal length L. The parameter h is the height of the panel and l is the length, *see chapter 3.2.1 Dimensions*.

$$A = L = \sqrt{h^2 + l^2} \tag{3.3}$$

The equivalent modulus of elasticity of the spring is calculated according to *Equation 3.4*. This is the equivalent value for the spring stiffness of the diagonal that considers the shear stiffness of a CLT panel.

$$E_{\text{ef}} = \frac{G \cdot d \cdot k_{88} \cdot L^2}{h \cdot l} \tag{3.4}$$

The equivalent spring stiffness E_{ef} can as well be derived from a shell element loaded in shear, *see Figure 3.6* and *Equations 3.5–3.9*. For an elastic element with a shear stiffness G and thickness d, the shear stress τ can be calculated, where $\gamma = \frac{\delta}{h}$ and δ is the horizontal displacement.

$$\tau = G \cdot \gamma \tag{3.5}$$

The shear stress τ is expressed in terms of an arbitrary force F that causes shear displacement.

$$F = \tau \cdot l \cdot d \tag{3.6}$$

A diagonal spring with stiffness k and length L representing the stiffness of the panel is used. By setting the horizontal force component in the spring, F_1 equal to the external force F, the spring stiffness k can be calculated. The stiffness reduction factor k_{88} is included in the final step and the factor is found in *Table 3.1*.

$$F_1 = k \cdot \cos^2\varphi \cdot u_1 = k \cdot \frac{l^2}{L^2} \cdot u_1 \tag{3.7}$$

$$F = G \cdot \gamma \cdot l \cdot d = G \cdot \frac{d \cdot l}{h} \cdot \delta \tag{3.8}$$

$$k = k_{88} \frac{G \cdot d \cdot L^2}{l \cdot h} \tag{3.9}$$

Note that *equations 3.4 and 3.9* present the same equation for the diagonal spring stiffness of the truss model.

3.2.4.2 Spring stiffness – Truss model B

The diagonal spring stiffness for Truss model B is based on equations presented in the state-of-the-art publication by Lukacs et al. (2019). To calculate the stiffness, the relation between the maximum force acting on a shear wall and the resulting displacements is used. The total displacement is a result of four mechanisms: bending, shear, translation (sliding) and rotation (rocking), *see Equation 3.10*. The equations, from the state-of-the-art article by Lukacs et al. (2019) are originally presented by Gavric et al. (2015b), Wallner-Novak et al. (2013) and Hummel et al. (2016).

$$\Delta_{\text{tot}} = \Delta_{\text{B}} + \Delta_{\text{S}} + \Delta_{\text{T}} + \Delta_{\text{R}} \tag{3.10}$$

A limitation is made and the displacement due to translation and rotation is neglected. The spring stiffness of Truss model B includes bending of the panel, by taking the displacement due to bending and shear into account (Δ_B+Δ_S). The displacements (bending and shear) are calculated with *Equations 3.11–3.19*. The parameters that are used are the horizontal force acting on the panel *F*, the height of the panel *h*, the effective moment of inertia I_{ef} (calculated with the effective panel thickness, d_{ef}), the modulus of elasticity *E*, the shear modulus *G,* and the shear area of the panel *A* (calculated with the panel thickness *d* and the length *l*).

Gavric:

$$\Delta_{\text{B}} = \frac{F \cdot h^3}{3 \cdot E I_{\text{ef}}} \tag{3.11}$$

$$\Delta_{\text{S}} = \frac{1.2 \cdot F \cdot h}{G \cdot A_{\text{ef}}} \tag{3.12}$$

The effective shear area A_{ef} is the area transferring the shear stresses when the panel is under loading, i.e. only the vertical lamellas of the panel. The effective shear area is calculated with the effective width of the panel d_{ef}.

$$A_{\text{ef}} = d_{\text{ef}} \cdot l \tag{3.13}$$

Wallner-Novak:

$$\Delta_B = \frac{F \cdot h^3}{3 \cdot EI_{ef}} \tag{3.14}$$

$$\Delta_S = \frac{F \cdot h}{G \cdot A} \tag{3.15}$$

The shear stiffness *GA* is calculated with a 25 % reduction of the shear modulus.

$$G \cdot A = (0.75 \cdot G)(d \cdot l) \tag{3.16}$$

Hummel:

$$\Delta_B = \frac{F \cdot h^3}{3 \cdot EI_{ef}} \tag{3.17}$$

$$\Delta_S = \frac{F \cdot h}{G \cdot A_{ef}} \tag{3.18}$$

The equation for shear displacement includes the effective area multiplied by the shear modulus. This is equivalent to the gross shear area multiplied by the effective shear modulus.

$$G \cdot A_{ef} = G_{eff} \cdot A \tag{3.19}$$

The equations for the displacement are based on Wallner-Novak et al. (2013) and are further used in the modelling, *see Equation 3.20*. The 25 % reduction of the shear stiffness is replaced with the stiffness reduction factor k_{88}, *see Table 3.1*. The other reduction factor related to edge gluing that effects torsion k_{33} is not relevant for this model since the models are restricted for out of plane movement.

$$\Delta_{tot} = \Delta_B + \Delta_S = F \cdot \left(\frac{h^3}{3 \cdot EI_{ef}} + \frac{h}{G \cdot A \cdot k_{88}} \right) \quad \rightarrow \quad \frac{F}{\Delta_{tot}} = \left(\frac{h^3}{3 \cdot EI_{ef}} + \frac{h}{G \cdot A \cdot k_{88}} \right)^{-1} \tag{3.20}$$

The horizontal force F_1 in a diagonal spring element from *Equation 3.21* is assumed to be equal to the external force *F*. In this case, the total displacement is equal to the horizontal displacement u_1.

$$F_1 = k \cdot \cos^2\alpha \cdot u_1 = k \cdot \cos^2\alpha \cdot \Delta_{tot} \quad \rightarrow \quad k = \frac{F}{\Delta_{tot}} \cdot \frac{1}{\cos^2\alpha} \tag{3.21}$$

Table 3.2: Input data for the corresponding equivalent stiffness for Truss model B.

Length of wall, l [m]	Effective moment of inertia, $I_{x,ef}$ [m^4]	Angle of the diagonal spring, α [°]
3	0.135	45
6	1.080	27
9	3.645	18
12	8.640	14
15	16.875	11

By combining *Equations 3.20* and *3.21* the equivalent diagonal stiffness k both including bending and shear is found, *see Equation 3.22*. The effective moment of inertia I_{ef} and the angle of the diagonal spring α is dependent on the wall length and the values are presented in *Table 3.2*.

$$k = \left(\frac{h^3}{3 \cdot EI_{ef}} + \frac{h}{G \cdot A \cdot k_{88}} \right)^{-1} \cdot \frac{1}{\cos^2 \alpha} \tag{3.22}$$

3.3 Models part 2 – Multi-storey

The single panels that are used in *Models part 1 – single panel*, are connected to create larger walls with multiple storeys. The panels are connected to create different configurations of varying height and length. Both the shell model and the truss models A and B are investigated. The horizontal global displacement of the different wall configurations is of interest and the aim is to analyse possible differences between the models. When modelling multiple panels on top of each other, the vertical displacement of the top part of the intermediate panels is partly restricted due to the connections between the panels. The horizontal displacement of the shell models becomes smaller, and a multi-storey wall should therefore give more comparable results between the shell and truss model.

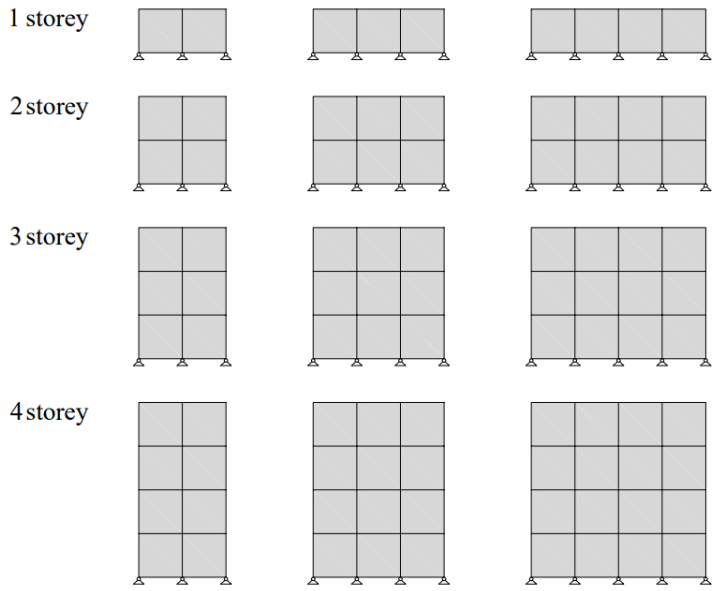

Figure 3.7: Configurations of panels for the models of multi-storey buildings.

3.3.1 Dimensions

The dimension of the panels of the multi-storey buildings are as for the panels of *Models part 1 – single panel* inspired by Sandoli et al. (2016) and Moroder et al. (2015). Thus, ideally one should have a panel height and length of the same value. If this is not the case, the panel should be subdivided to get as close as possible to the desired 45 degrees. (Moroder et al., 2015) The panels for the multi-storey buildings are therefore preferably modelled as square panels with a height h and a length l of 3 m respectively. Different configurations of panels are tested, the number of horizontal panels varies between 2, 3 and 4 panels and the number of vertical panels between 1, 2, 3 and 4, *see Figure 3.7*.

3.3.2 Load

The load is applied similarly to the models of *Part 1 – single panel*. For the truss model, the load acts as a horizontal point load of 3 kN at the top of each level. For the shell model, the load is applied as a horizontal line load on each level, with a load corresponding to a point load of 3 kN. Additional loads such as self-weight and live load are neglected.

3.3.3 Shell model

The shell model is built up of several panels of the add on module RF-laminate in RFEM. The panels are connected with line hinges, which allow rotation between the panels. The top support for the shell model is as for the model of the single panel modelled with nodal supports or with a line support preventing vertical displacement of the model. The later modelling choice will better mimic the behaviour of the truss model.

3.3.4 Truss model

The truss model panels are combined into larger truss models, both Truss model A and B are included. Like for the single panels, the model is restricted from out-of-plane movement in the y-direction. Member hinges are applied at the end of the rigid bars to allow rotation. *See Figure 3.8* for the placement of the member hinges in the truss model.

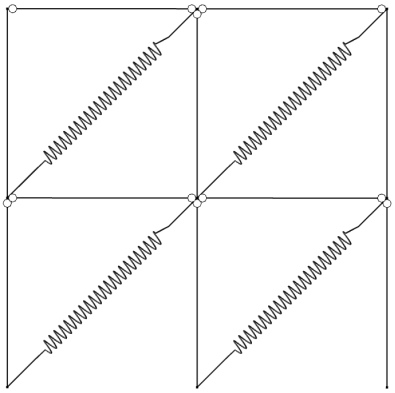

Figure 3.8: Truss model with member hinges (white dots) at the ends of some of the bar elements.

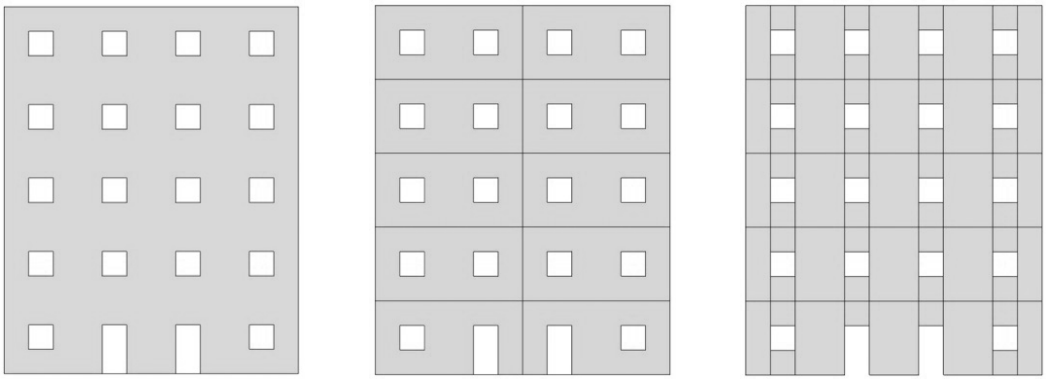

Figure 3.9: Subdivision types of the gable, One panel (left), Subdivision type 1 (middle) and Subdivision type 2 (right).

3.4 Models part 3 – Gable

The next modelling part is a further development of the shell model. The model is made to mimic a gable of a multi-storey building. Three different models of the gable are used to investigate the influence of how the subdivision of CLT walls influences the performance of a gable. The first model presents the gable as a single wall unit with cut-outs for openings and thus neglects the influence of joints between panels. The second and third models are subdivisions of the gable with smaller panel units, *see Figure 3.9*.

For the models of the gable, the inclusion of window and door openings and the resilience of panel connections are analysed. A calculated, more realistic, wind load is used. In the results, the global horizontal displacement of the gable is compared between the models. It is the horizontal displacement of the upper right node that is of interest. The displacement of the upper left node is greater due to local effects of the point load, but the local effects are neglected. The vertical reaction forces and the vertical internal force distribution is as well of interest for the result, both mean and maximal values. For the mean values the length of the gable excluding openings (door and windows) are used, instead of the full length of the gable (12 m). Comparisons are made with or without self-weight of the panels and adjacent floors.

3.4.1 Dimensions

Three symmetric gables that imitate a building are modelled, and the dimension of the gable and the openings are presented in *Figure 3.10*. The gables are 12 m long and 15 m high and have five storeys, each 3 m high. The openings that are made for windows and doors have the dimensions of 1×1 m^2 and 1×2 m^2, respectively. Two doors and two windows are placed on the first level and four windows are placed on each level above. One gable is modelled as one entire shell panel. The first subdivided gable (Subdivision type 1) has two panels on each floor, a total of 10 panels. The second (Subdivision type 2) is inspired by Casagrande et al. (2021a) and consists of wall segments, lintels, and parapets (*see Figure 3.9* for the three gables).

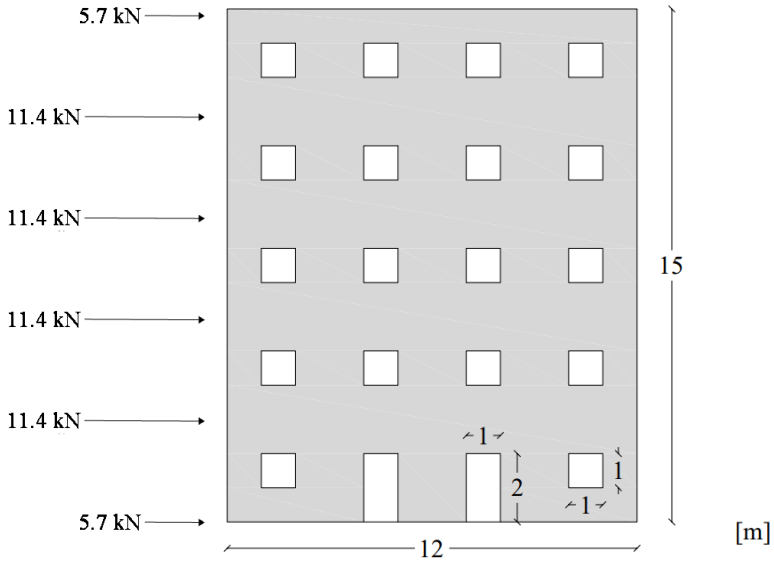

Figure 3.10: Dimensions of the gable and its openings with applied wind load on each floor.

3.4.2 Load

The multi-storey gable is subjected to a lateral wind load acting on the long side of the building. The chosen location of the studied building is in the south of Sweden. The basic wind velocity v_b is therefore 26 m/s and the terrain category is assumed to be number IV. With these factors, the characteristic wind pressure $q_p(z)$ can be interpolated to 0.543 kN/m^2 for a building of 15 m in height (*Table 1.11*, SS-EN 1991-1-4 (2008)).

The external pressure coefficient $c_{pe} = -1.2$ (*Table 1.12*, SS-EN 1991-1-4 (2008)). The internal pressure coefficient c_{pi} for a wall area with an unknown opening area is + 0.2 and – 0.3, which are the most unfavourable values. The most unfavourable wind load is a combination of external and internal wind load. The wind load is calculated with *Equations 3.24–3.26* using the characteristic wind pressure $q_p(z_e)$, the external pressure coefficients c_{pe} and either one of the internal pressure coefficients c_{pi}.

$$w_{e_1} = q_p(z_e) \cdot (c_{pe} - c_{pi_1}) = 0.543 \cdot (-1.2 - (-0.3)) \approx -0.49 \text{ kN/m}^2 \quad (3.24)$$

$$w_{e_2} = q_p(z_e) \cdot (c_{pe} - c_{pi_2}) = 0.543 \cdot (-1.2 - 0.2) \approx -0.76 \text{ kN/m}^2 \quad (3.25)$$

$$|w_{e_2}| > |w_{e_2}| \rightarrow w_e = 0.76 \text{ kN/m}^2 \quad (3.26)$$

The contributory width of the building is assumed to be 5 m. There are five levels, and the foundation and roof each takes half the amount of the load acting on one level, *see Figure 3.10*. The point wind loads are calculated with *Equations 3.27 and 3.28.*

$$P_{w,level} = (w_e \cdot h \cdot b_{influence})/n_{level} = (0.76 \cdot 15 \cdot 5)/5 \approx 11.4 \text{ kN} \quad (3.27)$$

$$P_{w,foundation,roof} = (w_e \cdot \frac{h}{2} \cdot b_{influence})/n_{level} = (0.76 \cdot \frac{15}{2} \cdot 5)/5 \approx 5.7 \text{ kN} \quad (3.28)$$

3.4.3 Connections

The supports of the gable are modelled to mimic the true behaviours of a building subjected to a lateral wind load. By applying nodal supports the shell model is restricted from out of plane movement in the *y*-direction. A line support is attached along the bottom panels to mimic the behaviour of a concrete foundation. The preconditions for the line support from RFEM *Failure if negative support force* is used in the *z*-direction. This means that the support cannot transfer tensile forces and is infinitely stiff in compression in the vertical direction and can therefore not deform below the *z*-axis. The line support restricts displacement in the global *x*-direction (preventing sliding) and *y*-direction and allows rotation around all axes.

3.4.3.1 Placement of hold-downs

The ground support also includes hold-downs that restrict the panel in the vertical direction, acting in the global *z*-direction. The support condition of RFEM *Failure if positive PZ'* is applied and the hold-downs can thereby only take tension and not compression. The hold-downs are placed at different positions of the gable, at the ends of each panel and at all nodes (at the ends of the panel and openings), *see Figure 3.11*.

The subdivided panels are interconnected along their edges by line hinges (springs). Consequently, along such interconnected edges, there are duplicate nodes at each node position, one node belonging to each of the two panels being joined. Thus, if a hold-down is placed at such a point (located at the corners of two panels) it will be connected to only one of these nodes. Which node the hold-down is connected to depends on how the line hinge between the panels is constructed in RFEM, i.e. to which panel the line hinge is primarily connected.

An alternative approach used is to apply two hold-downs in the connection of two panels. The hold-downs are placed 100 mm from the point of fixation of the panels, in both the *x*- and *z*-direction, *see Figure 3.12*. It is of interest to investigate to what extent the different hold-down placements affect the displacement and tension reaction forces of the model.

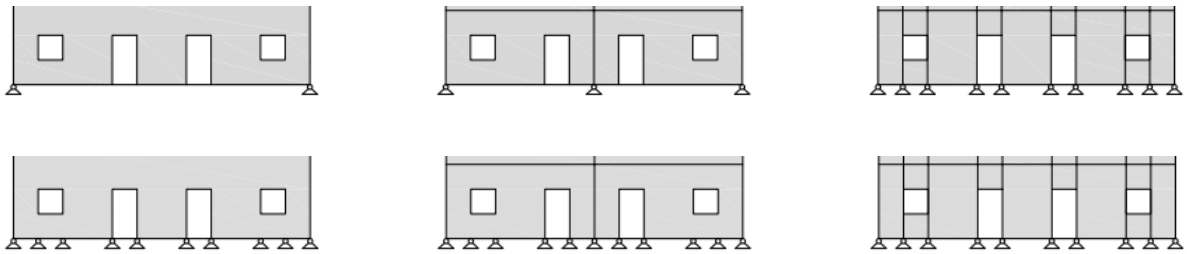

Figure 3.11: The gables with hold-downs only at the ends of the panels (upper) and hold downs at all nodes (lower): One pane (left), Subdivision type 1 (middle) and Subdivision type 2 (right).

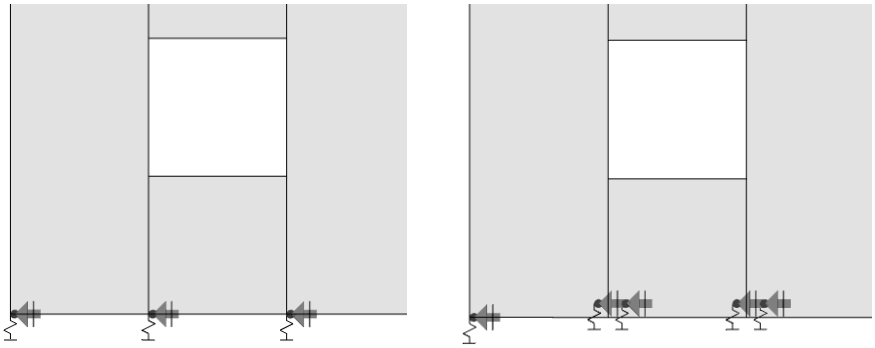

Figure 3.12: Placement of hold-downs for the connection between panels, single hold-downs (left) and double hold-downs (right).

3.4.3.2 Hold-down stiffness

The hold-downs are restrained in the global *x*-direction (preventing sliding), *y*-direction and in rotation around the *z*-axis. Initially, different values of the stiffnesses for the hold-downs are examined (10, 15 000 and 200 000 kN/m). Analyses are made to investigate to what extent the stiffness of the hold-downs affects the horizontal displacement, reaction forces and internal forces of the gable. The values later used for the modelling of the gable are 5000 kN/m and 15 000 kN/m, inspired by Casagrande et al. (2016) and Mestar et al. (2020). For the comparison including a self-weight, a value between the two mentioned stiffnesses is chosen, 10 000 kN/m, it is assumed that one hold-down stiffness is sufficient for the analyses.

3.4.3.3 Line hinge stiffness

The gables that are subdivided into several panels have connections between the sub-panels, these connections have a certain resilience. The connections are modelled in RFEM with so-called line hinges. The line hinges are modelled with translational releases in the local *x*-direction and *y*-direction of the connection, with a joint stiffness of 3 000 kN/m^2 inspired by Olausson (2021) and Shahnewaz et al. (2018). This is the stiffness of applying 1 fastener per meter line hinge. To analyse the effect of the line hinge stiffness, different numbers of fasteners are applied per meter, 1, 5 and 10 fasteners/meter**.** This gives line hinge stiffnesses of 3000 kN/m^2, 15 000 kN/m^2 and 30 000 kN/m^2, respectively. The connections between the panels are located both in the horizontal and vertical direction and in this case, they are modelled with the same varying stiffness.

3.4.4 Self-weight

The influence of self-weight is of interest for the results of the horizontal displacement, reaction forces and internal forces. The self-weight of the panels themselves and the self-weight of the adjacent floors are applied to the models of Subdivision types 1 and 2. A model without an applied self-weight will be on the safe side regarding the risk of turning over. According to Eurocode, calculations made with self-weight, which excludes live load, are a criterion.

Table 3.3: Input data and result for the total load of the self-weight.

	Parameter		Self-weight	Total self-weight
Gable	Area of gable (exc. openings)	158 m^2	5.9 kN/m	55.9 kN/m
	Total thickness of gable	0.09 m		
	Self-weight of gable	5 kN/m^3		
	Length of gable	12 m		
Adjacent floors	Self-weight of adjacent floors	2 kN/m^2	50 kN/m	
	Influence width	5 m		
	Number of floors	5		

A simple calculation is made to estimate the self-weight and to compare the result, *see Table 3.3* for the input data and the result. The assumed self-weight of a floor is 2 kN/m^2 (including isolation, interior walls etc.) The contributory width of the building is set to 5 m, and this gives a self-weight of 10 kN/m per storey. The self-weight of the floors is applied as a line load on five storeys including the roof and the self-weight of the panels is introduced by RF-laminate. The length of the gable is 12 m, the height is 3×5 m, and the panel thickness is 0.09 m. The gable has 18 window openings (18×1 m^2) and two door openings (2×2 m^2). The total load of the self-weight is 55.9 kN/m, considering the total gable length of 12 m.

3.4.5 Sections

The internal forces of the gable are analysed through three sections that are applied to the models in RFEM, *see Figure 3.13*. Section 1 is located on the first floor crossing the openings of this floor, Section 2 is located above the openings of the first floor and Section 3 is located on the second floor crossing the openings of this floor. The sections for Subdivision type 1 and type 2 are called 1.1, 2.1 and 3.1 respectively 1.2, 2.2 and 3.2.

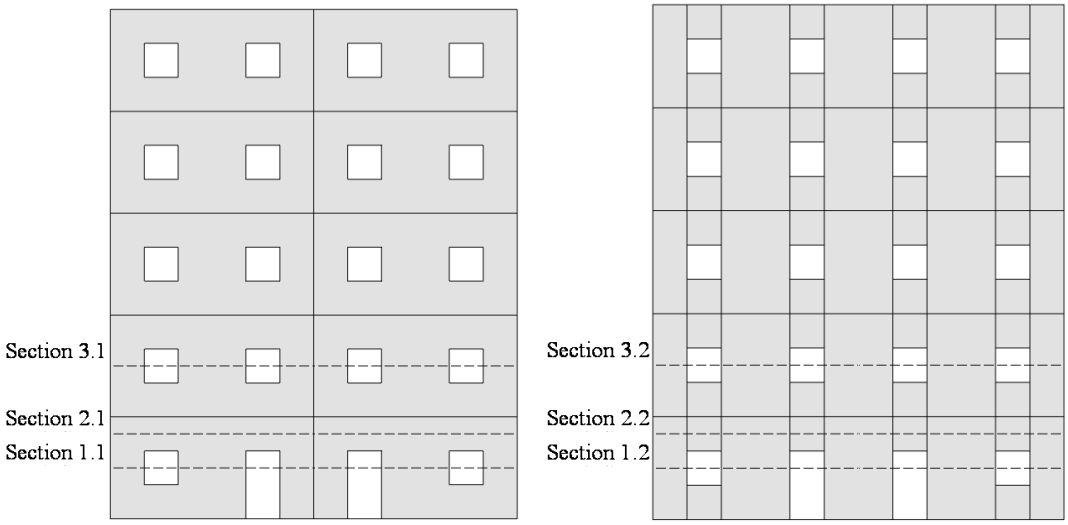

Figure 3.13: Subdivision type 1 (left) and Subdivision type 2 (right), with the locations of the sections.

4 Result

The results regarding the properties of interest for the models and the modelling approaches are presented in this chapter. The structure of this chapter is divided into three parts concerning the modelling of the single panel, the multi-storey building and the gable including openings.

4.1 Models part 1 – Single panel

The calculated values for the equivalent spring stiffness for the different lengths of the panels are presented in the following section, both for Truss models A and B. The horizontal displacement of the two truss models and the shell model are presented. The comparison of the models is made by noting the global horizontal displacement u_x of the upper right node, *see Figure 4.1*. The vertical displacement of the shell model is either restricted or free.

4.1.1 Study of convergence

A study of convergence is made to reassure that the results fulfil a convergence criterium. It is assumed that an iterative calculation method is not needed to fulfil the convergence. An iterative process will increase the time of the calculations but without a great improvement of the precision. The criterium is related to how small the elements need to be to not be affected by a change in the mesh size. The horizontal displacement of the upper right node of the shell model, with and without a restriction for vertical displacement, is of interest in the study of convergence. A limitation is made, and only panels with lengths of 3 and 12 m are used. The element mesh sizes used in the study of convergence have the range from 0.7 m to 0.05 m. The calculations in RFEM takes from a few seconds up to a couple of minutes to complete and the difference in time is considerably small for the element mesh sizes applied. Smaller elements (<0.05 m) would require an iterative calculation method which would take more than several minutes in RFEM. The values and the corresponding number of elements for each size are presented in *Table 4.1*.

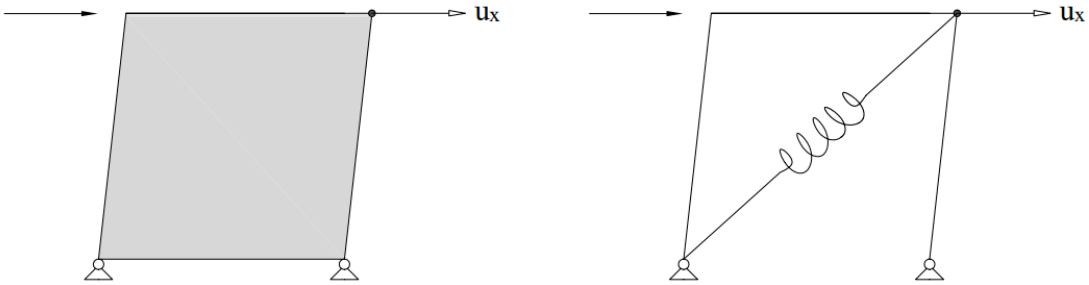

Figure 4.1: Horizontal displacement of the upper right node u_x of the shell and truss model.

Table 4.1: Number of elements of the panels by the mesh size used.

Element mesh size [m]		0.7	0.5	0.2	0.1	0.07	0.05
Number of elements	Panel of 3 m in length	18	36	225	900	1837	3600
	Panel of 12 m in length	73	144	900	3600	7347	14 400

The plot in *Figure 4.2* presents the displacement of the shell model of 3 m in length (with *no* restrictions for vertical displacement) and the corresponding number of elements used for the mesh. The plots of the model with the length 3 m with restricted vertical displacement, as well as the model of 12 m in length with and without restricted vertical displacement are found in *Appendix A: Figure A1-A3*. The model that requires the smallest mesh element size to make the plot converge, is decisive for the element mesh size used for further modelling, this is the model of 3 m with *no* restrictions for vertical displacement. The convergence criteria is fulfilled at a mesh size of 0.1 m since the difference is less than 2 % if more elements are used. It is therefore used for further modelling.

4.1.2 Equivalent spring stiffness

4.1.2.1 Truss model A

The calculated equivalent stiffness E_{ef} for Truss model A, with varying lengths, is calculated with *Equation 3.4* and the values are presented in *Table 4.2*. The calculations include a shear stiffness but no reduction for bending. The stiffness is reduced with the reduction factor k_{88} found in *Table 3.1*. The equivalent stiffness increases with the length of the panel.

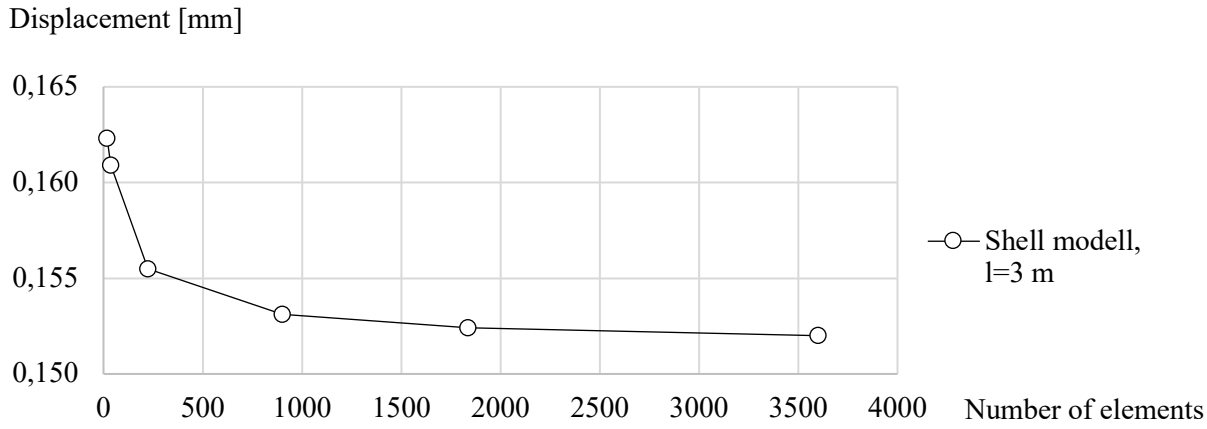

Figure 4.2: Plot of convergence for the shell model with *no* restrictions for vertical displacement with a length of 3 m.

Table 4.2: Values of equivalent stiffness for Truss model A for varying lengths of the panel.

Length of panel, l [m]	Equivalent stiffness, E_{ef} [kN/m]
3	62 100
6	77 625
9	103 500
12	131 963
15	161 460

Table 4.3: Values of equivalent stiffness for Truss model B for varying lengths of the panel.

Length of panel, l [m]	Equivalent stiffness, k [kN/m]
3	52 265
6	74 137
9	101 380
12	130 428
15	160 254

4.1.2.2 Truss model B

The spring stiffness that includes a reduction for bending is calculated with *Equation 3.22* and the result is presented in *Table 4.3*. The equivalent stiffnesses increases with the length of the panel. The contribution of bending deformation is much smaller for wider panels and as expected, the equivalent stiffness of Truss model B approaches the values of Truss model A for panels with greater lengths.

4.1.3 Displacement

The horizontal displacement varies for panels with different lengths and of different models (shell model, Truss model A and Truss model B). The diagram in *Figure 4.3* displays the difference in percentage of the displacement for the truss models, with the shell model as a reference, *see Appendix A: Table A1* for values. Both the truss models (Truss model A and B) experience smaller displacements than the shell model, regardless of the length of the panels.

For truss models with the length of 15 m, the horizontal displacement differs with about 15 % from the shell model. The shell model of 3 m in length differs (in displacement) to Truss model B (including a reduction for bending) with 25 % and to Truss model A (not including a reduction for bending) with 37 %. The values of displacement for Truss model B, are closer to the shell model for all lengths of the panel.

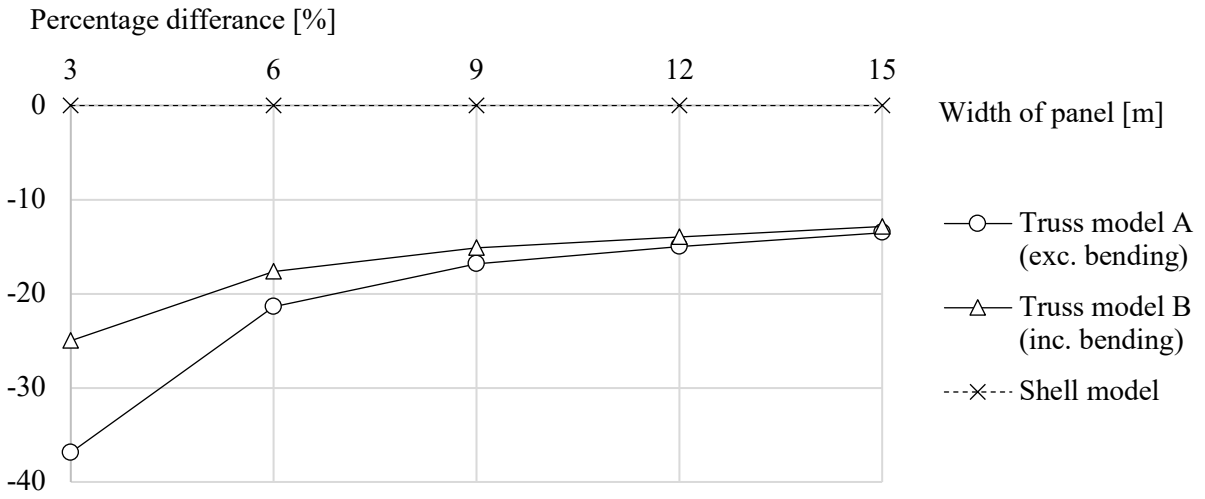

Figure 4.3: Percentage difference in displacement for the truss models with the shell model as a reference.

4.1.3.1 Shell model without vertical displacement

A linear support is applied to the top part of the shell model to mimic the behaviour of the top part of the truss model, where almost no vertical displacement is present. The horizontal displacement of the shell model, the altered shell model and both the truss models are presented in *Table 4.4*.

Preventing the shell model to move vertically, results in displacements similar to the displacements of Truss model B, *see Figure 4.4* for a diagram and *Appendix A: Table A1* for values. In general, the percentage difference between the models is smaller for longer walls and greater for shorter walls. For panels with a length of 3 m, the displacements of Truss model A and Truss model B differ from the shell model (restricted for vertical displacement) with 17 % and 1.5 %, respectively.

Table 4.4: Horizontal displacement for the truss and shell models with different lengths.

	Displacement			
Length of panel *l* [m]	Shell model [mm]	Shell model (restricted vertical displacement) [mm]	Truss model B [mm]	Truss model A [mm]
3	0,153	0,116	0,115	0,097
6	0,061	0,053	0,051	0,048
9	0,039	0,034	0,033	0,032
12	0,028	0,025	0,024	0,024
15	0,022	0,020	0,020	0,019

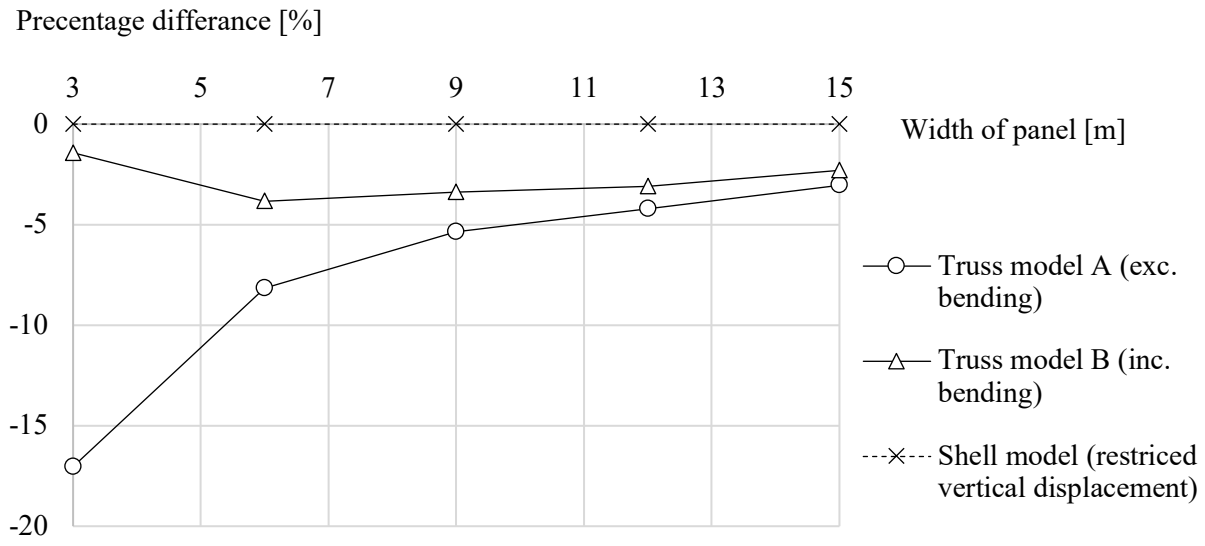

Figure 4.4: Percentage difference in displacement for the truss models to the shell model (including a restriction for vertical displacement) as a reference.

4.2 Models part 2 – multi-storey

The results regarding connected panels with a length and height of 3 m are presented in this chapter. Various number of panels both vertically and horizontally are combined, and the results are compared, *see Figure 3.7* for the configurations. The horizontal displacement of the shell model (both restricted and not restricted in vertical displacement at the top) and the truss models (including or not including a reduction for bending) are presented. The comparison of the models is made by noting the global horizontal displacement u_x of the upper right node of the models, *see Figure 4.1* for the placement of the node for the single panels. It is assumed that the study of convergence for *Models part 1 – single panel* is valid for the models analysed in this chapter.

4.2.1 Displacement

The diagrams in *Figures 4.5 and 4.6* present the displacement of the truss models and the shell model as well as the difference in displacement between the truss models and the shell model. The values for the displacement are found in *Appendix B: Table B1*. For every number of storeys, the shell model experiences a greater displacement than the truss models, where Truss model A has the smallest displacement. The number of storeys and panels horizontally makes a difference, the more slender the model is the greater the difference in the displacement of the truss model compared to the shell model.

The graph in *Figure 4.6* shows that Truss model B experiences displacements closer to the shell model, where the one-storey model of four panels in length has the smallest percentage difference in displacement relative to the shell model.

The effect of changing the support conditions for the upper part of the shell model i.e., not allowing any vertical displacement of the shell model, is presented in *Figures 4.7 and 4.8*, the values are found in *Appendix B: Table B2*. The figures present the displacement of the truss models and the shell model (with restrictions for vertical displacement) as well as the percentage difference in displacement between the truss models and the shell model (with restrictions for vertical displacement), respectively. The graph in *Figure 4.7* shows that when applying a restriction for vertical displacement of the upper support, the horizontal displacements of the truss models become more similar to the displacement of the shell model. Generally, the more slender the model is the greater the difference in displacement compared to the shell model.

The graph in *Figure 4.8* shows that a change of the upper support will result in a smaller difference in percentage for all modelling configurations of Truss model A (excluding bending), the model with one-storey has the smallest difference. For Truss model B (including bending) the model of 3-storeys becomes more similar to the shell model and the model of 1-storey becomes less similar when the support is changed.

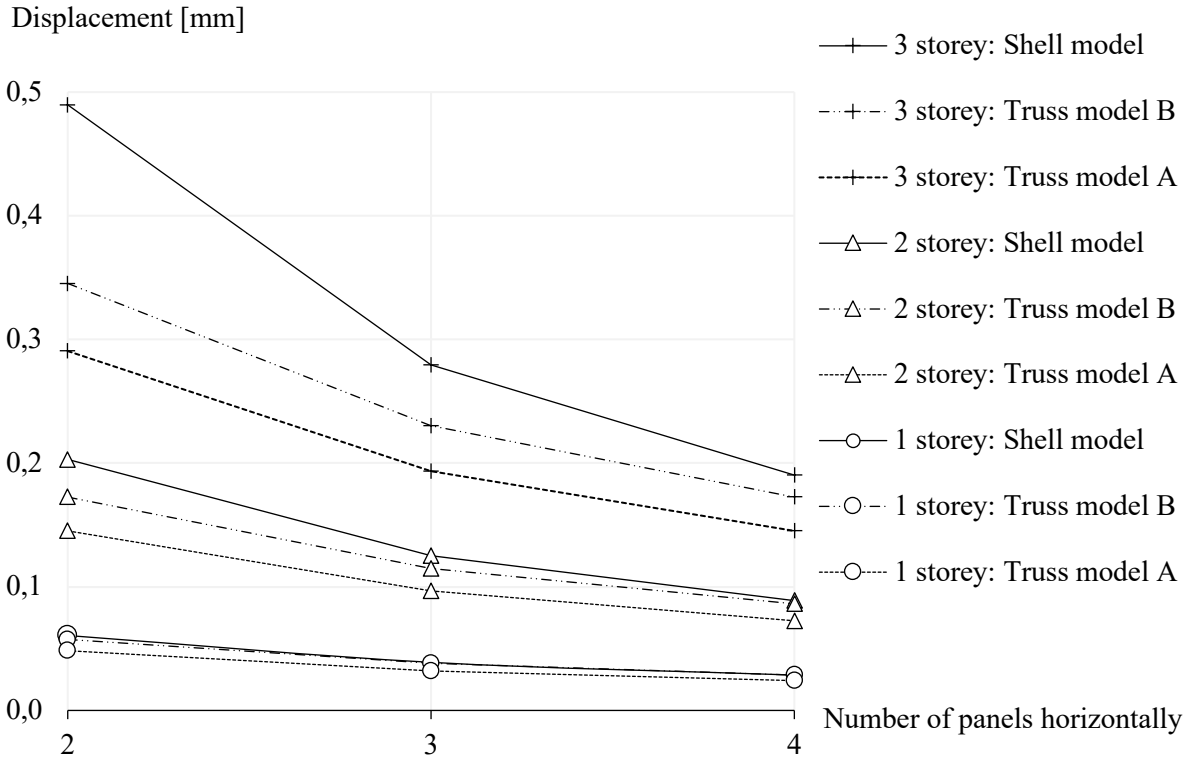

Figure 4.5: Horizontal displacement for the truss and shell models of different configurations.

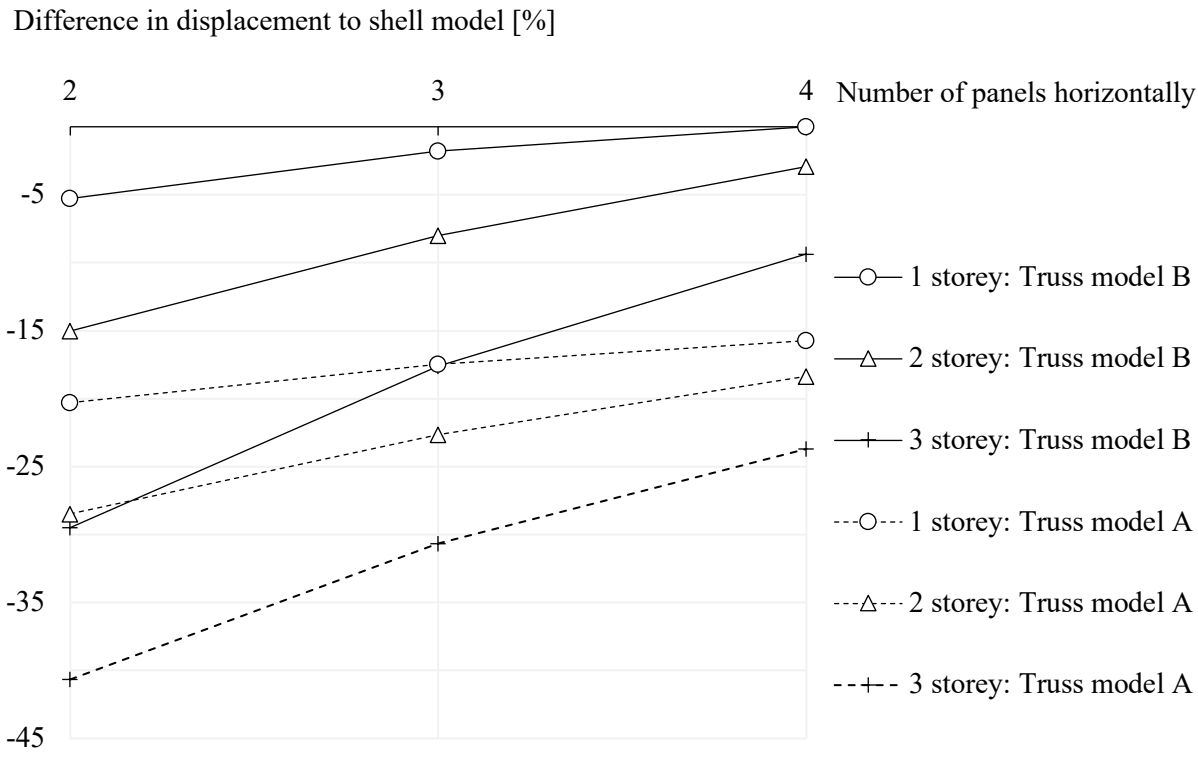

Figure 4.6: Difference in displacement for truss models of different configurations, with the shell models as a reference.

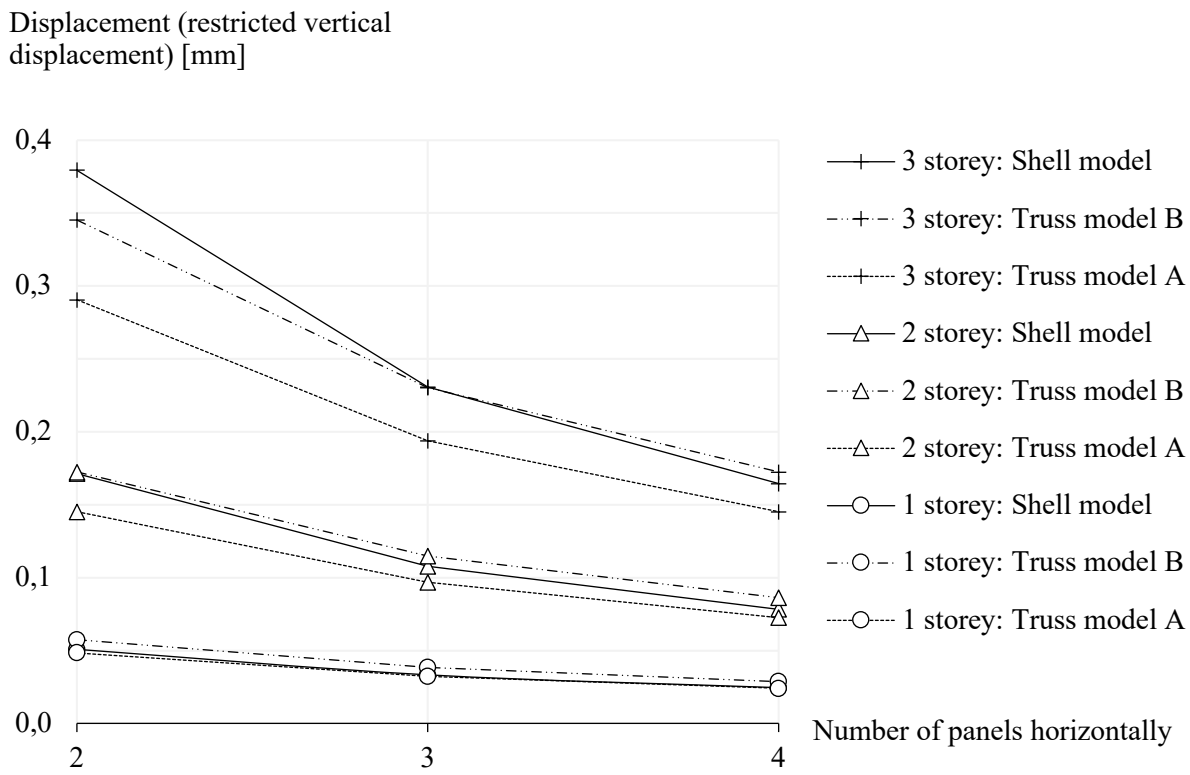

Figure 4.7: Horizontal displacement for the truss and shell models (restricted vertical displacement) of different configurations.

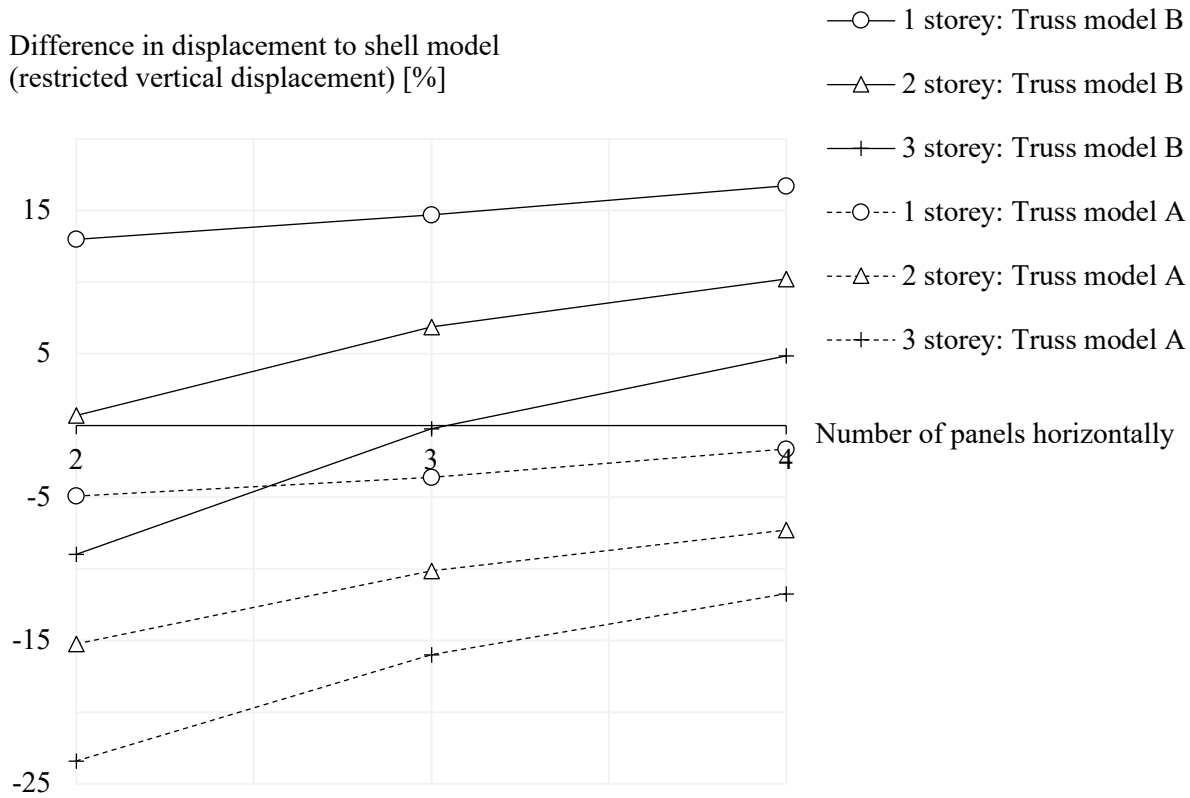

Figure 4.8: Difference in displacement for truss models of different configurations with the shell model (restricted vertical displacement) as a reference.

4.3 Models part 3 – Gable

The parameters of interest for part three are horizontal displacement, vertical reaction forces and vertical internal force distribution. The horizontal displacement u_x is noted in the upper right node of the models, *see Figure 4.1* for the placement of the node for the single panels. The first result that is presented is a convergence study of the mesh size for the shell model and a suitable mesh size is determined. The following chapter presents a parametrical study of the influence of panel configurations, the stiffness of line hinges and the stiffness of hold-downs. The impact of adding self-weight to the gable and the adjacent floors is also analysed.

4.3.1 Study of convergence

A study of convergence is made for the gable of Subdivision type 2 to reassure that the results (displacement, reaction forces and internal forces) fulfil a convergence criterium. It is assumed that linear problems do not need an iterative process to fulfil the convergence. The stiffness values for hold-downs and line hinges are 10 000 kN/m and 15 000 kN/m^2, respectively. The line hinge stiffness is applied for both the local x- and y-axis. The acceptable accuracy is reached when the results no longer are affected to any great extent by the mesh size.

The element mesh sizes used in the study of convergence have a range from 1 m to 0.05 m. The calculations in RFEM take from a few seconds up to a couple of minutes to complete and the difference in time is considerably small for the element mesh sizes applied. Smaller elements (< 0.05 m) would require an iterative calculation method which would take more than several minutes in RFEM. The values and the corresponding number of elements for each size are presented in *Table 4.5*.

Table 4.5: Number of elements of the panel (gable) by the mesh size used.

Element mesh size [m]	1	0.8	0.6	0.4	0.2	0.1	0.07	0.05
Number of elements	158	247	439	988	3950	15 800	32 245	63 200

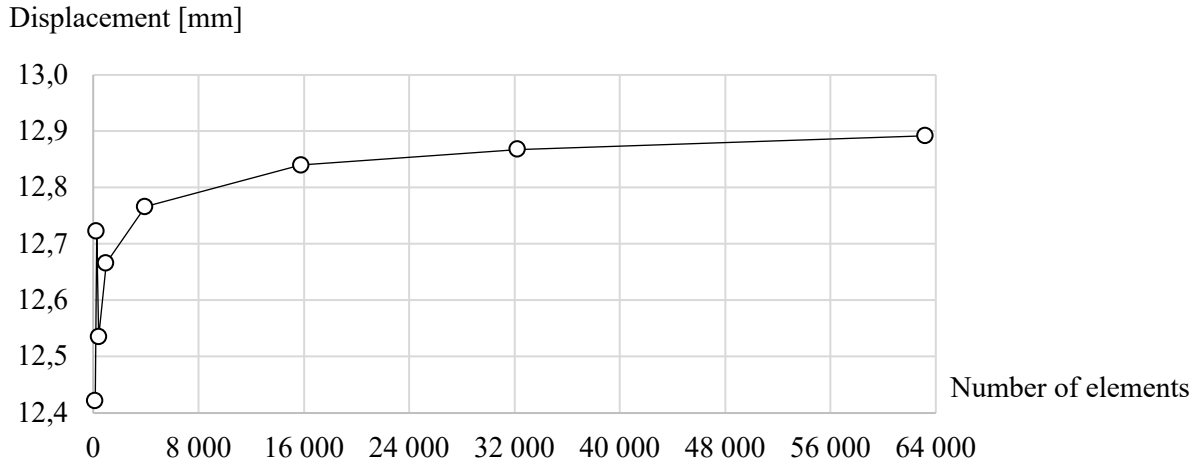

Figure 4.9: Plot of convergence for the displacement of the gable.

4.3.1.1 Displacement

The accuracy of the results for the displacement is investigated. The graph in *Figure 4.9* shows that the number of elements required for an acceptable accuracy is about 15 000 elements, which corresponds to an element mesh size of 0.1 m. From 15 000 elements up to about 63 000 elements, the difference in displacement is less than 0.4 %.

4.3.1.2 Reaction forces

The accuracy of the results for the reaction forces for both the line supports and the hold-downs is investigated. The graph in *Appendix C: Figure C1* shows that the number of elements required for an acceptable accuracy for the maximum reaction force (tension) in the hold-downs is 15 000 elements, which corresponds to a mesh size of 0.1 m. If the number of elements is increased, the difference in reaction force is not more than 0.7 %, i.e. the graph levels out.

The plot in *Appendix C: Figure C2* presents the convergence for the mean reaction force (compression) for the line support over the length of 10 m (not including the openings). It shows that the number of elements required for an acceptable accuracy is about 15 000 elements, which corresponds to a mesh size of 0.1 m. If the number of elements is increased the difference 0.1 %, i.e. the graph levels out.

4.3.1.3 Internal forces

The plots for the convergence study of basic internal forces are presented in *Appendix C: Figures C3–C5*. A limitation is made and only internal forces along Section 1.2 are used for this convergence study (*see Figure 3.13* for the location of the section). Section 1.2 is divided into two parts, Section 1a (left part of Section 1.2) and Section 1b (right part of Section 1.2). This is to better evaluate the mean internal forces of the gable since the right side of the gable will experience greater compression forces and the left side greater tension forces. The mean values of the internal forces are noted when adapting different element mesh sizes. For Section 1.2 there is a tendency of convergence at 15 000 elements, which corresponds to a mesh size of 0.1 m. For Section 1b and 1a, the tendency of convergence is noted after 32 000 elements, which corresponds to a mesh size of 0.07 m. The difference in internal force between 15 000 to 32 000 elements (i.e., an element mesh size of 0.1 to 0.07) is less than 0.1 % for Section 1a and 1b. This difference is small and a mesh size of 0.1 is assumed to be sufficient.

4.3.2 Parametric study

The effects of placement and stiffness of hold-downs and line hinges are studied through displacement and reaction forces. Due to the load application, the compression reaction forces generally act in the bottom right part of the gable and the tension forces in the bottom left. The maximum and mean values of the compression forces along the line support of the gable are noted as well as the maximum values of the tension forces in the hold-downs.

4.3.2.1 Hold downs

With a small hold-down stiffness of 10 kN/m, the horizontal displacement is similar to the displacement of a model without hold-downs. A greater stiffness of 200 000 kN/m results in similar displacement as for a model with infinitely stiff nodal supports. This sets the range of stiffnesses for the hold-downs and the stiffness values further used in the modelling are within this range.

When analyzing the effect of hold-down stiffness through the displacement and reaction forces of the models, see *Figure 4.10 – 4.13*, the line hinge stiffness is *not* varied, and the stiffness of 3 000 kN/m is used exclusively. Values for the displacement and the reaction forces for models with a different line-hinge stiffness of 15 000 kN/m^2 and 30 000 kN/m^2 are found in *Appendix C: Table C1 and C2*.

Changing the hold-down stiffness from 5 000 kN/m to 15 000 kN/m results in a decrease of the displacement varying from 5 – 45 mm, a change of 10–50 %, depending on the placement and subdivision of panels. *See Figure 4.*10 for the displacement of the different models and *Appendix C: Table C1 and C2* for the values for the graph. The model of Subdivision type 2 experiences the greatest displacement followed by the model of Subdivision type 1 and the model experiencing the smallest displacement is the One panel. The models with hold-downs at all nodes have a smaller displacement than if the hold-downs are placed exclusively at the ends of the gable. Using smaller/larger values on hold-down stiffness has the largest effect on the One panel model with hold-downs only at the ends, then the displacement changes from 12.4 to 6.3 mm. The smallest effect is found for the model of Subdivision type 2 where the displacement changes from 46.0 to 41.9 mm.

The maximum reaction forces in the line support (compression) of the models (One panel, Subdivision type 1 and Subdivision type 2) vary from 100–308 kN/m, *see Figure 4.11* for the graph and *Appendix C: Table C1 and C2* for the values. Subdivision type 2 experiences the greatest reaction forces and Subdivision type 1 the smallest, independent of the hold-down stiffnesses that are used. When changing the hold-down stiffness from 5 000 kN/m to 15 000 kN/m the maximum reaction forces (compression) decrease since hold-downs with higher stiffness better prevent displacement of the model. This results in smaller compression forces on the right side of the gable (the opposite side of the applied load) where most of the compression forces occur. The greatest difference in maximal reaction force when the hold-down stiffness is changed (from 5 000 kN/m to 15 000 kN/m) occurs for the One panel with nodal supports only at the ends, from 208.0 to 132.0 kN/m, about a 37 % decrease. The smallest difference occurs for Subdivision type 2, from 308.2 to 240.7 kN/m, about a 22 % decrease.

The mean value of the reaction forces (compression) in the line support varies between 3.6 – 7.5 kN/m, *see Figure 4.12* for the graph and *Appendix C: Table C1 and C2* for the values. There is only a 1 – 13 % change in reaction force when the hold down-stiffness is changed from 5 000 kN/m to 15 000 kN/m. The gable that experiences the greatest mean reaction force is Subdivision type 2.

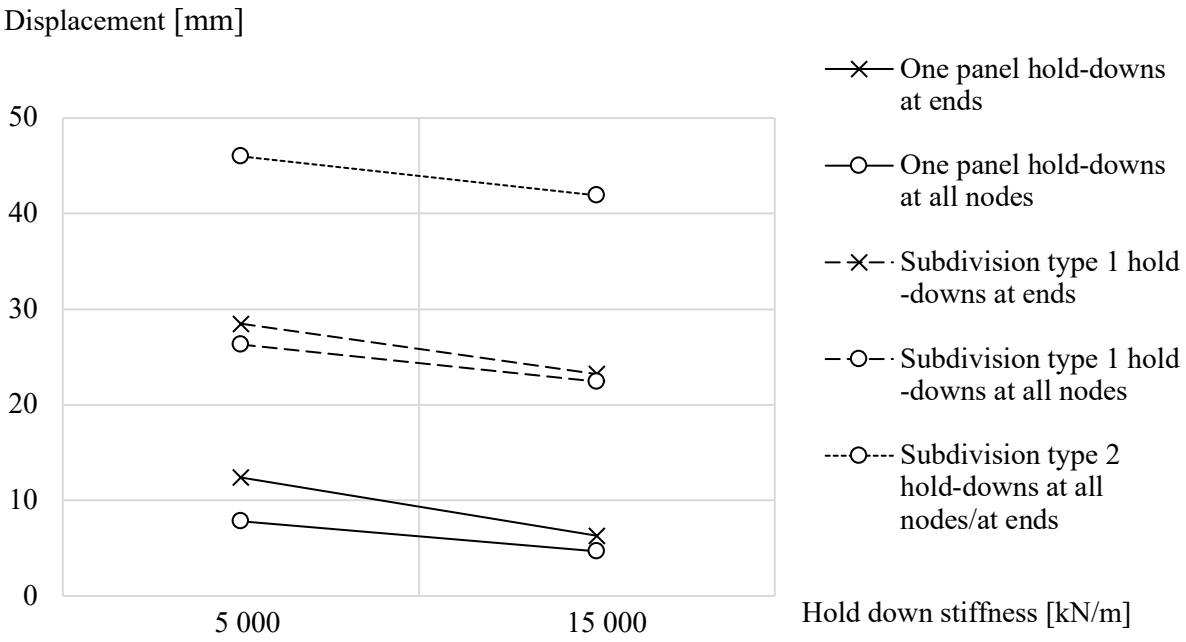

Figure 4.10: Horizontal displacement for the different models of the gable, with two different hold-down stiffnesses, 5 000 kN/m and 15 000 kN/m.

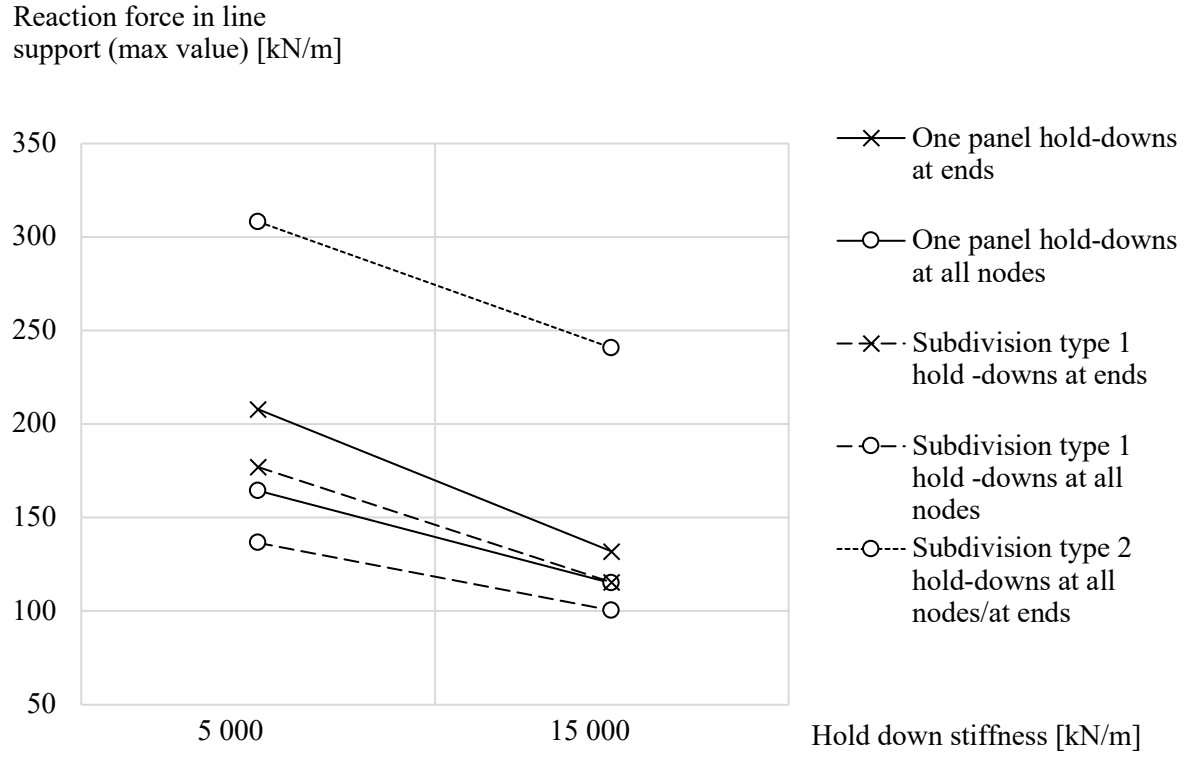

Figure 4.11: Reaction forces from line support (maximum value) for the different models of the gable, with two different hold-down stiffnesses, 5 000 kN/m and 15 000 kN/m.

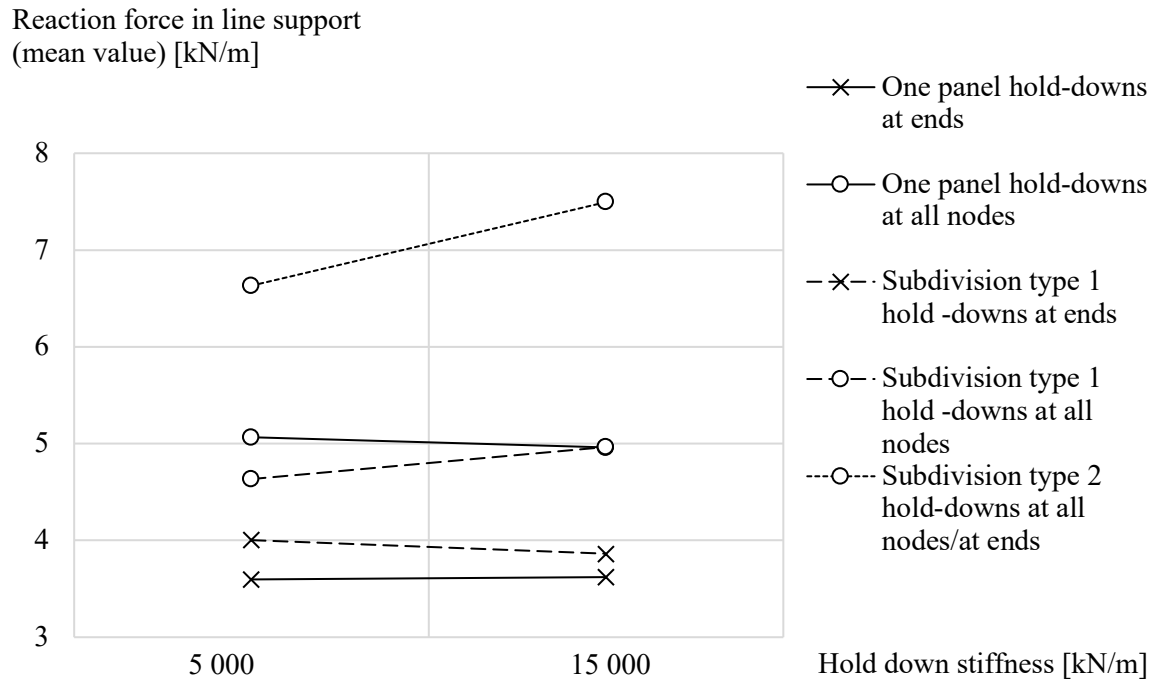

Figure 4.12: The effect of hold-down stiffness on mean reaction force in the line support for the different gables.

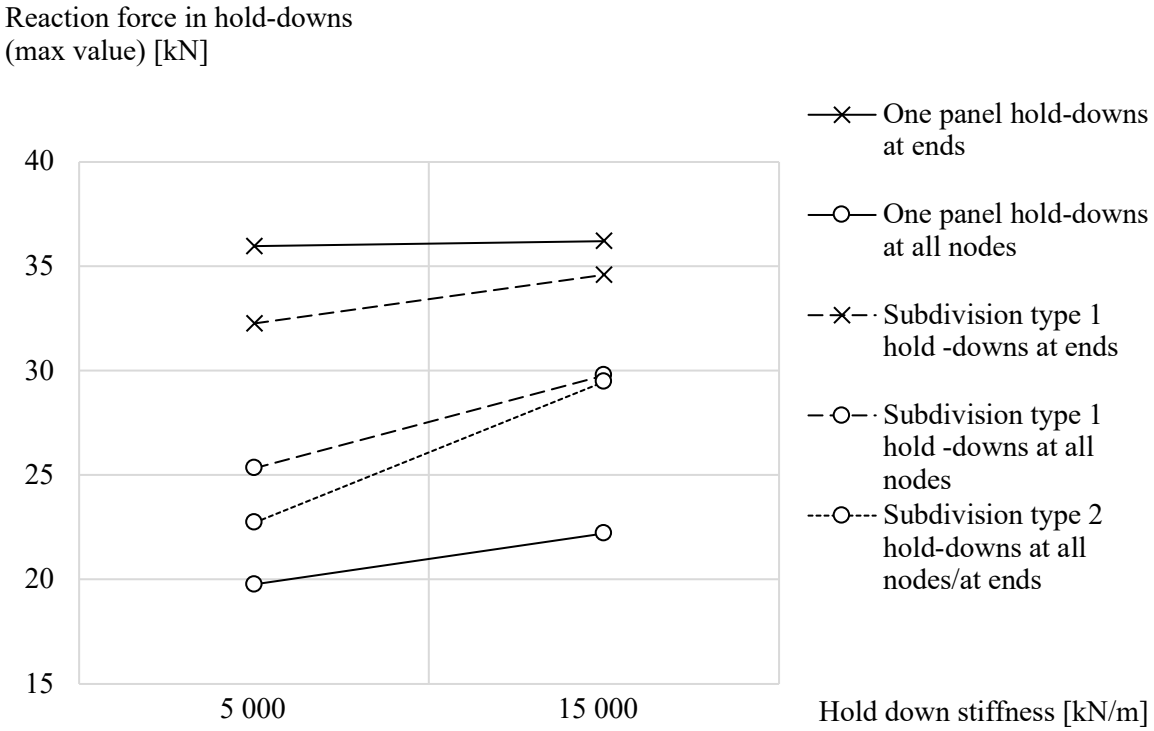

Figure 4.13: The effect of hold-down stiffness regarding reaction force in hold-downs for the different gables.

The maximum values for the tension reaction forces in the hold-downs vary between 18 – 37 kN, *see Figure 4.13* for the graph and *Appendix C: Table C1 and C2* for the values. The tension forces increase up to 30 % when the hold-down stiffness is increased from 5 000 to 15 000 kN/m. The largest difference occurs for the model of Subdivision type 2 and the smallest difference is noted for the One panel with hold-downs only at the ends. The model of the One panel with hold-downs only at ends experiences the greatest tension reaction force and the One panel with hold-downs at all nodes the smallest.

4.3.2.2 Line hinges

When analyzing the effect of line-hinge stiffness through the displacement and reaction forces of the models, see *Figure 4.14 – 4.16*, the hold-down stiffness is *not* varied, and the stiffness of 5 000 kN/m is used exclusively. Values for the displacement and the reaction forces for models with a different hold-down stiffness of 15 000 kN/m^2 are found in *Appendix C: Table C2*. The One panel model does not contain line hinges and is therefore not included.

The displacement of the models (Subdivision type 1 and Subdivision type 2) is affected by the values of the line hinge stiffness. The range of the global horizontal displacement for the models is between 10 – 46 mm, *see Figure 4.14* for the graph and *Appendix C: Table C1* for the values. Changing the line hinge stiffness from 3 000 to 30 000 kN/m^2 decreases the displacement by 55 – 77 % depending on the subdivision. A lower stiffness in the line hinge results in a greater displacement for the models. The gable of Subdivision type 2 is the model with the most line hinges, and the model is experiencing the greatest effect when the line hinge stiffness is varied.

The values for the maximum compression forces acting in the line support of the models are presented in *Figure 4.15, see Appendix C: Table C1* for the values. The reaction forces vary between 137 – 308 kN/m depending on the model. The model of Subdivision type 1 (with hold-downs at ends or all nodes) is not affected by the change of line hinge stiffness to any great extent. An increase of 8 % and 14 % for the model with hold-downs at ends and the model with hold-downs at all nodes, respectively, is noticed when the stiffness is changed from 3 000 to 30 000 kN/m^2. The model of Subdivision type 2 presents a greater difference in reaction force when the line hinge stiffness is changed, about 50 % decrease, from 308.2 to 156.1 kN/m.

The mean value of the reaction force varies with the same pattern as the maximum reaction forces, though the differences are smaller, *see Figure 4.16* for the graph and *Appendix C: Table C1* for the values. For Subdivision type 1 the mean reaction force increases by 4–9 % with an increased line hinge stiffness (3 000 kN/m^2 to 30 000 kN/m^2). For Subdivision type 2 the stiffness results in a decrease of the mean reaction force by 21 %, from 6.6 to 4.8 kN/m, with the same change in line hinge stiffness.

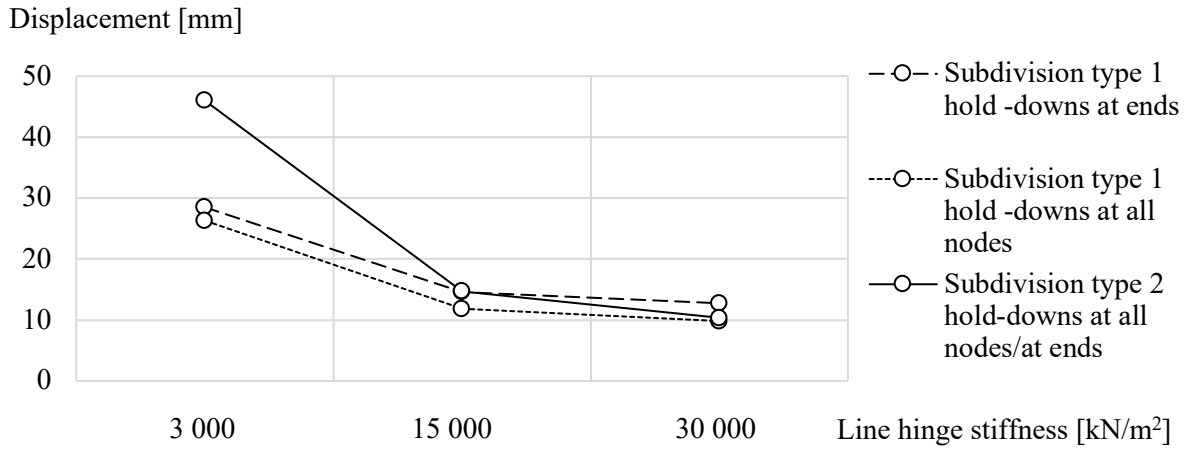

Figure 4.14: The effect of different line hinge stiffnesses regarding displacement for the gables with subdivisions.

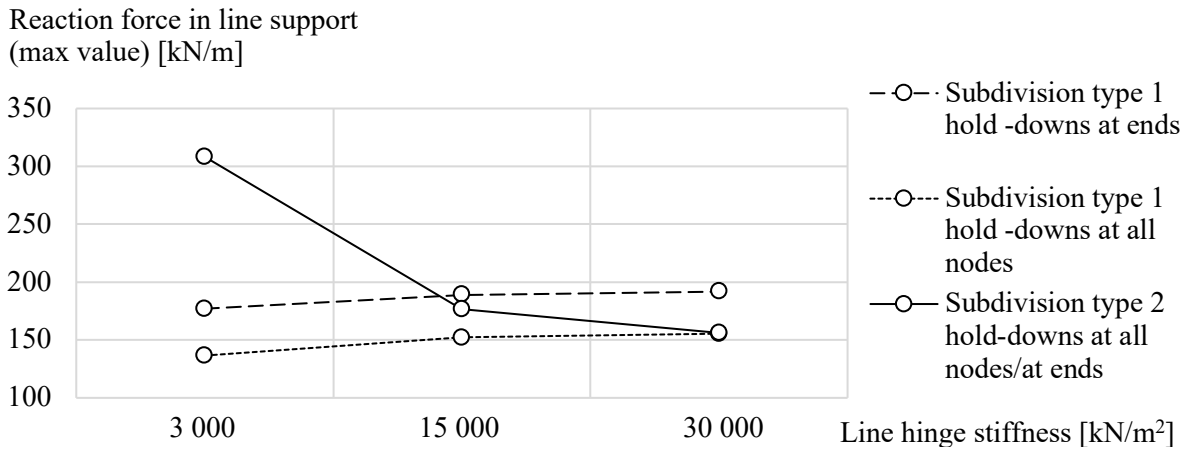

Figure 4.15: The effect of different line hinge stiffnesses regarding reaction force in line support (max values) for the gables with subdivisions.

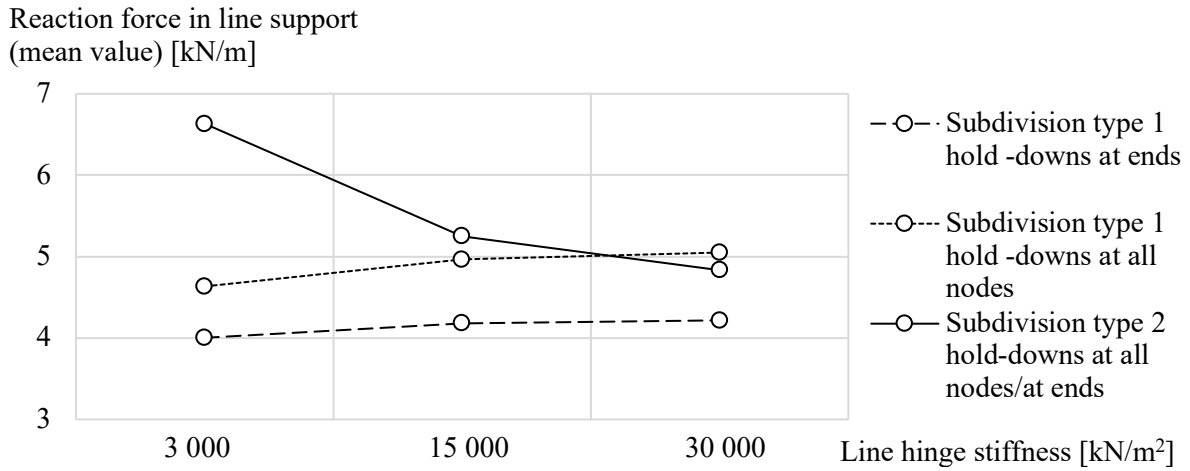

Figure 4.16: The effect of different line hinge stiffnesses regarding reaction force in line support (mean values) for the gables with subdivisions.

4.3.3 Alternative hold-down placement

The result for the different modelling approaches of the hold-downs, for the model of Subdivision type 2, is shown visually in *Figure 4.17*. The panels will move differently depending on how the hold-downs are placed, which will affect the reaction forces. The tension reaction forces in the hold-downs for the model of one hold-down respectively two hold-downs in the connection of two panels are shown in *Figures 4.18 and 4.19*. When the hold-down placement is changed, in the connection of two panels, all reaction forces are affected. The greatest difference in reaction force appears on the left side of the gable, where the tension forces are the greatest (due to the placement of the wind load). Changing the support conditions from one hold-down to two hold-downs at each point of fixation makes the tension reaction forces change from 9.1 kN and 8.8 kN to 7.1+5.7 kN and 5.3+11.5 kN on the left and right side of the left window of the gable, respectively.

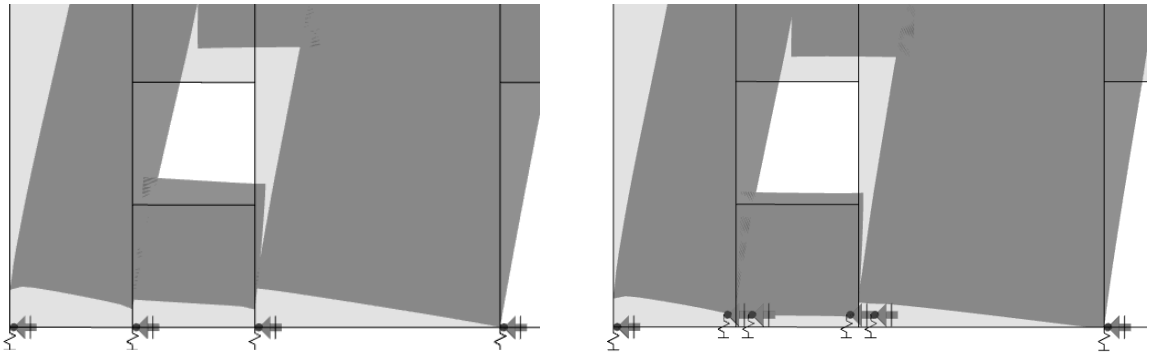

Figure 4.17: Modelling approach of hold-downs, one hold-down at each fixation point (left) and two hold-downs at each fixation point (right).

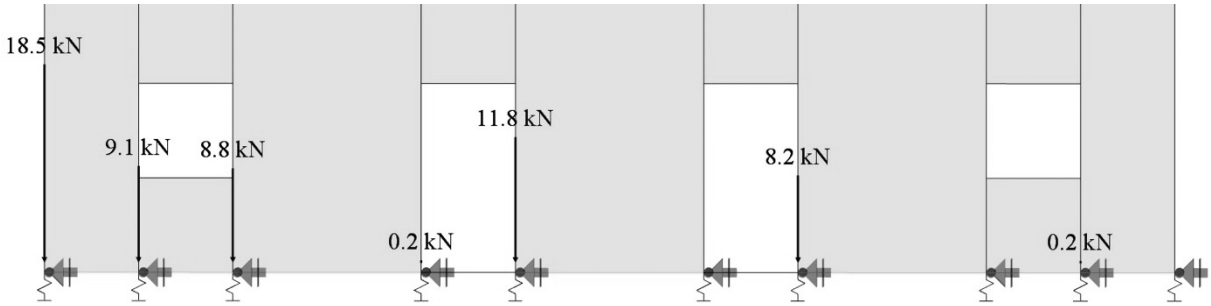

Figure 4.18: Tension reaction forces for the gable (Subdivision type 2) with the hold-down configuration of one hold-down for the connection of two panels.

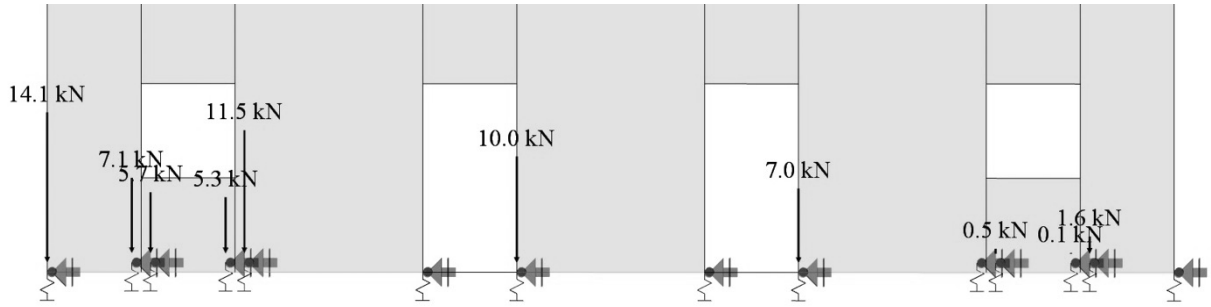

Figure 4.19: Tension reaction forces for the gable (Subdivision type 2) with the hold-down configuration of two hold-downs for the connection of two panels.

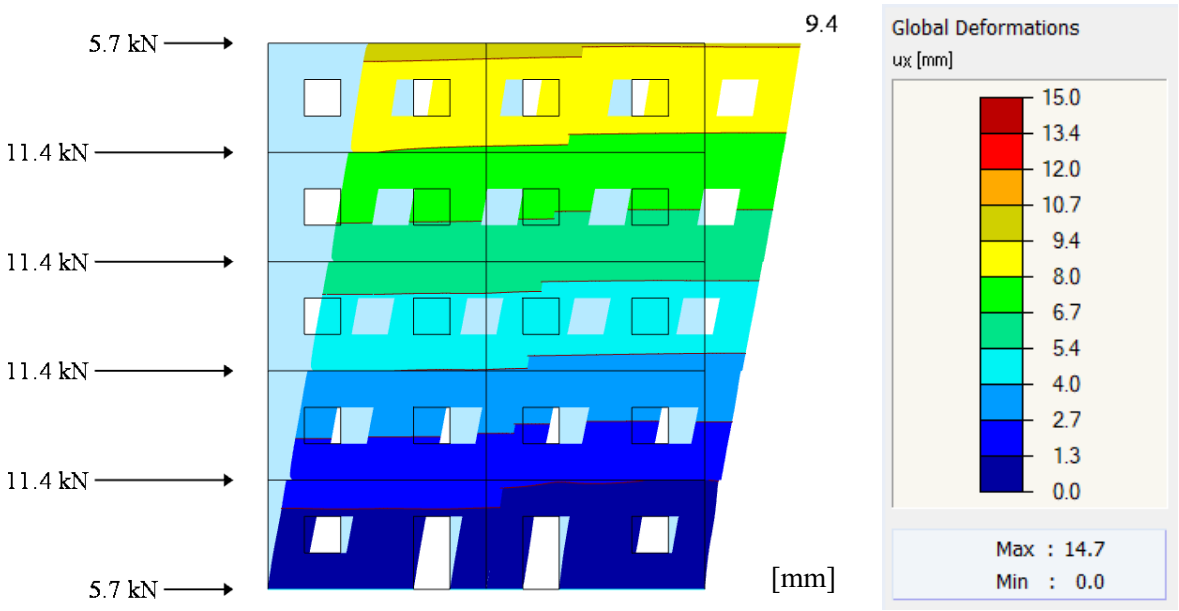

Figure 4.20: Horizontal displacement of the gable of Subdivision type 1 without self-weight.

4.3.4 Self-weight – Subdivision type 1

When self-weight is included the parameters of interest are affected in varying amounts. The interesting parameters are the horizontal displacement, reaction forces and internal forces. The compression reaction forces are analysed along the ground line support and the internal forces are analysed along three sections made through the gable, Section 1.1, Section 2.1, and Section 3.1, *see Figure 3.13* for the location of the sections.

4.3.4.1 Displacement

The global displacement of the gable due to the wind load and without self-weight is 9.4 mm, *see Figure 4.20*. When including self-weight, the global horizontal displacement decreases by 40 % to 5.7 mm, *see Appendix C: Figure C6*.

4.3.4.2 Reaction force

The line support takes compression but no tension, both for the case with and without self-weight. In the model without self-weight, there is no compression nor tension on the left side of the line support. The mean reaction force is 4.9 kN/m, and the maximum reaction force is 120.3 kN/m, *see Figure 4.21* and *Appendix C: Table C3*. The mean reaction force is calculated over the length of the gable not including openings, i.e 10 m. When including self-weight, the compression against the ground is spread out along the bottom line. The maximum and mean reaction force in compression becomes 123.3 kN/m and 60.0 kN/m, respectively, *see Figure 4.22* and *Appendix C: Table C3*. The mean value of the reaction force is increased by about 12 times the amount when a self-weight is included, and the maximum value of the reaction force is increased by 3 %.

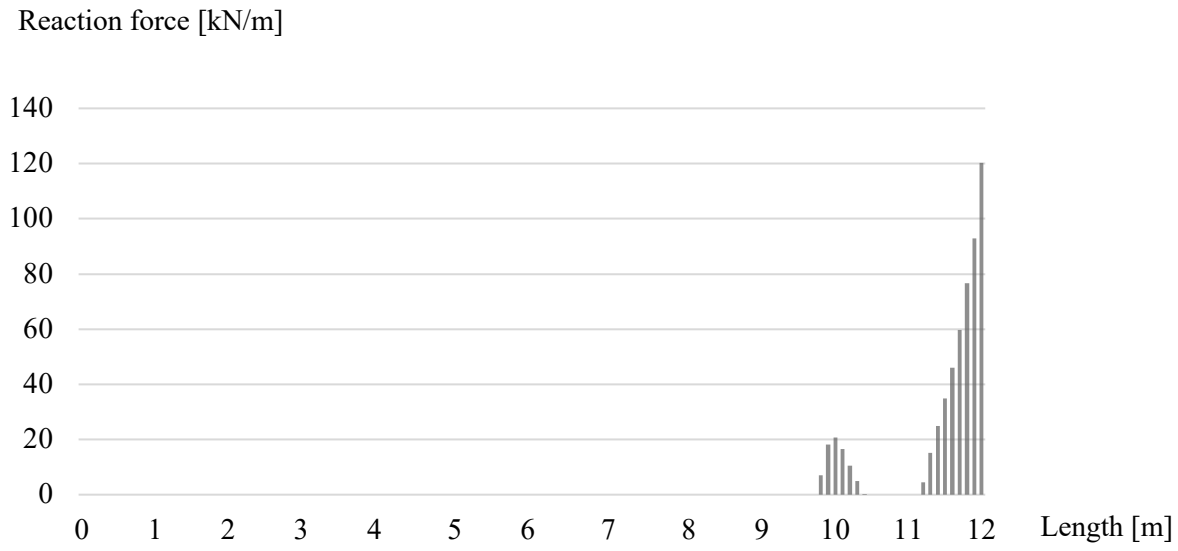

Figure 4.21: Result diagram for the reaction force in the line support of Subdivision type 1 without self-weight.

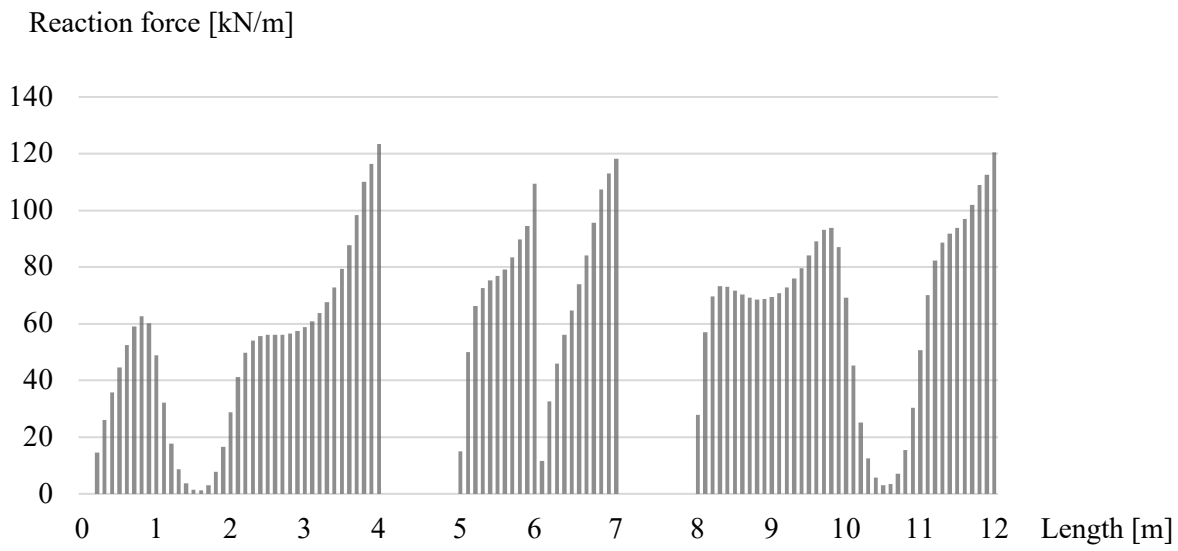

Figure 4.22: Result diagram for the reaction force in the line support of Subdivision type 1 including self-weight.

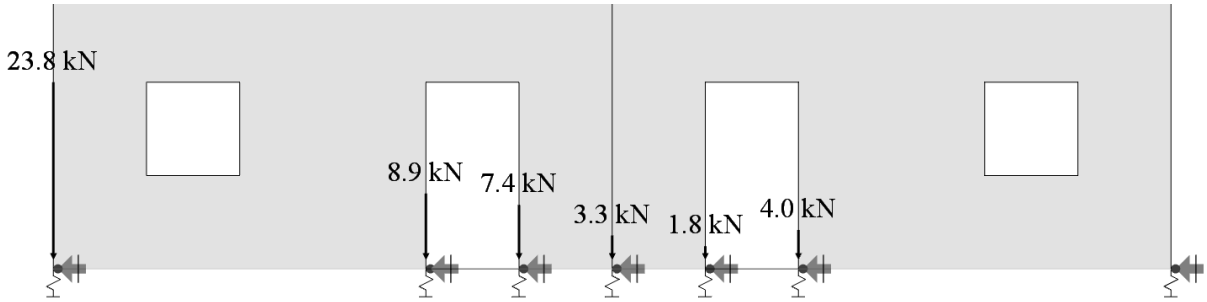

Figure 4.23: Reaction forces in hold-downs in the model of Subdivision type 1 without self-weight.

A simplified calculation is made to check the compression reaction forces. The self-weight of the adjacent floors and the gable is converted into a load per length of the gable, *see Table 3.3* for the input values and the result. The total load is 55.9 kN/m, similar to the 60.0 kN/m found in RFEM for the mean reaction force for the gable of Subdivision type 1 (including self-weight).

The maximum reaction force in the hold-downs, acting as tension force, is 23.8 kN when no self-weight is applied, and 0.1 kN when self-weight is included. The hold-down that takes the maximum tension force is located at the left corner of the panel. *See Figure 4.23* for the values and locations of the tension forces of the gable not including a self-weight and *Appendix C: Figure C7* for the gable including self-weight.

4.3.4.3 Internal forces

The result of the distribution of forces in the gable without self-weight is shown in a colour diagram in *Figure 4.24*. The bottom right corner is compressed and the bottom left corner experiences tension due to the uplift of the panel.

The result of the basic internal forces is presented in three sections; Section 1.1, Section 2.1, and Section 3.1, *see Figure 4.25–4.27* for force diagrams and *Appendix C: Table C4* for force diagrams of the sections and values. The force diagrams are arranged on top of each other to show how the internal forces are transferred through the gable to the ground support. As seen in the colour diagram, the diagrams show that the right side of the gable is compressed and that the left side experiences tension.

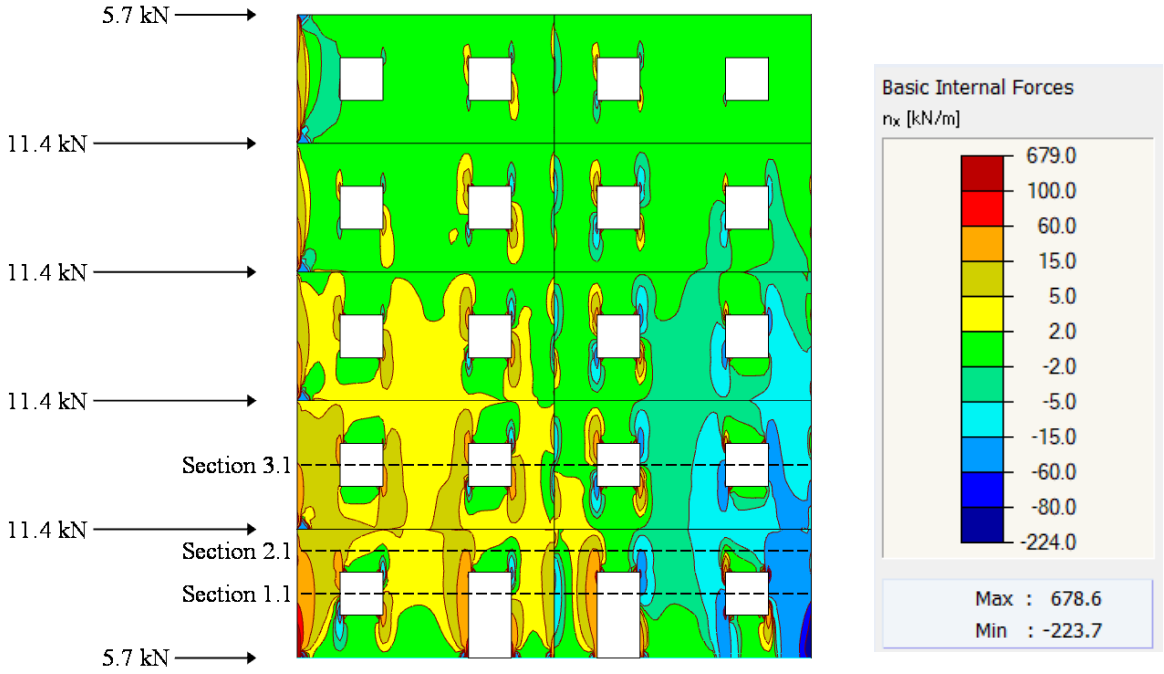

Figure 4.24: The distribution of vertical internal forces for the model Subdivision type 1 without self-weight.

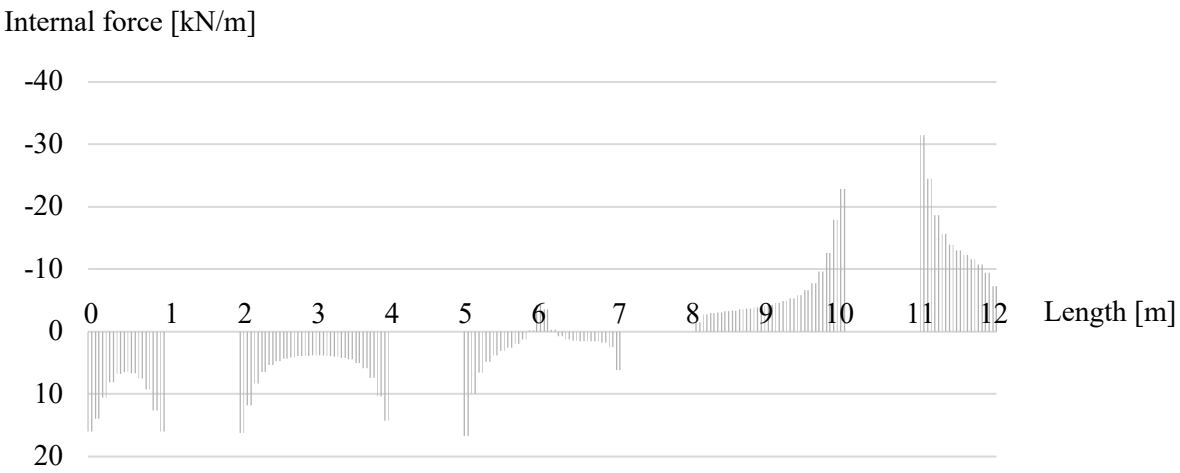

Figure 4.25: Internal force distribution of Subdivision type 1 without self-weight, Section 3.1.

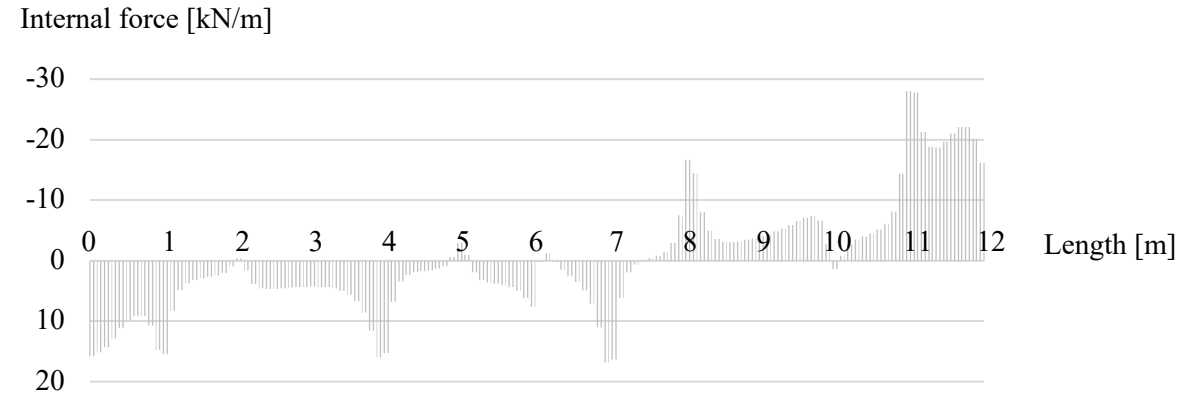

Figure 4.26: Internal force distribution of Subdivision type 1 without self-weight, Section 2.1.

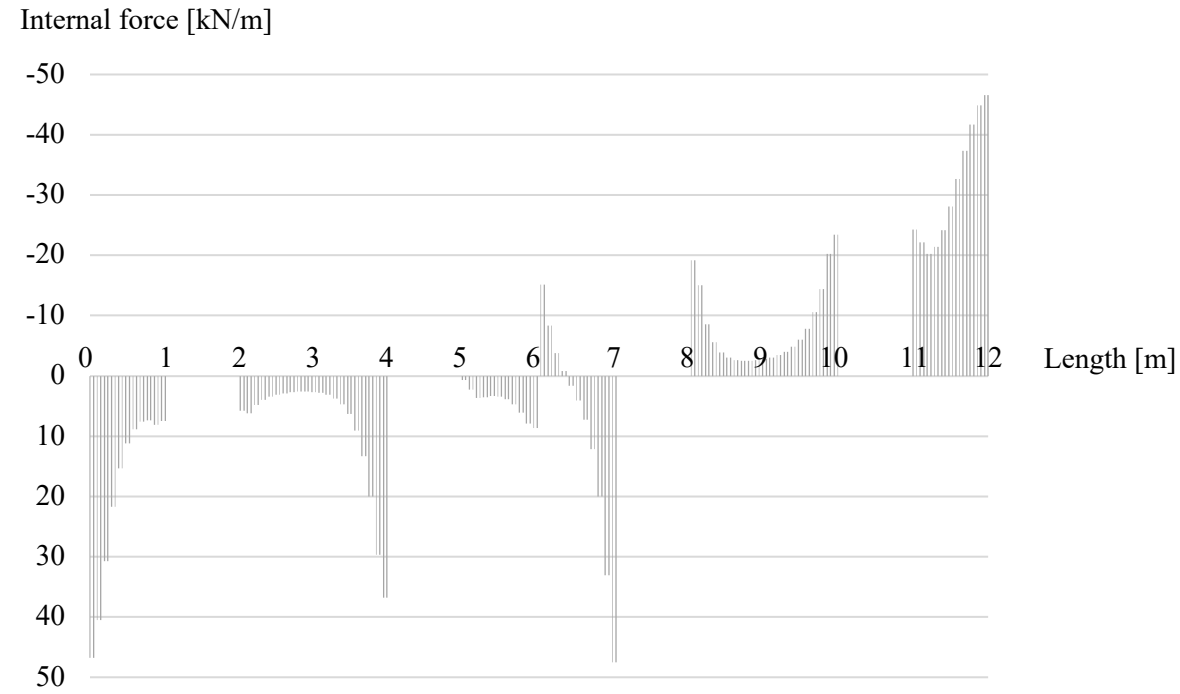

Figure 4.27: Internal force distribution of Subdivision type 1 without self-weight, Section 1.1.

The diagrams show the location of high stresses, which are located at the corners and around openings. The openings are placed between the lengths of 1–2 m, 4–5 m, 7–8 m and 10–11 m which is visualized in Sections 1.1 and 3.1 where no stresses are located. The mean value of the internal forces over one whole section evens out since equilibrium is fulfilled over the section.

The result of the distribution of the internal forces in the gable including self-weight is shown in a colour diagram in *Figure 4.28*. The bottom part of the gable is almost entirely compressed, and tension forces are only experienced in a small amount when a self-weight is included.

The internal forces for the gable including self-weight are presented in three different sections, Section 1.1, Section 2.1, and Section 3.1, *see Figure 4.29 – 4.31* for force diagrams and *Appendix C: Table C4*. The same conclusion as for the force diagrams can be drawn for the colour diagram; that the gable is compressed throughout almost the whole area. The diagrams show the location of high stresses, which are located at places like openings and corners. The maximum value of internal force in compression (170.0, 96.0 and 167.3 kN/m for Sections 1.1, 1.2 and 1.3, respectively) occurs one meter from the right end for all three sections. The mean value of the forces over one whole section is 75.1, 50.0 and 60.1 kN/m for Section 1.1, Section 2.1, and Section 3.1, respectively. The mean internal forces increase closer to the ground support.

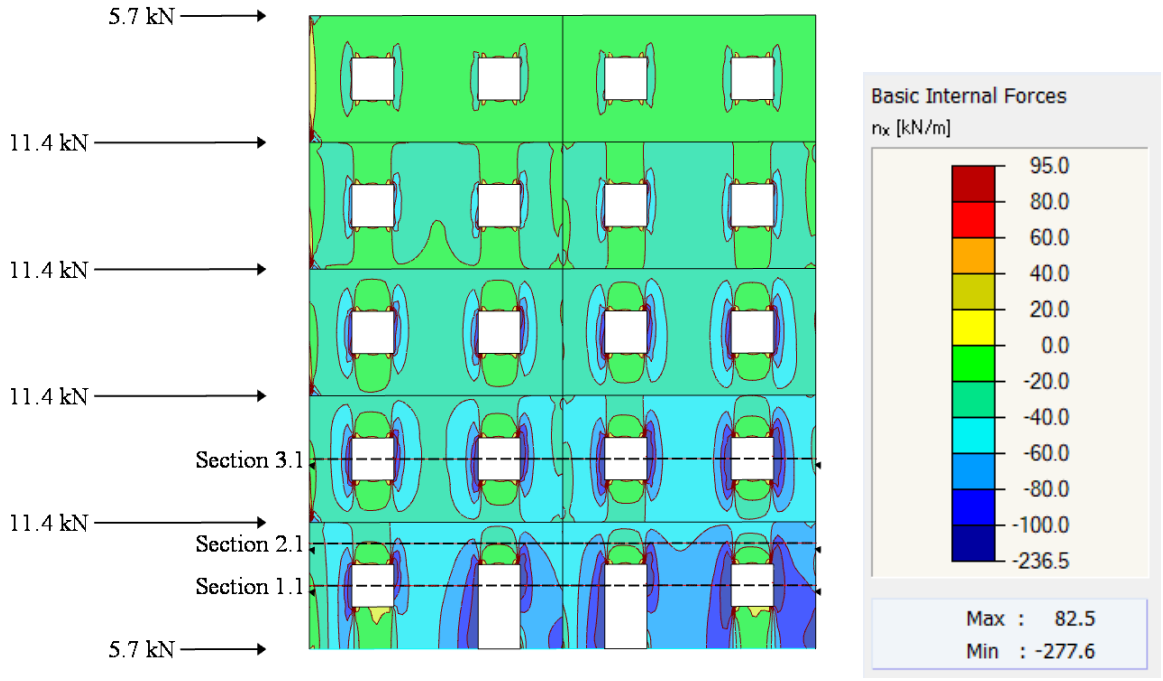

Figure 4.28: The distribution of vertical internal forces of Subdivision type 1 including self-weight.

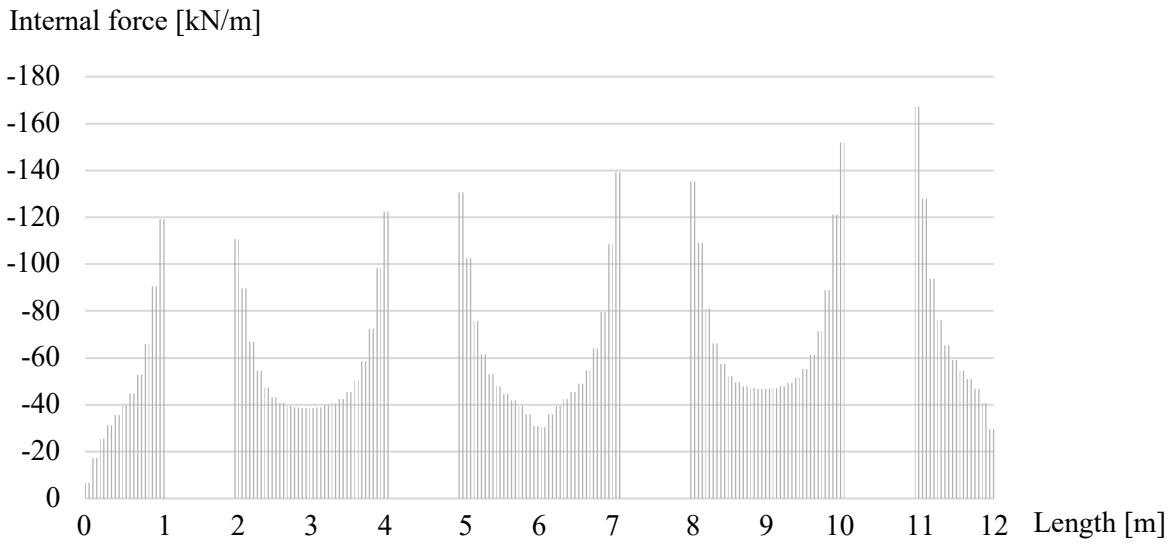

Figure 4.29: Internal force distribution of Subdivision type 1 including self-weight, Section 3.1.

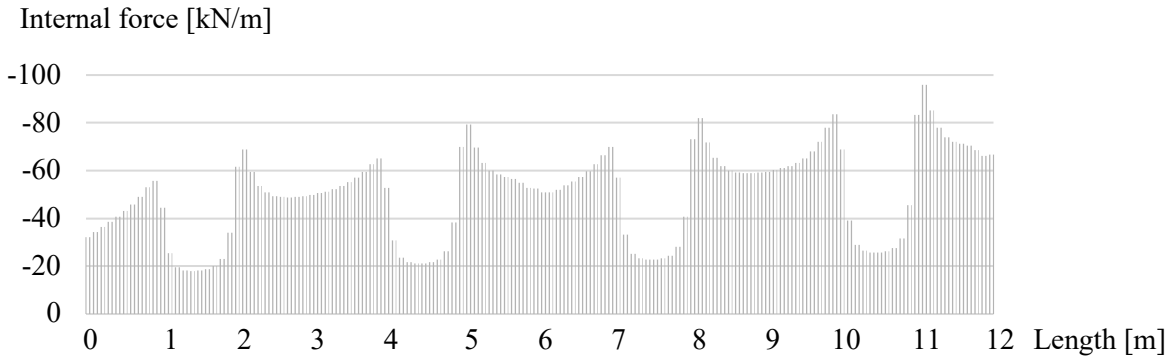

Figure 4.30: Internal force distribution of Subdivision type 1 including self-weight, Section 2.1.

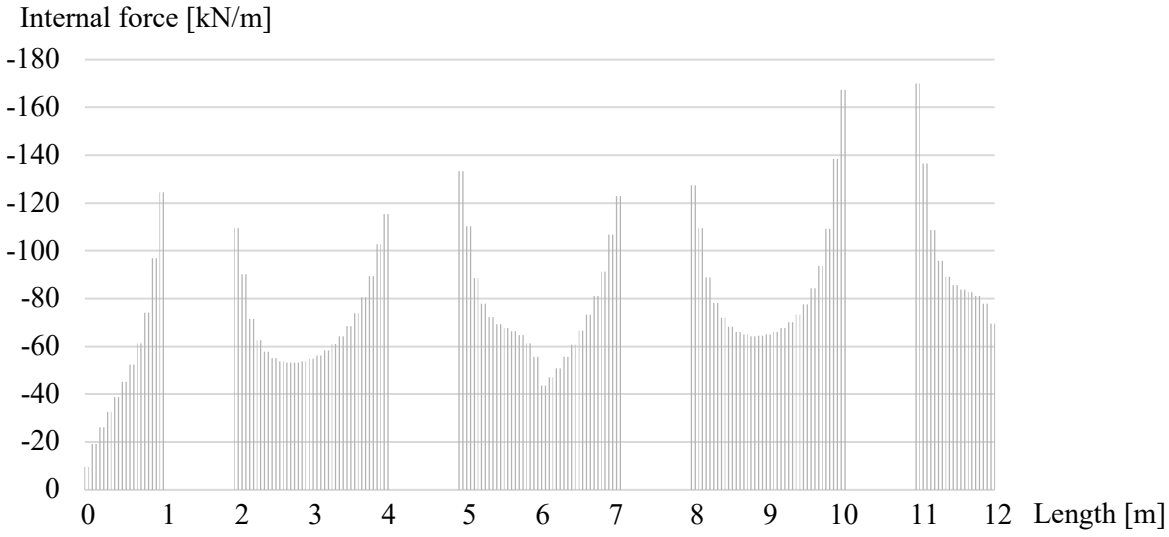

Figure 4.31: Internal force distribution of Subdivision type 1 including self-weight, Section 1.1.

4.3.5 Self-weight – Subdivision type 2

When the self-weight of the gable of Subdivision type 2 and a self-weight of adjacent floors are applied, the parameters of interest are affected in varying amounts. The interesting parameters are the horizontal displacement, reaction force and internal forces. The compression reaction force is analysed along the ground line support and the internal force is analysed along the three sections made through the gable, Section 1.2, Section 2.2, and Section 3.2.

4.3.5.1 Displacement

The displacement of the upper right corner of the gable is 12.8 mm, due to the wind load and without including self-weight, *see Figure 4.32*. When including self-weight, the global horizontal displacement decreases by 29 % to 9.1 mm, *see Appendix C: Figure C8*.

4.3.5.2 Reaction force

The influence of self-weight on the reaction force is investigated at the ground line support. The line support takes compression but no tension, both for the case with and without a self-weight. In the model without self-weight, there is no compression nor tension on the left side of the line support. The mean reaction force is 5.7 kN/m, and the maximum reaction force is 147.4 kN/m, *see Figure 4.33* and *Appendix C: Table C3*. The mean reaction force is calculated over the length of the gable not including openings, i.e. 10 m. When including self-weight, the compression against the ground is spread out along the bottom line. The maximum and mean reaction force in compression becomes 162.2 kN/m and 60.1 kN/m, respectively, *see Figure 4.34* and *Appendix C: Table C3*. The mean value of the reaction force is increased by about 11 times the amount when a self-weight is included, and the maximum value of the reaction force is increased by 10 % when a self-weight is included.

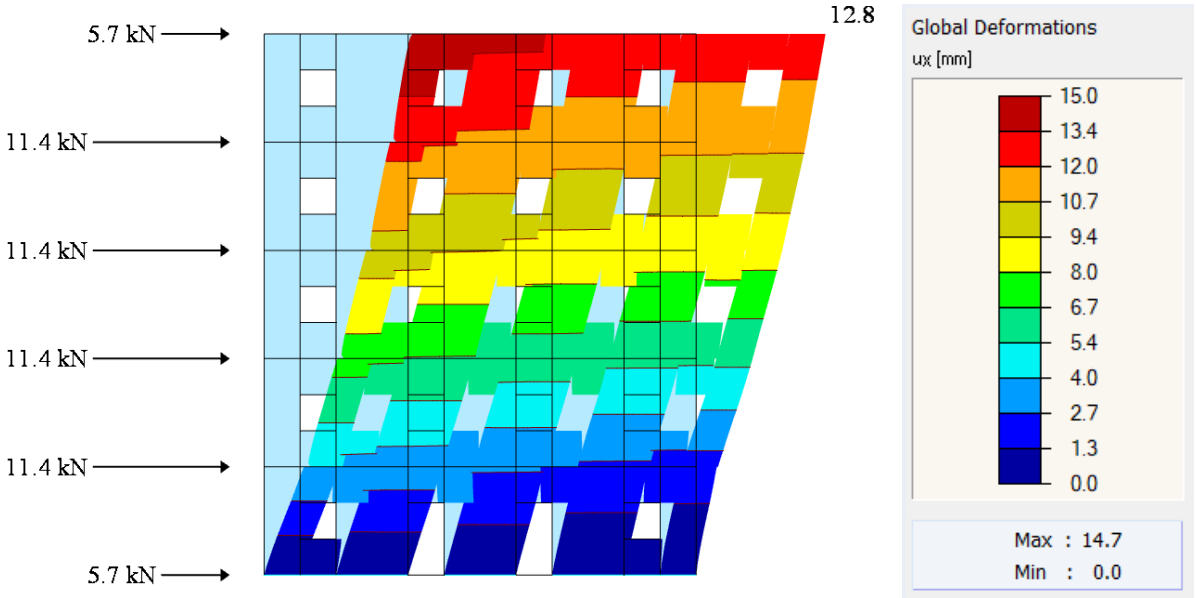

Figure 4.32: Horizontal displacement of the gable of Subdivision type 2 without self-weight.

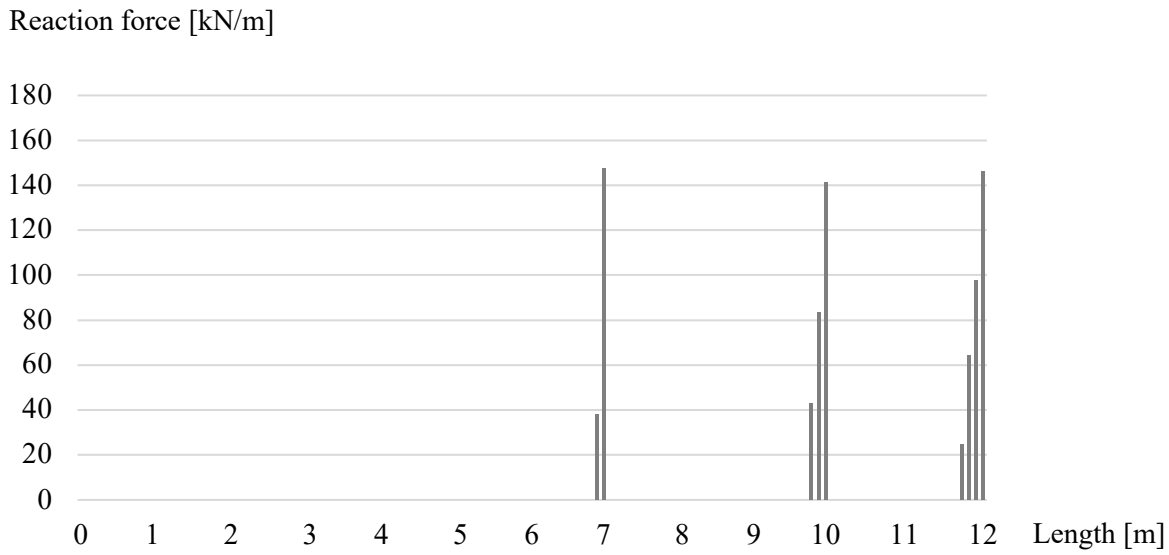

Figure 4.33: Result diagram for reaction forces in the line support of the gable (Subdivision type 2) without self-weight.

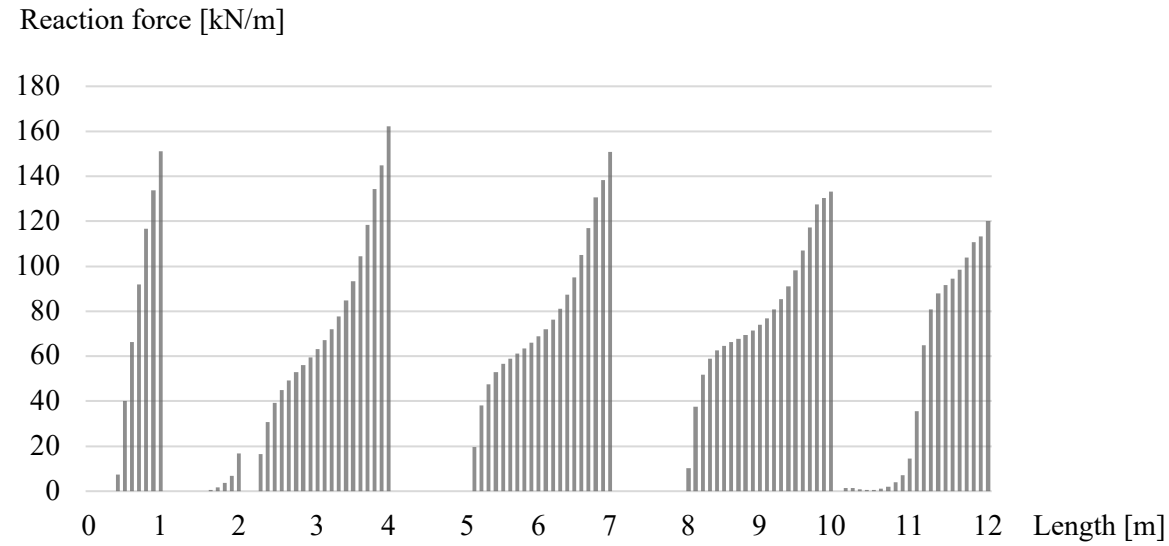

Figure 4.34: Result diagram for reaction forces in the line support of the gable (Subdivision type 2) including self-weight.

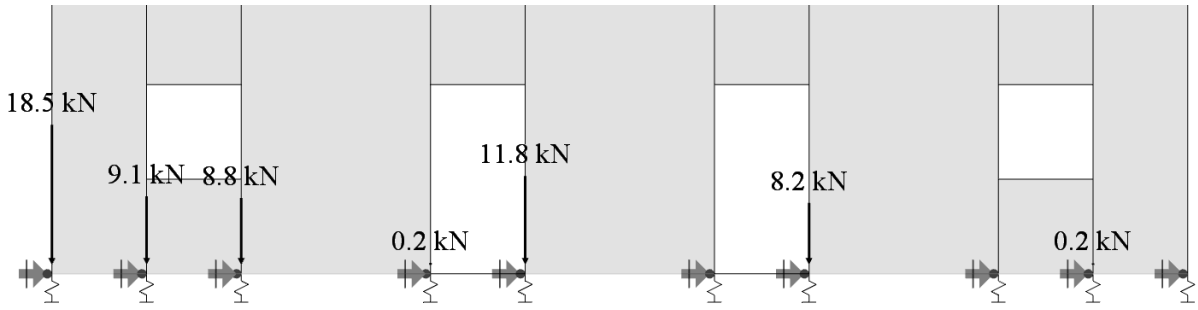

Figure 4.35: Reaction forces in the hold-downs of Subdivision type 2 without self-weight.

As for the model of Subdivision type 2 the mean reaction force of the model of Subdivision type 2 is compared to the calculated load of the self-weight, *see Table 3.3* for the input data and the result. The calculated total load is 55.9 kN/m, similar to the 60.1 kN/m found in RFEM for the mean reaction force for the gable of Subdivision type 2 (including self-weight).

The maximum reaction force in the hold-downs, acting as tension force is 18.5 kN when no self-weight is applied and 1.1 kN when self-weight is included. The hold-down that takes the maximum tension force is located at the left corner of the panel. *See Figure 4.35* for the value and location of the tension forces of the gable not including a self-weight and *Appendix C: Figure C9* for the gable including self-weight.

4.3.5.3 Internal forces

The result of the distribution of the forces in the gable without self-weight is shown in *Figure 4.36.* The bottom right corner is compressed and the bottom left corner experiences tension because of the uplift of the panel.

The result of the basic internal forces is presented in three sections; Section 1.2, Section 2.2, and Section 3.2, *see Figure 4.37 – 4.39* for force diagrams and *Appendix C: Table C4* for the values. The force diagrams are arranged on top of each other to show how the internal forces are transferred through the gable to the ground support. As seen in the colour diagram the force diagrams show that the right side of the gable is compressed and the left side experiences tension. The diagrams show the location of high stresses, which are located at places like openings and corners. The openings are placed at the length of 1–2 m, 4–5 m, 7–8 m and 10–11 m which is visualized for Sections 1.2 and 3.2 where no stresses are located. The mean value of the internal forces over one whole section evens out since equilibrium is fulfilled over the section.

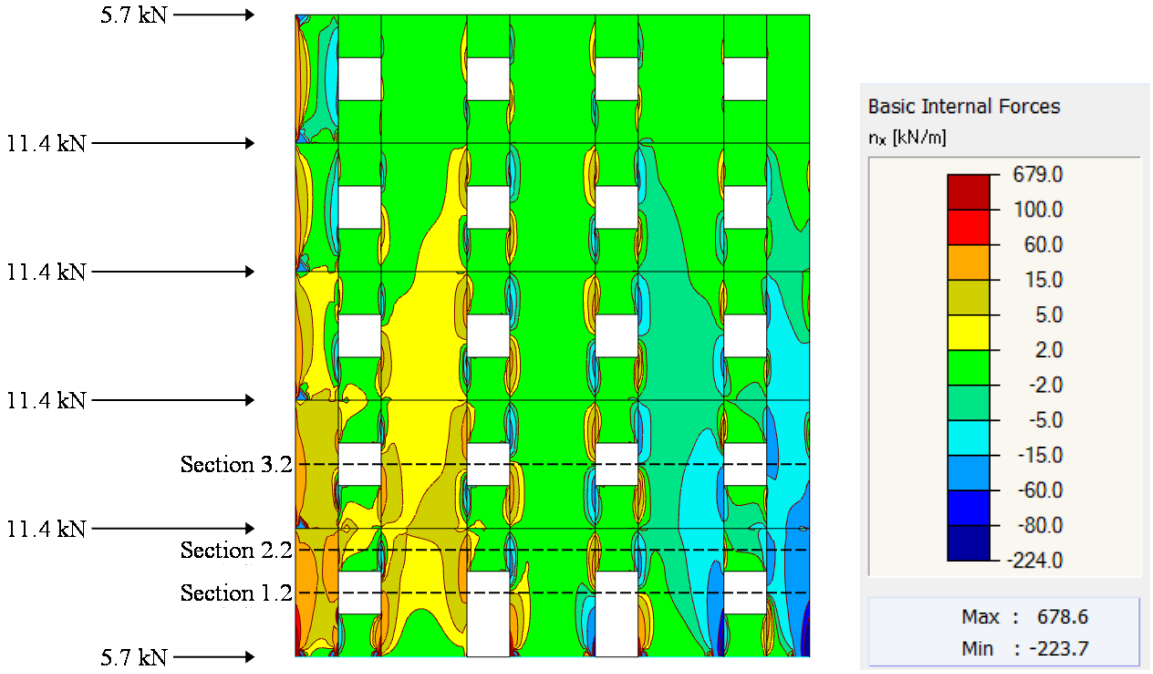

Figure 4.36: The distribution of vertical internal forces of Subdivision type 2 without self-weight.

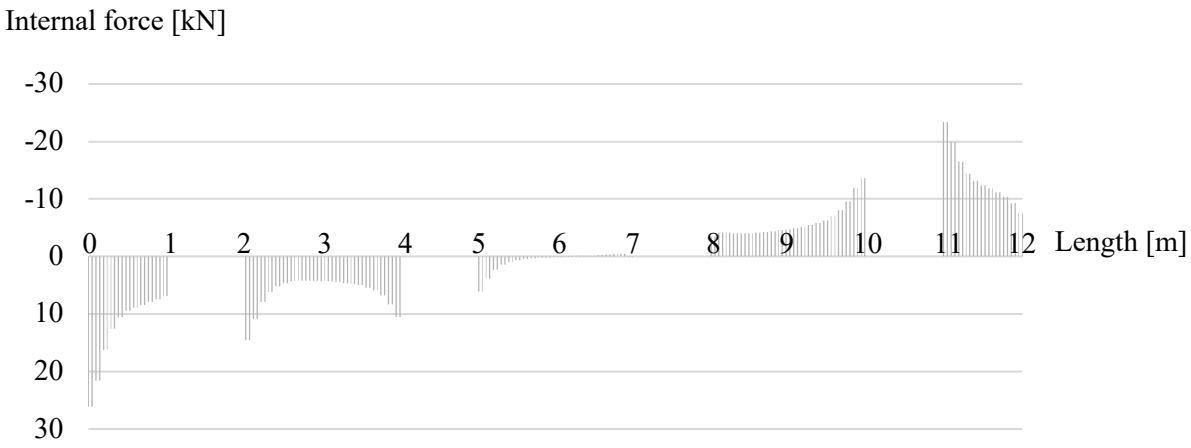

Figure 4.37: Internal force distribution of Subdivision type 2 without self-weight, Section 3.2.

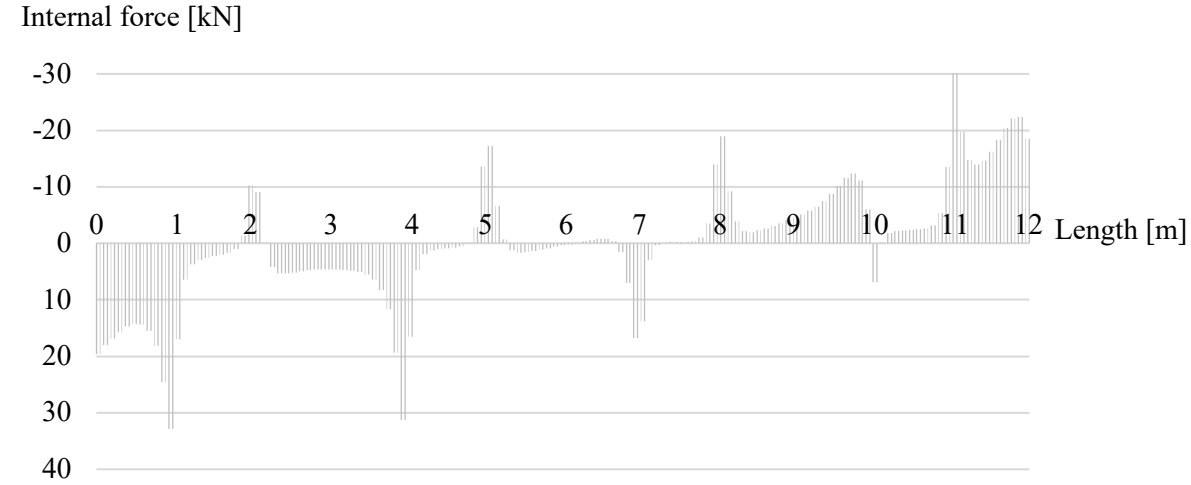

Figure 4.38: Internal force distribution of Subdivision type 2 without self-weight, Section 2.2.

Figure 4.39: Internal force distribution of Subdivision type 2 without self-weight, Section 1.2.

The result of the distribution of the internal forces in the gable including self-weight is shown in *Figure 4.40*. The bottom part of the gable is almost entirely compressed, and tension forces are only experienced in a small amount when self-weight is included. Tension forces are located at the bottom left corner of the gable and the bottom left parapet (panel underneath openings). The colour diagram shows that no or small stresses are occurring in the parapets and lintels (panels underneath and above openings). The load is almost exclusively transferred through the wall segments.

The internal force distribution of the gable including self-weight is presented in three different sections, Section 1.2, Section 2.2, and Section 3.2, *see Figure 4.41–4.*43 for force diagrams and *Appendix C: Table C4* for values. The same conclusion as for the force diagrams can be drawn for the colour diagram; that the gable is compressed throughout almost the whole area. The diagrams show the location of high stresses, which are located at places around openings and corners. The parapets of Section 2.2 (from 1–2 m, 4–5 m, 7–8 m and 10–11 m) have a low value of internal forces, this confirms the statement that the load almost exclusively is transferred through the wall segments. The existing but low value of internal forces in the parapets are most likely occurring due to the self-weight of the parapets themselves and above-placed parapets. The maximum value of internal force (139.2, 117.8 and 133.3 kN for Sections 1.2, 2.2 and 3.2, respectively) occurs one meter from the right end for all three sections. The mean value of the internal forces over the whole section are 75.0, 50.1 and 60.0 kN/m for Section 1.2, Section 2.2, and Section 3.2, respectively, values almost identical as for Subdivision 1. The compression increases closer to the ground support according to the mean values.

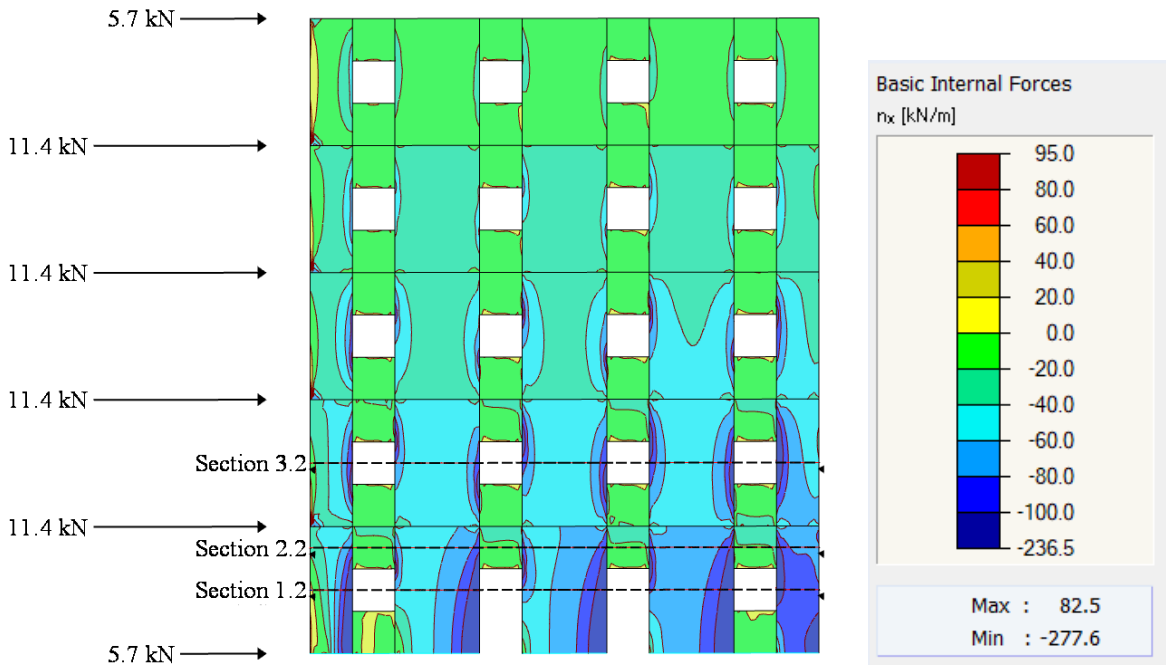

Figure 4.40: The distribution of vertical internal forces of Subdivision type 2 including self-weight.

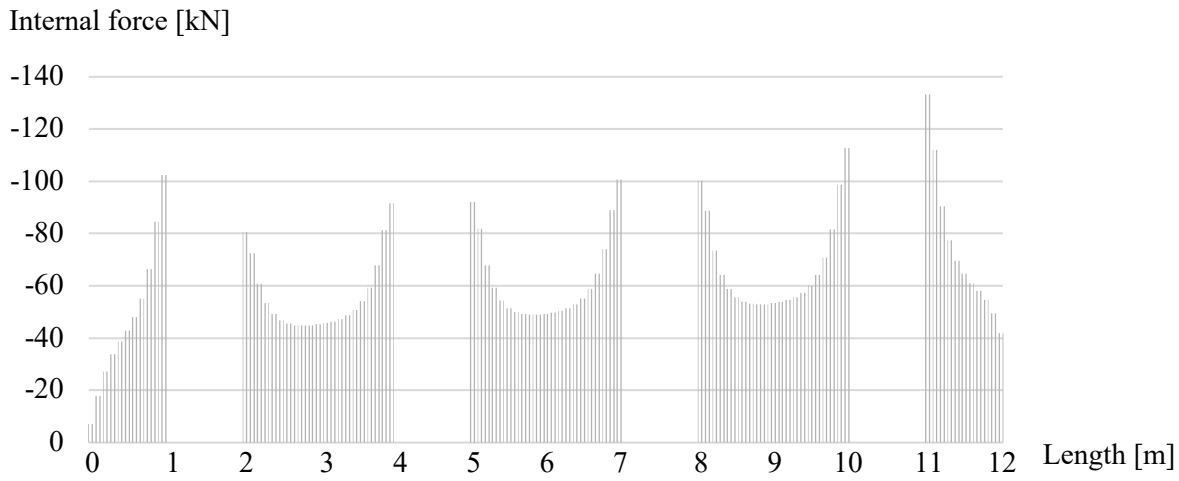

Figure 4.41: Internal force distribution of Subdivision type 2 including self-weight, Section 3.2.

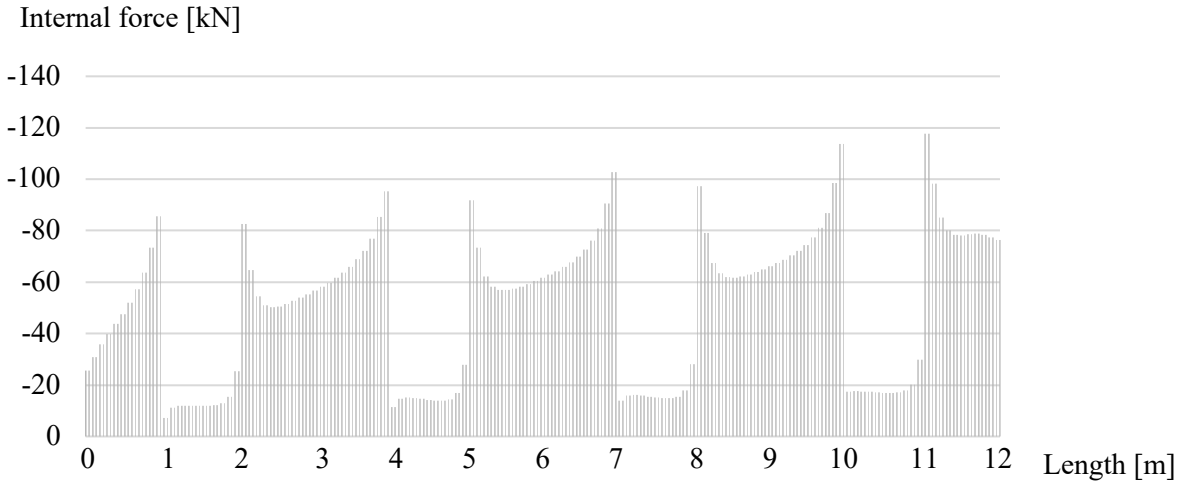

Figure 4.42: Internal force distribution of Subdivision type 2 including self-weight, Section 2.2.

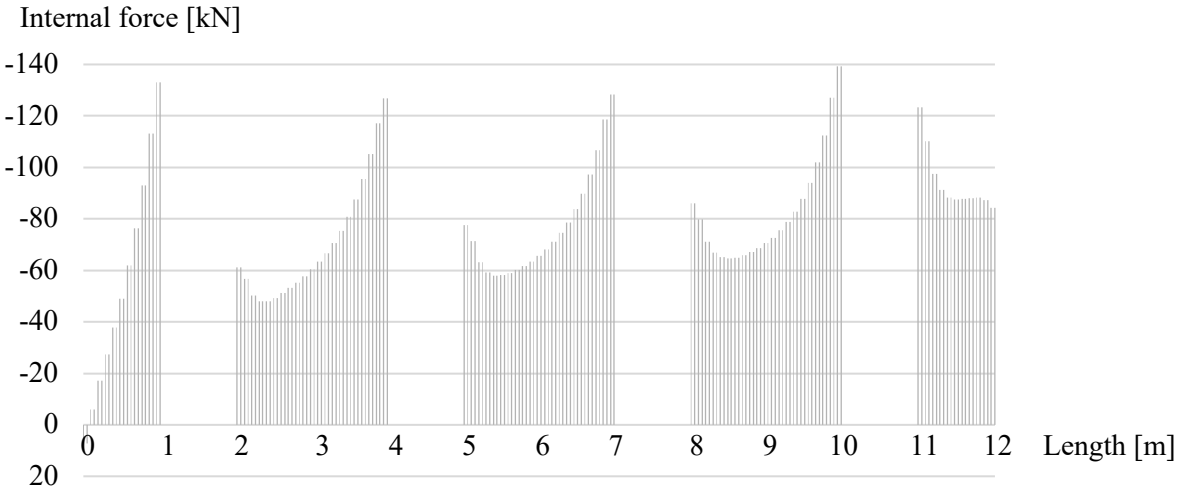

Figure 4.43: Internal force distribution of Subdivision type 2 including self-weight, Section 1.2.

5 Discussion

The discussion of the results is divided into chapters based on the different types of models. A general source of error that is of importance for all parts of the results is the mesh size of the FEM analysis. A study of convergence is made, and appropriate mesh size is chosen, the mesh size is therefore assumed not to contribute to any under- or overestimated results.

5.1 Models part 1 – Single panel

An assumed value for the wind load will be sufficient for the simplified models. The load on the truss model is applied as a point load but for the shell model, the load is applied as a linear load over the entire length of the model. This is done to avoid local effects, i.e. a line load will make the shell model behave more like the truss model that consists of rigid bar elements.

5.1.1 Equivalent stiffness

The calculated equivalent stiffness is derived from equations from scientific articles and is therefore assumed to be credible. The two equations for the equivalent stiffness for Truss model A and B differ, and it is the reduction for bending that is the main difference. In previous research, there are different ways to handle the reduction of bending. Gavric et al. (2015b), Wallner-Novak et al. (2013) and Hummel et al. (2016) all handled the kinematic behaviour of the CLT panels slightly different. The fact that the equivalent stiffness, as well as the reduction for bending, is calculated differently is an important variable to consider when comparing the results for Truss model A and B.

Since the same shear stiffness G is used for both the truss and the shell model, a relevant comparison can be made in that aspect. In this project, a reduction factor k_{88} is introduced to both the stiffness matrix of the shell model and for the equivalent stiffness of the truss models. The influence of the value of k_{88} is not investigated in this report but the value is estimated with the Austrian annexe and is therefore credible.

According to Moroder et al. (2015), the optimal truss model has a diagonal with an angle of 45 degrees. Though, in our results, the displacement of the truss model closest to the shell model was found for models with larger lengths, i.e. an angle smaller than 45 degrees. The inclusion of a reduction for bending does not change the fact that wider panels have a better outcome when comparing the displacement with the shell model. The statement that the most ideal angle of a diagonal is 45 degrees seems not to be accurate for the comparison between the shell model and the truss with an equivalent diagonal spring. This is since other parameters are more decisive (than the angle of the diagonal) for this comparison. Additionally, it is of importance to point out that the equation by Moroder et al. (2015) is based on timber diaphragms and not wall panels.

5.1.2 Displacement

The models of the single panel are simplified, and an assumed value for the wind load will be sufficient. However, the horizontal displacement of the models is small, and the assumed wind load might be too small. The relation between the horizontal displacement and the applied load is linear and a larger load would not change the result, only the size of the displacement. It is not the displacement itself that is of importance but the difference in displacement between models with different modelling approaches.

For a simplified and representative truss model of a CLT panel, a reduction for bending is one factor that is relevant to introduce to the equivalent stiffness. The result confirms that the reduction for bending is a relevant parameter since the horizontal displacement for Truss model B (including a reduction for bending) is closer to the displacement of the shell model. Not including a reduction for bending (Truss model A) is a too simplified approach and does not reflect the behaviour of the shell models as good as Truss model B.

For models with shorter lengths, the inclusion of bending has a greater effect on the displacement than for models with a larger length. For panels with greater length, the displacement of the truss models is more coinciding, and the displacements are as well more similar to the shell model. The short panels have a smaller equivalent stiffness, and they are therefore more affected by the reduction for bending. Slender panels have as well a higher risk of bending because of their geometry and moment of inertia.

5.1.3 Supports

To prevent larger global displacements of the shell model an improved support is applied that results in similar kinematic behaviour of the upper part of the model as for the truss model. With these improvements, the horizontal displacement of the shell model becomes more coincident with the displacement of the truss model. A frame with rigid bar elements that are subjected to a lateral load will have a vertical displacement of the top. It is of importance to mention that to notice the displacement for a small frame (3×3 m), the load must be very large, and the calculations must take non-linear geometry into account. When using linear calculations without consideration for large displacements this top vertical displacement of the truss model is not noticeable. That explains why the improvement of the shell model with no vertical displacements is a suitable approach.

Truss model B (including a reduction for bending) has a displacement that is more similar to the shell model when the upper support of the shell model is improved. There is no longer a significant difference in displacement to the shell model depending on the length of the panel. The coinciding displacement between the shell model and Truss model A (not including a reduction for bending) is also improving. But the phenomenon that a panel with a greater length has a result more similar to the shell model is still current.

5.2 Models part 2 – Multi-storey

The article by Moroder (2015) argues that a 45-degree angle of the diagonal is optimal which supports the decision to continue with the 3×3 m dimension of the panels. A line hinge stiffness is not introduced in the shell model and only rotation between the panels is allowed. The connections between the panels are decisive for the displacement of the entire model, something that is not further investigated in part 2.

The models of the multi-storey panels are simplified, and an assumed value for the wind load will be sufficient. The load is applied the same way as for the single panels, with a point load on the truss and a linear load over the entire length of the model for the shell model. By doing this, local effects from the load can be avoided and the models coincide better.

5.2.1 Displacement

The displacement of the truss models is overall smaller than for the shell models. As for the models of the single panels, the truss models in this part also include a reduction for bending (Truss model B). These models show a more coinciding result with the shell models. The more slender the multi-storey truss models (both A and B) are, the greater the differences are to the shell models. The difference in displacement between the shell model and the Truss model B is still distinct and it seems that the reduction used is not enough. Additional parameters that mimic the behaviour of the shell model need to be applied to the truss model. Furthermore, it seems that in this model of a multi-storey building, the bending effects are not captured accurately.

Member hinges are used for the truss model to allow rotation between the rigid bar elements, in the corners of the model. There is however a difference to the shell model, whose panels can rotate around the entire panel length. Therefore, a line support, preventing vertical displacement, is introduced to the top of the upper panels of the shell models. The restriction of the upper part of the multi-storey shell model makes the horizontal displacement of the models smaller and more similar to the displacement of the truss models.

For Truss model B, the fewer storeys the better the displacement coincides with the shell model. For Truss model A, the model of 2- and 3-storeys better coincides with the shell model. The truss model that best coincides with the shell model is the symmetric model of 3-storeys and 3 panels horizontally including bending (Truss model B), the difference in displacement is only about 0.2 % to the shell model with restriction in the vertical direction. Including a vertical restriction of the shell model improves the comparison as well.

5.3 Models part 3 – Gable

The result for the gable is displayed in both maximum and mean values, which is important to take into consideration when comparing the models. A great difference between the mean values and the maximum values can be noticed especially for the reaction forces. The loads that

are applied are point loads calculated according to Swedish Eurocode and they represent the wind load acting on the building. This is assumed to be a sufficient approximation of the load for this model. Different stiffnesses for the line hinges and the hold-downs have been used in this project and the lowest values were chosen for the presentation of the result of the parametric study of the gables, this is a source of error, and a mean value should have been chosen.

5.3.1 Hold-downs

The higher stiffness that is used for the hold-downs, the smaller the displacement of the gable is, the model with hold-downs at all nods has the smallest displacements. This is reasonable since a higher stiffness makes the gable withstand higher forces. This is as well the reason why the maximum reaction forces in the line support become lower when the stiffness in the hold-downs is increased. A higher hold-down stiffness better prevents the model to displace. This results in smaller compression forces on the right side of the gable where most of the compression forces occur (the opposite side of the applied load).

The mean reaction force in the line support does not present a change of result when the hold-down stiffness is changed. This is because of the equilibrium of forces, the total amount of compression forces in the line support and the total amount of tension forces in the hold-downs are both constant. The maximum forces can however change, because of the redistribution of forces within the line support respectively the hold-downs, when the stiffness in the hold-downs is changed.

The model that has the most obvious change in reaction force when the stiffness of the hold-downs is changed is Subdivision type 2, this is due to the number of hold-downs included in this model, 11 hold-downs. When the hold-down stiffness is changed it has a great effect, compared to when the hold-down stiffness is changed for the One panel with hold-downs only at the ends, that only has 2 hold-downs.

The reaction force that is taken up by the hold-downs is dependent on which side of the joint of the panel the line hinge is placed. The alternative modelling of the hold-downs (two hold-downs for one connection of panels) shows that the redistribution of reaction forces changes. On the left side of the gable a larger force is going down on the right side of the window on the right support i.e., the hold-down that is attached to the wall segment takes a higher force. These results show valuable information for designing hold-downs but also show another approach to how to handle reaction forces.

5.3.2 Line hinge

The global displacement is greater when the line hinge stiffness is lower, and this applies to all three models. The model of Subdivision type 2 is the model that experiences the greatest difference in both displacement and reaction force when the line hinge stiffness is changed, because of the greater amount of line hinges present in this model.

The stiffness values of the line hinges that are used are reasonable, although the values are inspired by connections between diaphragms, which should be an issue to consider. A modelling choice is made and the same value for line hinge stiffness is applied for both the vertical and horizontal connections. The modelling of the horizontal connections (between storeys) is therefore very simplified. Line hinge stiffness in *x*- and *y*-direction are set to the same value, a value that originally corresponds to the stiffness in the *x*-axis, which is a simplification.

The preconditions of the line hinge affect how the load is applied to the panels. Depending on which of the two panels in the connection are connected to the point of loading and which panel that only is connected to the first panel, the results will differ. It was discussed to what extent a line-load could be a solution to this inconvenience and whether this is a problem of importance for the modelling. The same dilemma was found for the hold-downs and the two connecting panels. Here, the support reaction affects one panel more because only one panel is connected to the hold-down, the other panel is through the line hinge connected to the first panel. The placement of the line hinge is decisive for which panel is transferring the load to the ground.

5.3.3 Self-weight

Taking self-weight into account makes the model more realistic. Without self-weight the results for displacement and tension reaction forces are on the safe side meanwhile the compression reaction forces are underestimated. However, the stiffness a load bearing capacity of a concrete foundation is significantly higher than for CLT panels and an applied self-weight to the model is not a great concern for the underestimated compression reaction forces.

5.3.3.1 Displacement

When self-weight is included the displacement of the gable is smaller than if a self-weight is not included. The gravity helps the gable withstand the wind load and this is accurate for both subdivision types. There is a difference in displacement decrease (when a self-weight is applied) for the two models, which depends on the stiffness of the connections between the panels and the connection to the ground.

5.3.3.2 *Reaction forces*

The compression reaction forces for Subdivision type 2 are in general larger than for Subdivision type 1. For both the subdivision models, without self-weight, the reaction forces are located at the right side of the gable. The compression reaction forces are greater on the right side of the panels close to the openings because the wind load is applied on the opposite side. The value of the maximum reaction force is affected by the length of the panels which depends on the subdivision type. With a self-weight applied the forces are more spread out, with a maximum value a bit to the left of the centre of the support, *see Figures 4.22 and 4.34* for the reaction force diagrams for Subdivision type 1 and 2, respectively. The distribution of the reaction forces is similar for both cases, the small difference correlates to the extra connection in the middle for Subdivision type 1.

The maximum reaction force in the line support (compression) has a small increase respectively decrease for the models of Subdivision type 1 and Subdivision type 2 when a self-weight is applied. Including the self-weight has a much greater effect on the mean reaction forces since the applied self-weight generates an equivalent reaction force. The smaller difference in the maximum reaction force when self-weight is applied is because the maximum reactions force is a result of the wind load.

The maximum reaction forces in the hold-downs (tension) have an expected result, they are decreased when the self-weight is applied, which is accurate for both the models (Subdivision type 1 and Subdivision type 2).

5.3.3.3 *Internal for*ces

The gable without self-weight is compressed on the right side and experiences tension on the left side because of the uplifting force of the panels due to the wind load. The gable experiences high forces (tension) at the points where the load is applied, which is a local effect caused by the modelling choice. There are also high stresses around the openings because of the abrupt change of geometry, and high stresses are also found close to the joints of the panels. The maximum forces for each section are located close to the edge of an opening or for Section 2, located above this edge of an opening, accurate for both the subdivisions.

The mean internal force for Section 1 (closest to the support) for the models with self-weight is larger than for the other sections, due to the greater amount of wind load applied to the area above the section. The mean internal forces for the different sections are similar for the two subdivisions, an expected result since the two models are similar. The small difference in mean internal force can be correlated to the different placement and the number of hold-downs or the different number of line hinges.

The colour diagram of *Figure 4.40* shows that parapets and lintels of Subdivision type 2 experience smaller internal forces than the wall segments. The same behaviour can be observed for the model of Subdivision type 1, the area underneath openings experience a low value of internal forces. This is the reason why hold-downs are not commonly placed so that they are connected to the parapets. The line hinge stiffness used (15 000 kN/m^2) influences the internal force distribution of the gable. A lower resilience of the line hinge would result in a smoother distribution of the internal forces between the sub-panels.

6 Conclusion

In this chapter, the summary of the results is presented together with recommendations and further development. The research questions that have been investigated in this project are:

- What type of modelling approaches is used in previous research for the design of CLT buildings experiencing lateral load?
- What is the effect of modelling choice (shell or truss models) for the predicted stiffness (displacement) of CLT panels experiencing lateral loads, in this case, wind loads?
- What is the effect of including self-weight in the models of CLT buildings in terms of displacement, internal force distribution and reaction forces?
- What is the effect of the subdivision of panels and their connections for models of CLT buildings in terms of lateral stiffness (displacement), internal force distribution and reaction forces?

6.1 Modelling recommendations

The study of previously used modelling approaches is presented in chapter *2.3 Scientific base.* The modelling approaches that are used for the models in this project are based on the previous research, comparisons and limitations were made to create the models in the best way.

The primary modelling approach that is used is a truss model with a spring element representing the stiffness of a CLT panel, which is a very simplified modelling approach. To make it compatible it is important to include the kinematic behaviours of CLT. Including a reduction for bending and a vertical restriction of the shell model are two recommended modelling approaches, since the inclusion of a reduction for bending to the truss model makes the kinematic behaviour of the truss model more similar to the shell model. A vertical restriction of the shell model makes its kinematic behaviour more similar to the truss model. We suggest that the panels are divided into sub-panels for the truss model, but a further investigation of their connections is necessary.

Another approach that is analysed is the dividing of a CLT wall into parapets, lintels, and wall segments. The choice of coupled or uncoupled panels is here an important modelling approach. A good way to model this phenomenon is with line hinges with an assigned stiffness. As a further development, a variation of the line hinge stiffness is recommended. It is noticed that the assigned stiffness is affecting the distribution of internal forces present in the lintels and parapets. This affects to what extent the lintels and parapets are contributing to the stiffness of the wall. We recommend that this is considered when modelling the connection between panels.

6.2 Summary of results

The modelling choice of applying a reduction for bending shows coinciding results (horizontal displacement) between the shell model and the truss model for both the single panels and multi-storey models. The inclusion improves the result, especially for the models with a shorter length since they are more affected by local effects and more influenced by bending. Applying a vertical restriction at the top of the shell model makes the comparison between the shell model and the truss model better. The displacement of the models with the greatest coinciding results is the multi-storey model of Truss model B and the shell model including a vertical restriction.

The line hinge stiffness that is used for the gable impacts the horizontal displacement, a lower stiffness results in a larger displacement. The panel configuration and the number of line hinges used for the models affect the displacement, the more line hinges the greater the displacement. The properties of the hold-downs are as well affecting the displacement, the higher the stiffness and the greater number of hold-downs, the smaller the displacement. Applying a self-weight to the subdivided models of the gable gives as well as expected a lower horizontal displacement.

Both the placement and the stiffness of hold-downs affect the reaction forces. A higher hold-down stiffness results in higher maximum tension support reactions. Depending on the model of subdivision that is used, the more hold-downs applied the smaller the reaction force in the individual hold-downs. An applied self-weight to the gable decreases the tension reaction forces as expected. The compression reaction forces increase when a self-weight is applied, for both the subdivisions. The locations and values of the compression reaction forces both maximum and mean are affected by the panel configuration i.e., the subdivision of the models.

The modelling approach that is chosen affects the internal force distribution in the gable. The locations of high internal forces are close to openings and the point of loading. The effect of applying a self-weight gives as expected an increase of internal compression forces to the gable. The internal forces are greater closer to the ground support, this is due to the greater amount of load affecting the section. The chosen subdivision type influences the internal force distribution. A lower value for the line hinge stiffness and fewer subdivisions both result in smoother internal force distribution.

6.3 Recommendations and further development

The subject of this study is under constant improvement and this chapter presents some of the possible further developments. To continue with model part 4 and make a truss model of the subdivided gable would be an interesting further development. Starting with one story and comparing the results with Subdivision type 2 would be the next step in investigating the truss model. Including the deformation types of translation (sliding) and rotation (rocking) in the models would also be an interesting development. For the models of the gable, the influence of size and placing of openings was of interest. The model of the gable is a generic model and different sizes, and placing is something that can be further investigated.

For a more comprehensive comparison between the truss model and the shell model, further parameters can be investigated. The anchorage forces and their distribution to the foundation are such parameters. However, a limitation was made, and these parameters are not included in the modelling part 1 and part 2. The improvement of the top support of the shell model can as well be further improved. An even better comparison can be made if the line support allows the top to be something in between free and fixed i.e., the top can move down vertically without rotation.

The modelling of the horizontal connections (between storeys) for the gable is simplified and the same stiffness values are used for both the horizontal connections and the vertical connections. A further development would be to use line releases (specific term for RFEM). Then it is possible to include non-linearity between the panels on different storeys so that the horizontal connection only takes compression and not tension. Further development would as well be to continue to investigate the stiffness of the line hinges and the effect it has on the internal force distribution in the lintels and parapets of the gable.

Bibliography

Brandner R, Flatscher G, Ringhofer A, Schickhofer G, Thiel A (2016) *Cross laminated timber (CLT): overview and development.* European Journal of Wood and Wood Products. 74;331–351. https://doi.org/10.1007/s00107-015-0999-5

Brandt, K (2015) *CLT-the future has historic roots*. Wood magazine: Issue 4. https://www.swedishwood.com/publications/wood-magazine/2015-4/clt_the_future_has_historic_roots/ [2021-09-13]

Casagrande D, Polastri A, Sartori T, Loss C, Chiodega M (2016) *Experimental campaign for the mechanical characterization of connection systems in the seismic design of timber buildings.* Proceedings of the 14th World Conference on Timber Engineering (WCTE), Vienna, Austria.

Casagrande D, Doudak G, Vettori M, Fanti R (2021a) *Proposal for an equivalent frame model for the analysis of multi-storey monolithic CLT shear walls*. Engineering Structures Volume:245,112894. https://doi.org/10.1016/j.engstruct.2021.112894

Casagrande D, Fanti R, Greco M, Gavric I, Polastri A (2021b) *On the distribution of internal forces for single-storey CLT symmetric shear-walls with openings*. Structures: Volume 33:4718-4742. https://doi.org/10.1016/j.istruc.2021.06.084

Dlubal (2021a) *RFEM 6: FEM Structural Analysis Software*. https://www.dlubal.com/en/products/rfem-fea-software/what-is-rfem [2021-12-01]

Dlubal (2021bb) *Frequently asked questions.* What are the stiffness reduction factors k33 and k88 in RF-LAMINATE? | Dlubal Software [2021-12-15]

Dlubal (2021cc) *4.7 Nodal Supports*. *https://www.dlubal.com/en/downloads-and-information/documents/online-manuals/rfem-5/04/07* [2021-12-08]

Dlubal (2021dd) *4.8 Line Supports. https://www.dlubal.com/en/downloads-and-information/documents/online-manuals/rfem-5/04/08* [2021-12-08]

Dlubal (2021ee) *4.10 Line Hinges.* https://www.dlubal.com/en/downloads-and-information/documents/online-manuals/rfem-5/04/10 [2022-02-10]

Dlubal (2021ff) *4.14 Member Hinges.* https://www.dlubal.com/en/downloads-and-information/documents/online-manuals/rfem-5/04/14 [2021-12-08]

Dlubal (2022) *RFEM 5 Manual: 8.17 Surfaces – Design Internal Forces.* https://www.dlubal.com/en/downloads-and-information/documents/online-manuals/rfem-5/08/17 [2022-03-28]

Dujic, B, Klobcar, S, Zarnic S.R (2007) *Influence of Openings on Shear Capacity of Wooden Walls*. Proceedings of the 40th CIB-W18. Bled: Slovenia

European Commission (2021a) *Buildings and construction.* https://ec.europa.eu/growth/industry/sustainability/buildings-and-construction_en [2021-22-24]

Gavric I, Fragiacomo M, Ceccotti A (2015a) *Cyclic behaviour of typical metal connectors for cross-laminated (CLT) structures*. Materials and Structures: 48, 18-41-1857. https://doi.org/10.1617/s11527-014-0278-7

Gavric I, Fragiacomo M, Ceccotti A (2015b) *Cyclic behaviour of CLT wall systems: experimental tests and analytical prediction models*. Journal of Structural Engineering 141(11):04015034. https://doi.org/10.1061/(ASCE)ST.1943-541X.0001246

Hummel J, Seim W, Otto S (2016) *Steifigkeit und Eigenfrequenzen im Mehrgeschossingen Holzabau*. Bautechnik: Volume 93, 781–94. https://doi.org/10.1002/bate.201500105

IMARC Group (2021) *European Cross-Laminated Timber Market: Industry Trends, Share, Size, Growth, Opportunity and Forecast 2021-2026*. https://www.imarcgroup.com/european-cross-laminated-timber-market [2021-12-03]

Liu G.R & Quek S.S (2003) *The finite element method- A practical course*. Oxford: Butterworth-Heinemann.

Lukacs I, Björnfot A, Tomasi R (2019) *Strength and stiffness of dross-laminated timber (CLT) shear walls: State of the art of analytical approaches*. Engineering Structures: Volume 178, 136-147. https://doi.org/10.1016/j.engstruct.2018.05.126

Mestar M, Doudak G, Polastri A, Casagrande D (2020) *Investigating the kinematic modes of CLT shear-walls with openings.* Engineering structures: Volume 228, 111475. https://doi.org/10.1016/j.engstruct.2020.111475

Moroder D, Smith T, Pampanin S, Buchanan A.H (2015) *An equivalent truss method for the analysis of timber diaphragms.* Proceedings of the Tenth Pacific Conference on Earthquake Engineering (PCEE). Sydney, Australia.

Ottosen Saabye N & Petersson H (1992) *Introduction to the Finite Element Method*. Prentice Hall Europe. Lund: Lund University.

Olausson G (2021) *Shear stiffness of cross laminated timber diaphragms- A study of the influence of connection and member stiffness.* Master thesis, Civil engineering. Lund: Lund University.

Sandoli A, Moroder D, Pampanin S, Calderoni B (2016) *Simplified analytical models for coupled CLT walls.* World Conference on Timber Engineering, WCTE 2016:4649.

Shahnewaz Md, Tannert T, Shahria Alam M, Popovski M (2016) *In-Plane stiffness of CLT panels with and without openings.* World Conference on Timber Engineering, WCTE 2016.

Shahnewaz Md, Alam S, Tannert T (2018) *In-plane strength and stiffness of cross-laminated timber shear walls*. Buildings 2018, 8(8),100. https://doi.org/10.3390/buildings8080100

SS-EN 1991-1-4:2005 (2008) Eurocode 1: Actions on structures – Part 1-4: General actions – Wind actions.

Swedish wood (2016) *Design of timber structures Volume 1- Structural aspects of timber construction.* https://www.svenskttra.se/siteassets/5-publikationer/pdfer/design-of-timber-structures-1-2016.pdf [2021-11-29]

Swedish Wood (2019) *The CLT Handbook.* https://www.svenskttra.se/siteassets/5-publikationer/pdfer/clt-handbook-2019-eng-m-svensk-standard-2019.pdf [2021-11-16]

Swedish Wood (2021) *Properties of softwood.* https://www.swedishwood.com/wood-facts/about-wood/from-log-to-plank/properties-of-softwood/ [2021-11-24]

Wallner-Novak M, Koppelhuber J, Pock K (2013) *Information Brettsperrholz Bemessung Grundlagen für Statik und Konstruktion nach Eurocode*. proHolz Austria; ISBN 978-3-902926-03-6

World Green Building Council (2021) *Bringing Embodied Carbon Upfront* https://www.worldgbc.org/embodied-carbon [2021-12-21]

Zhu B (2018) *The Finite Element Method- Fundamental and Applications in Civil, Hydraulic, Mechanical and Aeronautical Engineering*. John Wiley & Sons Singapore Pte. Ltd. Tsinghua University.

ÖNORM B EN 1995-1-1:2019-07 (2010) *Eurocode 5: Design of timber structures - Part 1-1: General- Common rules and rules for buildings- National specifications, national comments and national supplements concerning ÖNORM EN 1995-1-1.* Austrian Standards Institute.

Appendix A: Models part 1 – Single panel

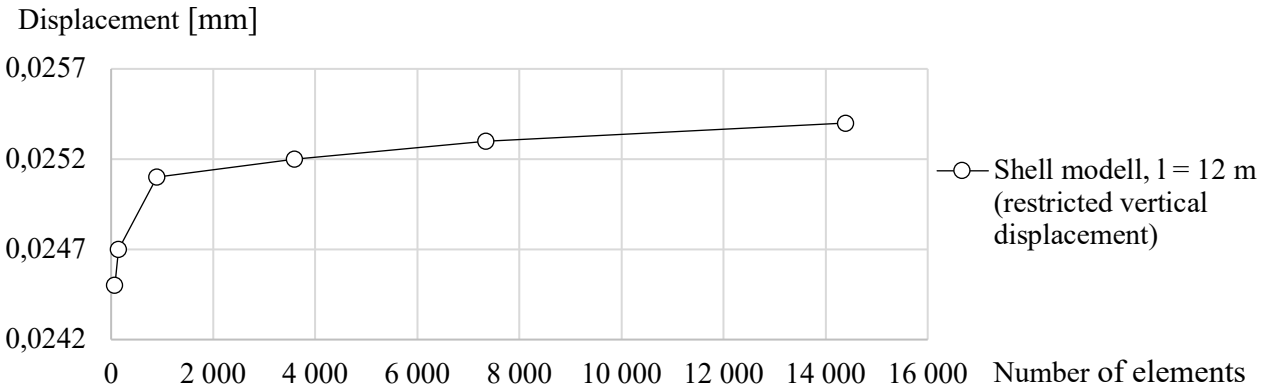

Figure A1: Plot of convergence for the shell model, with restrictions for vertical displacement, with a length of 12 m.

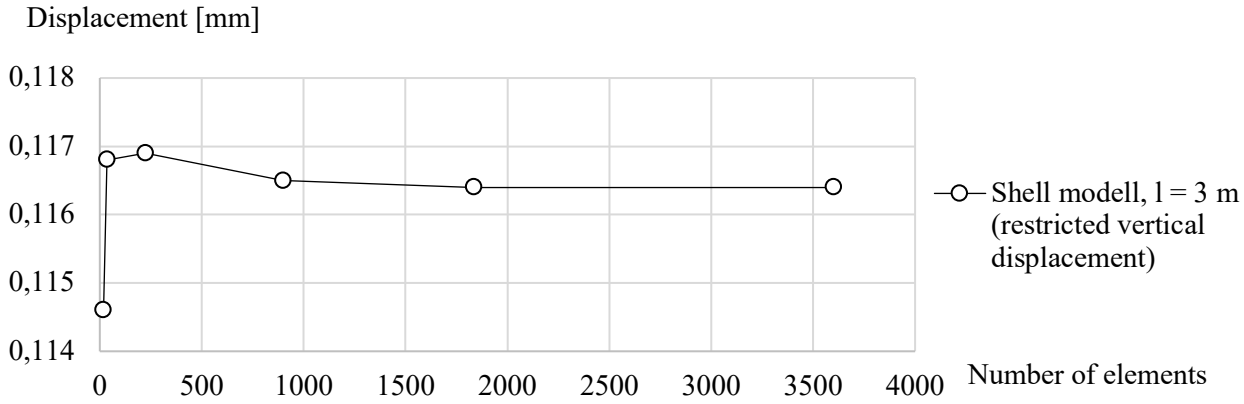

Figure A2: Plot of convergence for the shell model with *no* restrictions for vertical displacement with a length of 3 m.

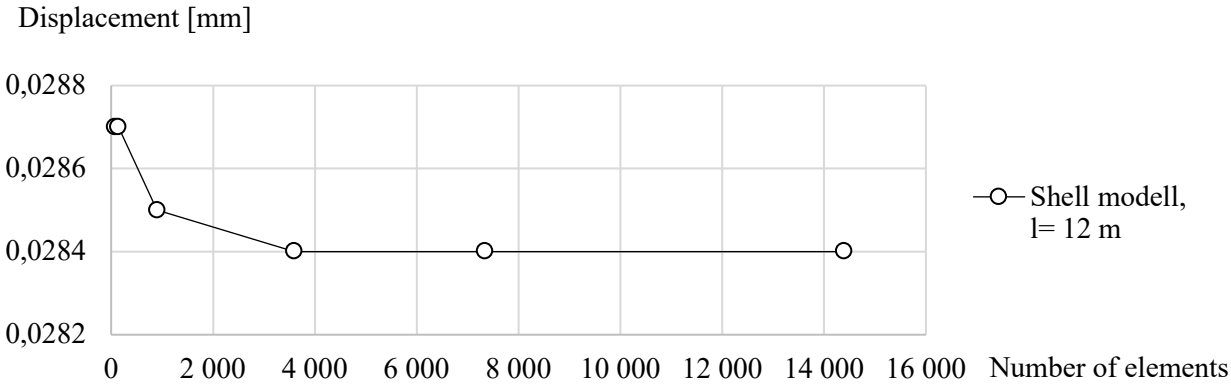

Figure A3: Plot of convergence for the shell model with *no* restrictions for vertical displacement with a length of 12 m.

Table A1: Values for the difference in displacement for Truss model A and B with the shell model as a reference.

Width of truss structure, b [m]	Difference in displacement [%]			
	Shell model as reference		Shell model (restricted vertical displacement) as reference	
	Truss model A	Truss model B	Truss model A	Truss model B
3	-17,0	-25,0	-17,0	-1,4
6	-8,2	-17,7	-8,2	-3,8
9	-5,3	-15,1	-5,3	-3,4
12	-4,2	-14,0	-4,2	-3,1
15	-3,0	-12,9	-3,0	-2,3

Appendix B: Models part 2 – Multi-storey

Table B1: Values for displacement and difference in displacement for the configurations of the multi-storey models with the shell model as a reference.

Geometry		Deformation			Difference in deformation			
Number of elements horizontally	Number of elements vertically	Shell model [mm]	Truss model B [mm]	Truss model A [mm]	Truss model B [mm]	Truss model A [mm]	Truss model B [%]	Truss model A [%]
2	1	0,06	0,06	0,05	0,00	-0,01	-5,28	-20,30
3	1	0,04	0,04	0,03	0,00	-0,01	-1,80	-17,48
4	1	0,03	0,03	0,02	0,00	0,00	0,00	-15,73
2	2	0,20	0,17	0,15	-0,03	-0,06	-15,02	-28,47
3	2	0,13	0,12	0,10	-0,01	-0,03	-8,00	-22,64
4	2	0,09	0,09	0,07	0,00	-0,02	-2,93	-18,36
2	3	0,49	0,35	0,29	-0,14	-0,20	-29,49	-40,66
3	3	0,28	0,23	0,19	-0,05	-0,09	-17,62	-30,65
4	3	0,19	0,17	0,15	-0,02	-0,05	-9,35	-23,70

Table B2: Values for displacement and difference in displacement for the configurations of the multi-storey models with the shell model restricted for vertical displacement as a reference.

Geometry		Deformation			Difference in deformation			
Number of elements horizontally	Number of elements vertically	Shell model (restricted) [mm]	Truss model B [mm]	Truss model A [mm]	Truss model B [mm]	Truss model A [mm]	Truss model B [%]	Truss model A [%]
2	1	0,05	0,06	0,05	0,01	0,00	12,99	-4,92
3	1	0,03	0,04	0,03	0,00	0,00	14,71	-3,60
4	1	0,02	0,03	0,02	0,00	0,00	16,73	-1,63
2	2	0,17	0,17	0,15	0,00	-0,03	0,70	-15,24
3	2	0,11	0,12	0,10	0,01	-0,01	6,88	-10,13
4	2	0,08	0,09	0,07	0,01	-0,01	10,23	-7,29
2	3	0,38	0,35	0,29	-0,03	-0,09	-8,99	-23,41
3	3	0,23	0,23	0,19	0,00	-0,04	-0,22	-16,00
4	3	0,16	0,17	0,15	0,01	-0,02	4,86	-11,73

Appendix C: Models part 3 – Gable

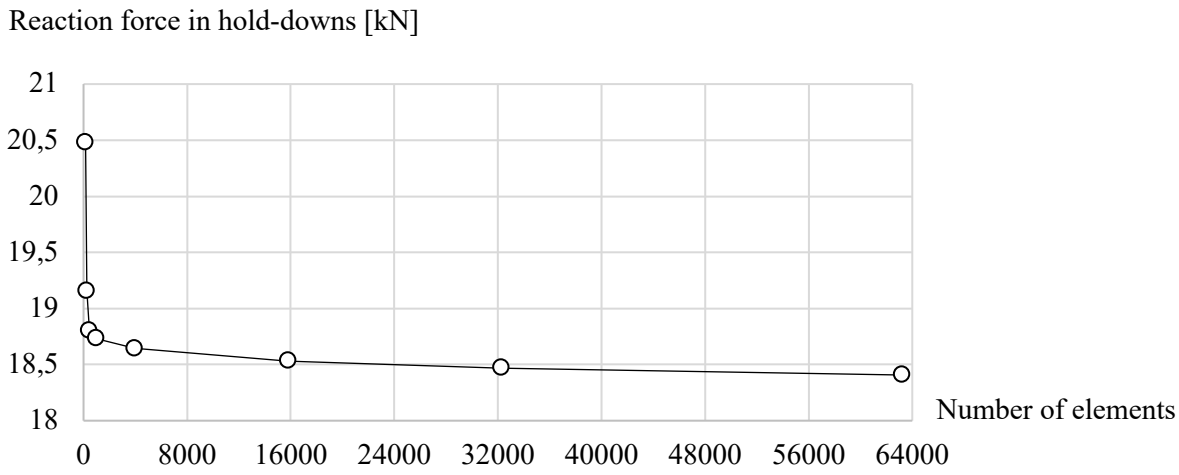

Figure C1: Plot of convergence for maximum tension reaction force in the hold-downs.

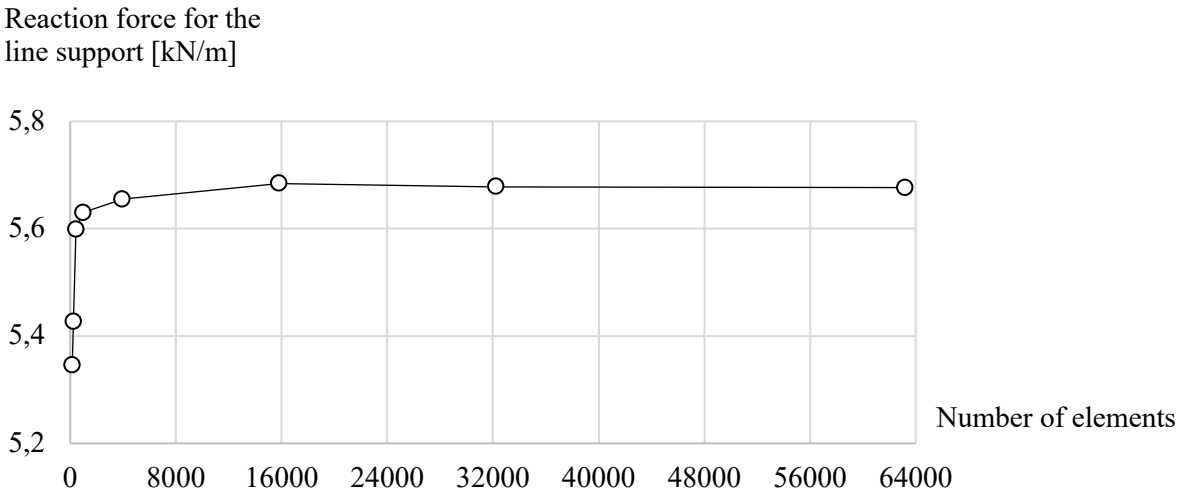

Figure C2: Plot of convergence for compression reaction force (mean) of the line support.

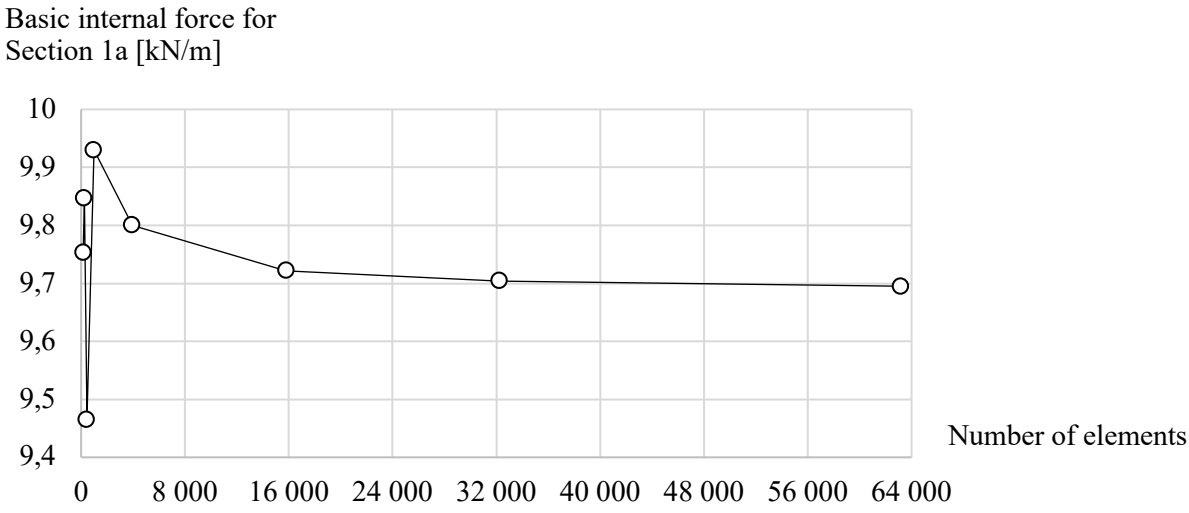

Figure C3: Plot of convergence for mean basic internal forces in Section 1.

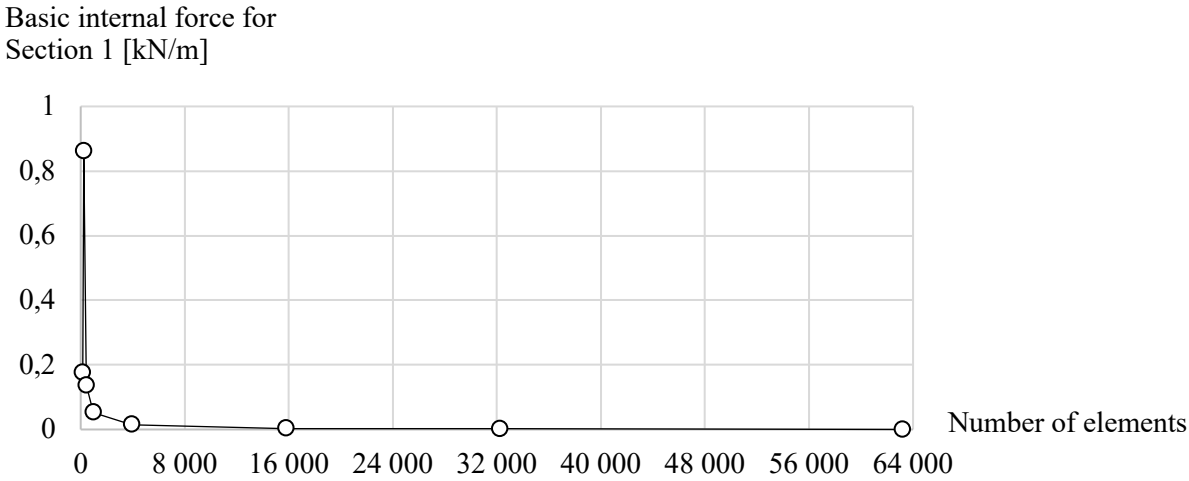

Figure C4: Plot of convergence for mean basic internal forces in Section 1a.

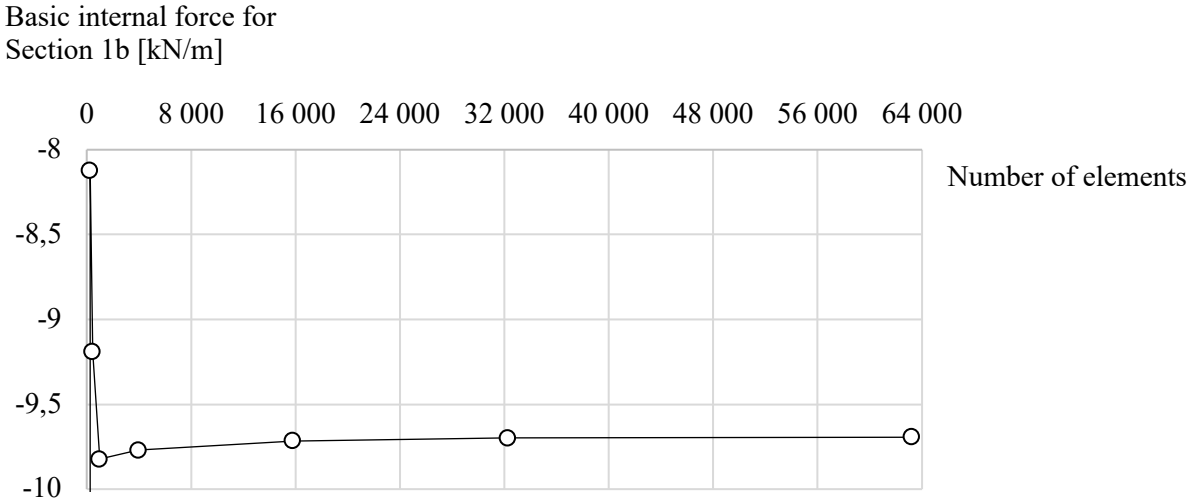

Figure C5: Plot of convergence for mean basic internal forces in Section 1b.

Table C1: Values for displacement and reaction force for the models of the gable with a hold-down stiffness of 5000 kN/m.

Hold down stiffness: 5 000 kN/m		Line hinge stiffness								
		3000 kN/m2			15 000 kN/m2			30 000 kN/m2		
		Hold down placement			Hold down placement			Hold down placement		
Parameter	Type of model	At ends	At all nodes	Difference [%]	At ends	At all nodes	Difference [%]	At ends	At all nodes	Difference [%]
Displacement, max [mm]	One panel	12,4	7,8	-36,9	12,4	7,8	36,9	12,4	7,8	36,9
	Sub. div. 1	28,5	26,3	-7,7	14,6	11,8	-19,1	12,7	9,8	-22,9
	Sub. div. 2	46,0	46,0	0,0	14,7	14,7	0,0	10,4	10,4	0,0
Support force (line support) max [kN/m]	One panel	208,0	164,4	20,9	208,0	164,4	20,9	208,0	164,4	20,9
	Sub. div. 1	177,1	136,5	22,9	189,0	152,1	19,5	191,8	155,5	18,9
	Sub. div. 2	308,2	308,2	0,0	176,7	176,7	0,0	156,1	156,1	0,0
Support force (line support) mean [kN/m]	One panel	3,6	5,1	-40,8	3,6	5,1	-40,8	3,6	5,1	-40,8
	Sub. div. 1	4,0	4,6	-15,8	4,2	5,0	-18,7	4,2	5,1	-19,8
	Sub. div. 2	6,6	6,6	0,0	5,3	5,3	0,0	4,8	4,8	0,0
Support force (hold-downs) max [kN]	One panel	36,0	19,8	45,0	36,0	19,8	45,0	36,0	19,8	45,0
	Sub. div. 1	32,3	25,3	21,5	30,5	21,1	30,9	30,1	20,1	33,3
	Sub. div. 2	22,7	22,7	0,0	16,2	16,2	0,0	14,4	14,4	0,0

Table C2: Values for displacement and reaction force for the models of the gable with a hold-down stiffness of 15 000 kN/m.

Hold down stiffness: 15 000 kN/m		Line hinge stiffness								
		3000 kN/m^2			15 000 kN/m^2			30 000 kN/m^2		
		Hold down placement			Hold down placement			Hold down placement		
Parameters	Type of model	At ends	At all nodes	Difference [%]	At ends	At all nodes	Difference [%]	At ends	At all nodes	Difference [%]
Displacement, max [mm]	One panel	6,3	4,7	25,9	6,3	4,7	25,9	6,3	4,7	25,9
	Sub. div. 1	23,2	22,4	3,4	9,5	8,5	10,4	7,7	6,7	13,4
	Sub. div. 2	41,9	41,9	0,0	12,1	12,1	0,0	8,1	8,1	0,0
Support force (line support) max [kN/m]	One panel	132,0	115,0	12,9	132,0	115,0	12,9	132,0	115,0	12,9
	Sub. div. 1	115,4	100,4	13,0	120,9	108,2	10,5	123,3	110,1	10,7
	Sub. div. 2	240,7	240,7	0,0	145,5	145,5	0,0	119,1	119,1	0,0
Support force (line support) mean [kN/m]	One panel	3,6	5,0	-37,0	3,6	5,0	-37,0	3,6	5,0	-37,0
	Sub. div. 1	3,9	5,0	-28,5	4,1	4,9	-19,0	4,2	5,0	-19,7
	Sub. div. 2	7,5	7,5	0,0	6,0	6,0	0,0	5,5	5,5	0,0
Support force (hold-downs) max [kN]	One panel	36,2	22,2	38,7	36,2	22,2	38,7	36,2	22,2	38,7
	Sub. div. 1	34,6	29,8	13,9	32,3	25,4	21,5	31,6	24,0	23,9
	Sub. div. 2	29,5	29,5	0,0	20,0	20,0	0,0	17,6	17,6	0,0

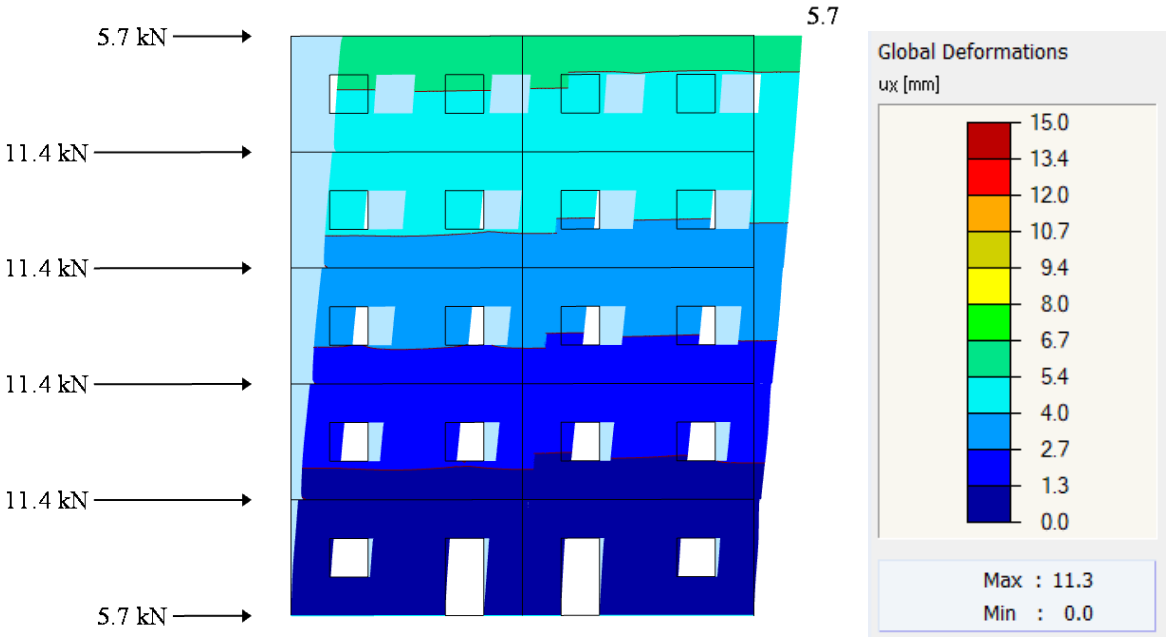

Figure C6: Horizontal displacement of the gable of Subdivision type 1 including self-weight.

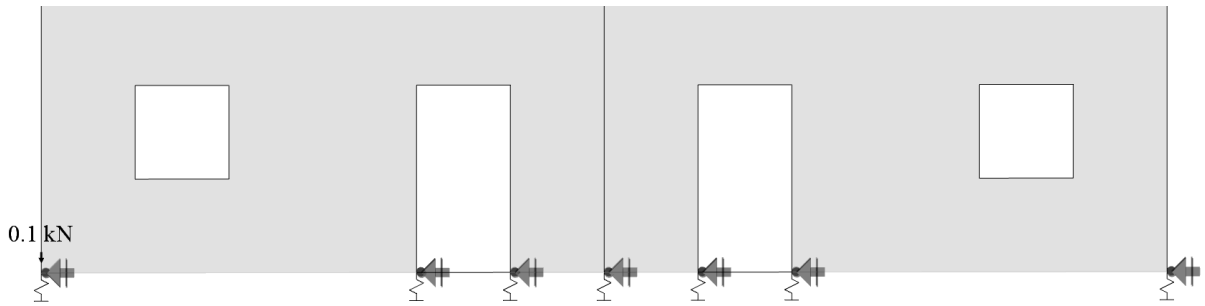

Figure C7: Reaction forces in the hold-downs of Subdivision type 1 including self-weight.

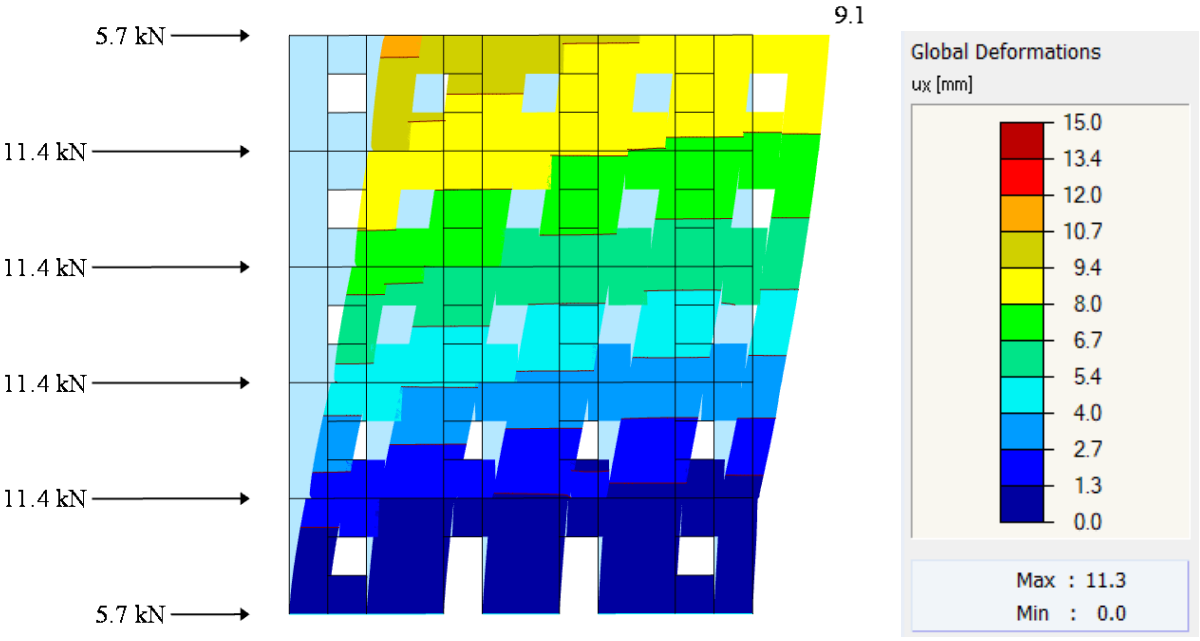

Figure C8: Horizontal displacement of the gable of Subdivision type 2 including self-weight.

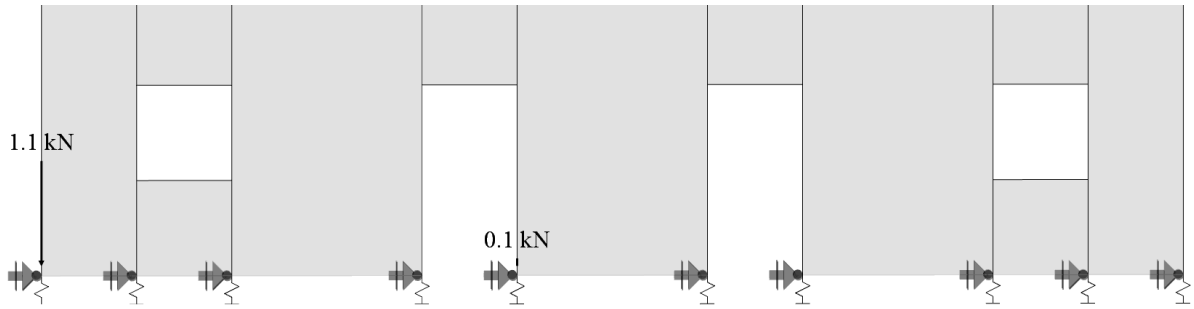

Figure C9: Reaction forces in the hold-downs of Subdivision type 2 including self-weight.

Table C3: Maximum and mean reaction force in the line support of the gable.

Reaction force		Max [kN]	Mean [kN]
No self-weight	Sub. div. 1	120,3	4,9
	Sub. div. 2	147,4	5,7
Self-weight	Sub. div. 1	123,3	60,0
	Sub. div. 2	162,2	60,1

Table C4: Maximum and mean internal forces in the gable.

Internal force			Max [kN]	Mean [kN]
No self-weight	Sub. div. 1	Section 1.1	47,5	-
		Section 2.1	-28,0	-
		Section 3.1	-31,5	-
	Sub. div. 2	Section 1.2	-51,1	-
		Section 2.2	32,9	-
		Section 3.2	26,1	-
Self-weight	Sub. div. 1	Section 1.1	-170,0	-75,1
		Section 2.1	-96,0	-50,0
		Section 3.1	-167,3	-60,1
	Sub. div. 2	Section 1.2	-139,2	-75,0
		Section 2.2	-117,8	-50,1
		Section 3.2	-133,2	-60,0